IOWA STATE UNIVERSITY
Digital Repository

2009

Titanium dioxide photocatalysis: studies of the degradation of organic molecules and characterization of photocatalysts using mechanistic organic chemistry

Timothy Lee Hathway
Iowa State University

Recommended Citation

Titanium dioxide photocatalysis: studies of the degradation of organic molecules and characterization of photocatalysts using mechanistic organic chemistry

by

Timothy Lee Hathway

A dissertation submitted to the graduate faculty

in partial fulfillment of the requirements for the degree of

DOCTOR OF PHILOSOPHY

Major: Organic Chemistry

Program of Study Committee:
William Jenks, Major Professor
Richard Larock
Nicola Pohl
Klaus Schmidt-Rohr
Yan Zhao

Iowa State University

Ames, Iowa

2009

Table of Contents

Chapter 1

General Introduction

1.1. Introduction

The cleanup of wastewater and air pollution has become increasingly important in the past decades, and burgeoning populations require more and more energy and resources to sustain a comfortable standard of living. Two major types of pollution can be identified that encompass all others: technological and agricultural. Technological pollution is that produced from human sources: industrial, military, etc. Compounds with low solubility in water characterize this type of pollution. A separate layer forms on the surface that negatively affects the physical properties of the water (oxygen uptake, surface tension), which also hampers any living thing that makes contact with the surface. The second major type of pollution is that of high concentrations of nutrients that leach into the soil and drain into water sources mainly from agriculture. The most notable effect of this form of pollution is the overgrowth of algae and other plants in the water source that cannot be removed by natural means, which build up in and prematurely age a water source.[1] With these issues in mind, freshwater sources are of particular concern as they are the major source of drinking water for the world's population. Chemical runoff from pollution sources enters bodies of water not naturally able to contain and remediate it.[2] Although the prevention of pollution is

critical to cleanup efforts, repairing the current damage is a great concern.

Many different types of chemicals enter ground and surface water sources, both inorganic and organic. Heavy metals, nitrates, and organometallics (especially tin compounds) are the most common inorganic sources of pollution, both technologically and agriculturally based.[3] Some of the most common and harmful organic pollutants in wastewater and other polluted sources are organic molecules, including polychlorinated biphenyls (PCBs), chlorinated and brominated phenols, chlorinated hydrocarbons, atrazines, surfactants, and a plethora of aromatics contained in pesticide runoff, sewage, and industrial sources.[3] Although this is by no means an exhaustive list, it does highlight the fact that many of these are small molecules that are at least mildly soluble in water and are toxic to all forms of life. Physical means of removing waste include filtration, distillation, ion exchange, and reverse osmosis. Most of these methods, though, are useful only for insoluble or inorganic compounds.[1] Chemical methods for removal of organics include waste incineration, anaerobic digestion, and physicochemical methods. Chemical oxidation is a physicochemical method involving highly oxidizing materials used to convert organic pollutants to carbon dioxide, water, and other fully oxidized species like nitrates and sulfates. By oxidative means, harmful organic compounds can be broken down into substances that the other methods (ion exchange, distillation) can easily separate from water.

These chemical oxidation processes can be divided into two major classes: conventional and advanced. Conventional processes[4] involve wet chemical oxidizing agents, including ozone, persulfate, and Fenton reagents (Fe^{3+}/H_2O_2). These methods have been proven effective in the remediation of a wide array of organics, but have several disadvantages. These include toxicity and potential safety hazards of the strongly oxidizing

agents (like H_2O_2 or permanganate). Also their high reactivity can lead to a short lifetime and thus incomplete oxidation of organics, producing intermediates that may be more toxic than the original pollutant.[4]

The premier alternative to conventional oxidation is that of advanced oxidation using sonolysis, radiolysis, or photolysis. Advanced oxidation processes (AOPs) are those processes that involve the creation of *in situ* oxidants with high oxidation potentials.[5] Of particular interest is photolysis, known as photodegradation, in terms of waste treatment. The most widely employed light-assisted remediation methods are direct photolysis, degradation with UV/H_2O_2, photolysis with ozone, and photocatalysis.[6]

As many organic compounds are resistant to direct photolysis under visible or UV light, a sensitizer or photocatalyst must be employed. Solution phase UV reagents, like H_2O_2, have many of the same downfalls that non-AOP chemical oxidizers have, including the tendency to react completely before the intended pollutant is sufficiently destroyed. Photocatalysts, being generally water-insoluble, do not suffer from this limitation, as many are rugged under aqueous conditions and resistant to photochemical degradation. Both of these methods generate hydroxyl radicals and other strongly oxidizing species in solution.[5] Therefore, photocatalysis and homogenous photodegradation share many of the same mechanistic traits, including an exceptional ability to degrade organic molecules to fully oxidized forms, as shown in Reaction 1.

$$C_xH_{2x} + xO_2 \xrightarrow[h\nu]{TiO_2} xCO_2 + \frac{x}{2}H_2O$$
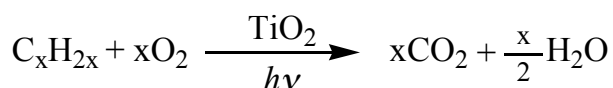
Reaction 1. Destruction of a generic hydrocarbon using titanium dioxide and light

Semiconductor photocatalysis relies on the use of metal chalcogenides to create oxidized holes, which directly react with adsorbed molecules. This subject is explained in further detail in section 1.3. In particular, titanium dioxide (TiO_2) has emerged as the most studied of these photocatalysts for its high degradation efficiency with almost any organic molecule and many other attractive properties, including physical and chemical stability and low cost.[7]

Although many of the degradation characteristics of TiO_2 are known, many of the initial chemical processes of degradation that occur directly after excitation are still unclear. This dissertation describes a study of the mechanistic organic chemistry occurring in the initial stages of the oxidative degradation of organic molecules at the surface of titanium dioxide photocatalysts. Specifically, the present studies focuses first on the effect of catalyst particle size on the degradation mechanism of organic molecules at various pH values. Also, organic molecules with well-defined oxidation chemistry are required in order to effectively study degradation mechanisms. Herein, work is described in which multiple probe molecules are characterized for use in this research, as well as work using a few of these molecules in the characterization of tungstated titanium dioxide nanoparticles.

1.2. Dissertation Organization

This dissertation is divided into five chapters. Chapter 1 is a general introduction to the subject of remediation and chemical oxidation of water pollutants. It explains the background information needed to understand the chemistry behind photocatalysis, with

titanium dioxide as the subject of interest. The properties of titania in terms of its ability to degrade organic molecules are discussed.

Chapter 2 describes the effects of titania particle size on the degradation of *para*-anisyl neopentanol (AN) and 4-methoxyresorcinol (MR). These two probe molecules provide well-studied degradation chemistry in order to ascertain the mechanism based on product ratios and kinetics. Nanometer scale titanium dioxide has shown the highest activity for the degradation of organic pollutants, but an optimum size has yet to be reached with the best charge carrier recombination to surface area ratio. To attain this, the Millennium PC catalyst series is studied and compared to a known catalyst, Degussa P25. The PC series are differentiated by size based on the extent of sintering performed. Each catalyst in the PC series is produced using the same procedure, with only the final sintering step varied by the amount of time spent annealing. This method produces catalysts that differ only by particle size and surface area, which can change other pertinent solid surface chemistry like defect formation.

Chapter 3 entails the study of the chemical degradation paths of AN and quinoline when a tungsten-modified titanium dioxide (WO_x-TiO_2) photocatalyst is employed. Tungstated titanium dioxide materials have recently been implicated for increased degradation efficiency and possible visible light absorption capabilities.[8] This work uses kinetic and product formation data to compare tungstated catalysts to pure titania catalysts at 350 and 419 nm irradiation. In this submitted manuscript, Timothy Hathway performed the AN degradation experiments and wrote the initial drafts of the paper. Erin Rockafellow performed the quinoline degradations and Youn-Chul Oh prepared the homemade tungstated catalysts.

Chapter 4 explores the reactivity differences between three similar biphenyl carboxylic acids. By slightly altering the placement of the carboxylic acid group and adding a hydroxy group, the electronic demand and adsorption capabilities of these compounds cause differences in the TiO_2 photocatalyzed degradation reactions of these compounds. Also, a simple method employing *ab initio* computations is proposed in the use of predicting major hydroxylation products of these biphenyl probes. This method is meant to be general to any functionalized aromatic compound.

1.3. Semiconductor Photocatalysis

Semiconductors used for the photocatalytic degradation of organic molecules are usually metal oxides or metal sulfides. The most commonly studied semiconductors include TiO_2, ZnO, WO_3, Fe_2O_3, and ZnS.[9] In searching for an ideal photocatalyst for remediation of organic molecules using sunlight, several factors must be taken into account; chief among them are oxidation potential and energy of the band gap. The oxidation potential is important, since the ability to form photogenerated valence band holes (h^+_{vb}) and to create hydroxyl radicals ($HO^•_{ads}$) in water is key to its use as a photocatalyst for the oxidation of organic molecules. This is also true of the reducing power of the excited conduction band electron (e^-_{cb}), which must be of sufficient energy to reduce molecular oxygen to superoxide.[6] These two chemical processes are the key to the photocatalysis of organic molecules to simple gaseous products (H_2O, CO_2) and inorganic ions (NO_3^-, SO_4^{2-}).

The energy of the band gap of the semiconductor defines the energy of light needed to excite an electron to the conduction band, which leaves a positively charged hole in the

valence band, h^+_{vb}.[10] If the required wavelength for a given semiconductor to form charge carriers is outside the range of the solar spectrum, then that semiconductor is of no use for the degradation of organics using sunlight without significant electronic modification. Titanium dioxide (TiO_2) has both a high oxidation potential and a band gap that allows for absorption of the UV portion of sunlight. Unfortunately, the UV portion makes up only about five percent of the solar emission spectrum.[7]

Despite the low solar absorbance, titania is considered the best choice for general photocatalytic needs as it fits other desirable criteria. TiO_2 is cheap, nontoxic, photolytically and chemically stable, and reusable with a high turnover rate. It is also simple to modify the chemical and physical characteristics of TiO_2, including absorption range and particle size, which can be considered the most important means of modification of titania's oxidation capabilities. Methods of electronic modification of TiO_2 to extend the band gap to higher wavelengths will be discussed later.

$$TiO_2 + h\nu \longrightarrow e^-_{cb} + h^+_{vb} \quad (1)$$

$$H_2O_{ads} + h^+_{vb} \longrightarrow HO^{\bullet}_{ads} + H^+ \quad (2)$$

$$O_2 + e^-_{cb} \longrightarrow O_2^{\bullet-} \quad (3)$$

$$O_2^{\bullet-} + H^+ \longrightarrow HO_2^{\bullet} \quad (4)$$

$$HO_2^{\bullet} + HO_2^{\bullet} \longrightarrow H_2O_2 + O_2 \quad (5)$$

$$H_2O_2 + e^-_{cb} \longrightarrow HO^{\bullet} + HO^- \quad (6)$$

$$D + h^+_{vb} \longrightarrow D^{\bullet+} \quad (7)$$

$$A + e^-_{cb} \longrightarrow A^{\bullet-} \quad (8)$$

$$e^-_{cb} + h^+_{vb} \longrightarrow TiO_2 + heat \quad (9)$$
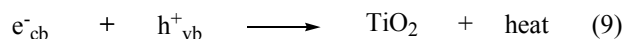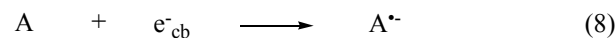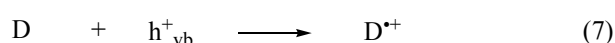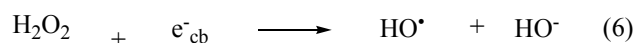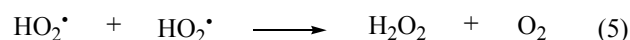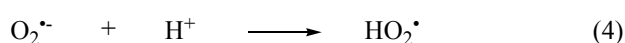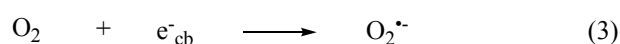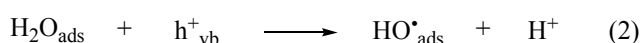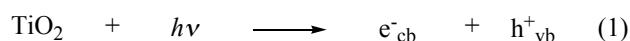
The chemical mechanism of titanium dioxide photocatalysis in water is shown in Equations 1-9. Figure 1 serves to show a pictorial representation of these processes. Equation 1 shows the initial reaction of titanium dioxide with light, producing a hole and an electron that act as the active excited species, which then react with water and oxygen as shown in equations 2-5. In aqueous conditions, Ti-OH groups are abundant and are the major source of hydroxyl radicals on the TiO_2 surface.[11] The downstream products of reactions with molecular oxygen are superoxide ($O_2{}^{\bullet-}$, Eq. 3) and often hydroxyl radical (HO$^\bullet$, Eq. 5), which can react with a nearby organic molecule. Equations 5 and 6 show the formation of hydrogen peroxide, which is known to split into two hydroxyl radicals through aqueous photolysis or to accept an electron as in equation 6.[12] The hole, h^+_{vb}, can also react directly with an adsorbed organic donor (**D**) as in equation 7. In systems where TiO_2 is used to reduce molecules, as in a dye-sensitized solar cell, **A** is the organic molecule and **D** (Eq. 7) is a hole trap.[13] Equation 8 describes the reduction of an adsorbed molecule by the conduction band hole. In this case, **A** is considered an adsorbed molecule that can accept electrons. Reductive titanium dioxide photocatalysis is less studied due to the lower reducing power of e^-_{cb} compared to the high oxidizing power of h^+_{vb}.[9] Finally, equation 9 describes the recombination of the two charge carriers that releases heat. This process is known to occur for approximately ninety percent of all charge carriers formed, and is thus the major reaction competing with all "useful" chemistry in this system.
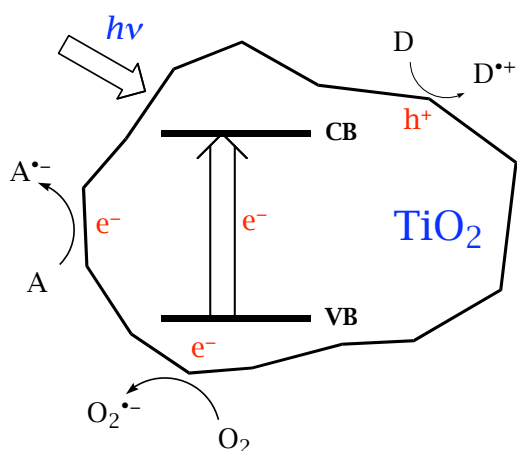
Figure 1. Pictorial view of TiO_2 excitation

A great deal of work has been carried out to understand surface recombination and many modifications of titania are based on reducing recombination.[14] The constant addition of an electron acceptor to a reaction is required; otherwise, Equation 9 becomes the primary surface reaction since the charge carriers are not physically separated. A common oxidant is molecular oxygen (Equation 8), which is added to titania reactions since it acts as a stoichiometric oxidant (Reaction 1).[3] Due to its high reduction potential and also the fact that the produced superoxide ion ($O_2^{\bullet-}$) reacts further to produce more hydroxyl radicals (Equations 3-5), O_2 makes an ideal trap for surface e_{cb}^-. O_2 is a better electron acceptor than most organic molecules studied in this chemistry; thus equation 3 becomes an important process in aqueous photocatalysis.

Titanium dioxide exists naturally in three crystalline phases: anatase, rutile, and brookite. Of the three, brookite is the only photochemically inactive one, and is unimportant in the field of photocatalysis from a reactivity standpoint. The synthesis of titanium dioxide from well-known precursors can result in the formation of brookite, but careful control of pH

and temperature will eliminate the brookite crystallization.[15] On this note, the synthesis of titanium dioxide at low temperatures can also yield an amorphous catalyst that has been studied recently for photocatalytic activity, but was found to be well below the activity of rutile and anatase in terms of degradation efficiency.[16]

Rutile was the first morphology to be studied in detail and thus much of the early experimental and theoretical work on TiO_2 was based on it.[17,18] Rutile is the more thermodynamically stable of the two photochemically active phases. Having a band gap energy of 3.0 eV (418 nm), rutile would seem more ideal than anatase (3.2 eV, 387 nm). As studies have shown, rutile is actually less effective then anatase in the degradation of many organic molecules.[7] This is likely due to the more tightly packed crystal structure in rutile, which has less defect sites in the bulk to trap photoexcited holes and electrons and thus reduce charge carrier recombination. Most of the research on remediation chemistry in the past few years has been performed on the anatase phase. Its high band gap energy leads to a higher reduction potential, which allows for the oxidation of less reactive organic materials, like substituted benzenes. This, however, has the disadvantage of shifting the absorption band of the anatase catalyst to the blue, which results in less sunlight absorption.

Modifications to the electronic structure of titanium dioxide in order to shift the absorption into the visible range are under intense study in the photocatalysis field. The most common types of alterations include pure titania modifications and doping with other elements or semiconductors. Pure titania variations involve changing the morphology and surface area (particle size). In terms of morphology, having both photoactive crystal phases present makes a large difference in photocatalytic activity. Degussa P25 is a catalyst that contains 80% anatase and 20% rutile prepared by high temperature sintering.[19] When

compared to the overwhelming majority of single-phase catalysts, P25 performs better in terms of degradation efficiency. This heightened photocatalytic activity has been attributed to the ability of excited electrons from the surface of anatase to become trapped in the lattice of the rutile phase, minimizing charge carrier recombination.[20]

The optimal particle size (and thus surface area) of titania has been studied by many groups over the years and affects both the amount of pollutants that can adsorb to the surface and the amount of charge carrier recombination that can occur, since recombination is a surface process.[21-23] Particle size considerations are discussed in further detail in chapter 2. In general, nanoscale titanium dioxide (1-100 nm) is considered the most active in the degradation of organic compounds, although many micrometer scale catalysts are available and moderately effective. For reference, P25 has been measured to have a particle size of 25-35 nm.[19]

Other morphological modifications include the coating of titanium dioxide onto the surfaces of polymers and silica of multiple sizes and shapes for use in realistic water and air treatment (as opposed to laboratory research). In addition, mesoporous TiO_2 and zeolites embedded with titania have been employed in efforts to dramatically increase surface area and allow for selective oxidations (i.e. chemical synthesis applications).[24]

The doping of titanium dioxide is a quickly progressing field where all manner of metals, non-metals, and other metal oxides have been coated onto or co-produced with titania crystallites in the interest of improving visible light absorption and/or decreasing recombination. One of the first and most successful doping strategies is the deposition of noble metals (like Pt or Au) onto the titanium dioxide surface, with the goal of splitting water into H_2 and O_2, which cannot be performed on naked TiO_2. When small (~2 nm) particles of

Pt are deposited on the titania surface, an increase in the production of H_2 from adsorbed water molecules is observed.[7,25] This is due to the movement of electrons from the TiO_2 surface to the metal, which reduces the H_2O to H_2. In most cases, the deposition of noble metals is used for H_2 production as opposed to water purification. It should also be noted that the photoactivity of the rutile phase is greatly increased (for H_2 production) by the deposition of noble metals, especially platinum.[16] Unfortunately, noble metals are too expensive to utilize on a large scale. The use of transition metals, including Fe and Cr, as dopants has been tested, but in many cases these metals act as electron and hole traps, and adversely increase the recombination rate instead of lowering it.[14]

Titania has also been prepared as a homogenous mixture with other metal oxides, including SnO_2 and WO_3.[26] Tungstate doping in particular has been shown to shift the band gap of TiO_2 closer to the visible spectrum (2.86 eV vs. 3.21 eV for pure anatase).[27] This result is highly encouraging, as mentioned before, since increasing the sunlight absorption is one of the major goals of titania research. Increased degradative ability (i.e. rate of oxidation of organic molecules) is also reported for many of these catalysts compared to pure anatase and P25. This has been attributed to both increased surface acidity[28] of the mixed catalyst surface, as well as charge carrier trapping,[29] much like noble metal doping. Tungstated titania catalysts are investigated in depth in chapter 3.

The most recent form of titania doping employs main group elements, especially C, S, and N. These elements substitute for O or Ti atoms in the titania lattice and introduce mid-gap levels in the electronic band structure where lower energy (and thus longer wavelength) excitations could occur, thus extending the band gap into the visible region, much like the case of tungstate doping.[14,27]

1.4. Degradation of Organic Molecules with TiO_2

Reaction 1 shows the most general degradation of organic compounds with titanium dioxide. Much of the oxidative chemistry of titania is attributed to the action of highly oxidizing species like surface-adsorbed hydroxyl radical, $HO^{\bullet}_{ads}$, which are formed *in situ* in aqueous photolyses of titania. The mechanism of organic pollutant degradation is highly dependent on reaction conditions and the structure of the organic molecule. For the most part, the titania surface acts as an adsorption center for organic molecules, which can bind to it specifically or onto an ad-layer of water molecules within a few angstroms of the surface. From here, the molecule is oxidized, either by direct single electron transfer or by addition of surface-adsorbed hydroxyl radicals. After this, a cascade of radical reactions and hydrolyses ensue leading ultimately to CO_2 and H_2O. In a few isolated cases, recalcitrant species are formed that cannot be degraded further by TiO_2 alone, which will be expanded upon below.[3,30]

To give a more specific example of the mechanism of degradation, the case of 4-chlorophenol (4CP) will be discussed. 4CP has been used extensively in mechanistic research as a model for a halogenated aromatic molecule.[31,32] This class of molecules is ubiquitous in terms of being found in polluted waters of many sources. In particular, 4CP has a set of photocatalytic products that can be confidently assigned to the action of certain oxidative processes. These include hydroxylation of the aromatic ring either directly or by *ipso* substitution of the chlorine, both of which are attributed to $HO^{\bullet}_{ads}$ chemistry.[31,32]

The other major process in the degradation of 4CP is opening of the aromatic ring,

which is attributed to chemistry initiated by direct electron transfer from the aromatic ring to the titania surface.[33] This type of single electron transfer (SET) to the titania surface is thought to occur alongside hydroxyl radical chemistry, although due to the requirement of specific binding (for efficient electron transfer), it can be largely disfavored in the degradation of some molecules. In the case of phenols and especially catechols (1,2-benzenediols), SET chemistry manifests itself through the formation of ring-opened products where molecular oxygen has attacked the adsorbed molecule and two carboxylic acid groups are formed through a proposed dioxetane intermediate.[32] This matter will be discussed in detail in chapter 2.

It has been stated multiple times that titania degrades almost any compound that it comes into contact with. However, there are exceptions, most notably cyanuric acid (Figure 2), which is the ultimate degradation product of a wide variety of triazines.[34,35] In a recent paper by the Hidaka group, cyanuric acid was found to degrade completely to inorganic products using titanium dioxide, but only through the addition of additional oxidants (O_3 and H_2O_2).[30] Although compounds like triazines are isolated cases, the phenomenon of incomplete degradation is very important as it can lead to insights into the chemical mechanisms governing the degradation of the molecules themselves, not to mention the prevalent processes on a given titania surface. Equations 1-9 only show the initial processes of aqueous phase degradations without going into any detail about the degradation of the chemicals themselves. By looking at the early products of degradation, and thus the early reaction steps, mechanistic insight can be gained, which can help lead to a greater understanding of how to improve the efficiency of the catalysts as a whole. The rest of this dissertation describes work in pursuing these chemical concerns.
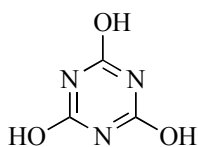
Figure 2. Cyanuric acid

1.6. References

(1)   Lorch, W. *Handbook of Water Purification*; Second ed.; Ellis Horword: Chichester, 1987.

(2)   Management, Office of Waste Water; United States Environmental Protection Agency: 1998.

(3)   Hoffmann, M. R.; Martin, S. T.; Choi, W.; Bahnemann, D. W. *Chem. Rev.* **1995**, *95*, 69-96.

(4)   Huling, S. G.; Pivetz, B. E.; United States Environmental Protection Agency: 2006.

(5)   Legrini, O.; Oliveros, E.; Braun, A. M. *Chem. Rev.* **1993**, *93*, 671-698.

(6)   Halmann, M. M. *Photodegradation of Water Pollutants*; CRC Press: New York, 1996.

(7)   Linsebigler, A. L.; Lu, G.; Yates Jr., J. T. *Chem. Rev.* **1995**, *95*, 735-758.

(8)   Li, X. Z.; Li, F. B.; Yang, C. L.; Ge, W. K. *J. Photochem. Photobiol. A* **2001**, *141*, 209-217.

(9)   Fox, M. A. *Chem. Rev.* **1993**, *93*, 341-357.

(10)   Oppenländer, T. *Photochemical Purification of Water and Air*; Wiley-VCH: London, 2003.

(11)   Murakami, Y.; Kenji, E.; Nosaka, A. Y.; Nosaka, Y. *J. Phys. Chem. B* **2006**, *108*, 8751-8755.

(12)   Turro, N. J. *Modern Molecular Photochemistry*; University Science Books: Sausalito, California, 1991.

(13)   O'Regan, B.; Grätzel, M. *Nature* **1991**, *353*, 737-740.

(14)   Thompson, T. L.; Yates, J. T. *Chem. Rev.* **2006**, *106*, 4428-4453.

(15)   Isley, S. L.; Penn, R. L. *J. Phys. Chem. B* **2006**, *110*, 15134-15139.

(16)   Zhang, Z.; Maggard, P. A. *J. Photochem. Photobiol. A* **2007**, *186*, 8-13.

(17)   Bakaev, V. A.; Steele, W. A. *Langmuir* **1992**, *8*, 1372-1378.

(18)   Ghosh, A. K.; Wakim, F. G.; Addiss Jr, R. R. *Phys. Rev.* **1969**, *184*, 979-988.

(19)   Tahiri, H.; Serpone, N.; Le van Mao, R. *J. Photochem. Photobiol. A* **1996**, *93*, 199-203.

(20)   Hurum, D. C.; Gray, K. A. *J. Phys. Chem. B* **2005**, *109*, 977-980.

(21)   Serpone, N.; Lawless, D.; Khairutdinov, R.; Pelizzetti, E. *J. Phys. Chem.* **1995**, *99*, 16655-16661.

(22)   Calza, P.; Pelizzetti, E.; Mogyorósi, K.; Kun, R.; Dékány, I. *Appl. Catal. B* **2007**, *72*, 314-321.

(23)   Zhang, Z.; Wang, C.-C.; Zakaria, R.; Ying, J. Y. *J. Phys. Chem. B* **1998**, *102*, 10871-10878.

(24)   Shiraishi, Y.; Saito, N.; Hirai, T. *J. Am. Chem. Soc.* **2005**, *127*, 12820-12822.

(25)   Emilio, C. A.; Litter, M. I.; Kunst, M.; Bouchard, M.; Colbeauu-Justin, C. *Langmuir* **2006**, *22*, 3606-3613.

(26)   Wu, Q.; Li, D.; Chen, Z.; Fu, X. *Photochem. Photobiol. Sci.* **2006**, *5*, 653-655.

(27)   Song, H.; Jiang, H.; Liu, X.; Meng, G. *J. Photochem. Photobiol. A* **2006**, *181*, 421-428.

(28)   Engweiler, J.; Harf, J.; Balker, A. *J. Catal.* **1995**, *159*, 259-269.

(29)   Do, Y. R.; Lee, W.; Dwight, K.; Wold, A. *J. Solid State Chem.* **1994**, *108*, 198-201.

(30)   Yanagisawa, I.; Oyama, T.; Serpone, N.; Hidaka, H. *J. Phys. Chem. C* **2008**, *112*, 18125-18133.

(31)   Li, X.; Cubbage, J. W.; Tetzlaff, T. A.; Jenks, W. S. *J. Org. Chem.* **1999**, *64*, 8509-8524.

(32)   Li, X.; Cubbage, J. W.; Jenks, W. S. *J. Org. Chem.* **1999**, *64*, 8525-8536.

(33)   Bouquet-Somrani, C.; Finiels, A.; Graffin, P.; Olivé, J.-L. *Appl. Catal. B*

1996, *8*, 101-106.

(34)   Oh, Y.-C.; Jenks, W. S. *J. Photochem. Photobiol. A* **2004**, *162*, 323-328.

(35)   Watanabe, N.; Horikoshi, S.; Hidaka, H.; Serpone, N. *J. Photochem. Photobiol. A* **2005**, *174*, 229-238.

Chapter 2

Effects of sintering of TiO$_2$ particles on the mechanisms of photocatalytic degradation or organic molecules in water

Timothy Hathway and William S. Jenks

Abstract

Partial degradations of 4-methoxyresorcinol and *p*-anisyl 1-neopentyl alcohol were carried out with the PC series of photocatalysts from Millenium chemicals and with Degussa P25. The PC series of anatase catalysts varies only in the degree of sintering, and thus particle size and type of crystal defects. The initial product distributions were not substantially sensitive to catalyst, implying that none of the major products depended on particular binding sites that could be annealed away. Rate constants varied from catalyst to catalyst, but not dramatically, on a weight-to-volume basis. Thus there was also not a direct connection between available surface area and the rate of degradation. The product distribution as a function of suspension pH is also discussed.

1.0   Introduction

Titanium dioxide has been given considerable attention as a degradative photocatalyst in both air and water due to its exceptional ability to decompose organic molecules having a multitude of functionalities [1-4]. Despite the enormous potential of this method, there are two major limiting factors: the lack of absorption of significant portions of the visible spectrum (meaning that solar irradiation is used inefficiently), and a low efficiency of photons that are absorbed. At least in part due to these limitations, photocatalytic degradation of organic compounds in water currently remains in limited use. Research on extending the useful range of light absorption by the catalysts is extremely active, but beyond the scope of this paper. Instead, we now focus on how the properties of a set of closely related catalysts affect the efficiency and chemistry induced by the catalysts. Our approach is to use the well-established chemistry of certain organic probe molecules to report on the effects of the structural variation of the catalyst. Because "home made" catalysts are subject to subtle reproducibility issues, we take this approach first with a series of commercially available catalysts: the PC series of materials from Millenium Chemicals. Surface area and defect concentration are the largest variables within this series. Recent work by Nowotny points out explicitly, in trying to understand the effects of defects in both undoped and doped TiO_2-based photocatalysts [5], that detailed characterization of defect type is critical to predicting defect behavior. In the absence of atomic-scale understanding of the defect structure, a strong implication for reproducible results is that comparisons of such effects are

best carried out with a standard set of materials whose members are subject to minimal processing differences and are widely available.

The catalysts in the Millennium PC series all derive from PC 500, which is an anatase TiO_2 catalyst with 5-10 nm particle size. Its name correlates with the approximate surface area of the material, as seen in Table 1. The rest of the catalysts in the series are produced by sintering PC500, causing larger particles to be formed and greater crystallinity within the particles. We also include the industry standard Degussa P25 catalyst in our experiments, for comparison.

Table 1. Physical Characteristics of TiO_2 Photocatalysts

Catalyst	Surface area (BET)	Average Particle
	m^2/g	Size, nm
PC 10	11	75
PC 50	50	25
PC 100	87	20
PC 500	335	8
P25	55	35

In optimizing the conditions for degradation, it has been shown multiple times that the recombination of the two charge carriers, electrons (e^-) and holes (h^+), is the major cause of low degradation efficiency in titania [6]. Simply put, electron-hole recombination competes with the ability of the holes either to directly oxidize organic species or to cause hydroxyl-radical-like chemistry.

Sintering affects these dynamics. The greater particle size induced by sintering stems

from the merging of smaller particles and crystal annealing. This lowers the number of large-scale surface defects (boundaries, shear planes, etc.) and some small-scale defects (islands, vacancies, etc.). Reduction in defects in turn increases the h^+ lifetimes by slowing recombination. Thus, the fraction of h^+ that achieves useful chemistry should increase. At the same time, sintering can increase surface electron trapping sites (Ti^{3+} centers and oxygen vacancies) [6]. Such centers can increase the average charge separation distance if they are in the bulk of the crystal by localizing e^-, but surface traps can again induce recombination. The latter effect is ameliorated by electron scavengers like O_2. Additionally, O_2 can help lead to surface hydroxyl formation on anatase [7-9]. In short, it is probably an oversimplification to say that sintering universally reduces the number of defect sites, but it is generally accepted that it minimizes the types of defect sites that are most damaging to photonic efficiency in the process of particle merger and crystal annealing [6,10,11].

Table 1 shows the effects of sintering PC 500 on the average particle size, which is of the order of 10 mm diameter in the originally prepared material. On the assumption that the rate of a given photocatalytic degradation step is affected by photon flux, available surface for adsorption, and the efficiency of recombination, sintering should lead to opposite-trending effects: slowing down the observed rate because of lower surface area, and raising the observed rate because of fewer recombination sites. Indeed, Pichat has carried out experiments testing just these ideas using several probes and identified varying trends, depending on the substrate [12-14]. Here, we expand on this notion by exploring the type of reactivity observed in addition to the simple rates. The essential hypothesis to test is whether the reduced number of "defects" also affects the type of chemistry (single-electron-transfer based or hydroxyl-like), i.e., whether surface defects (steps, vacancies, etc.) represent sites

for preferred types of photocatalytic reactions, in addition to being traps for recombination. We use the previously studied compounds methoxyresorcinol (**MR**) [15] and 1-*p*-anisyl neopentanol (**AN**) [16] to carry this out.

MR   **AN**
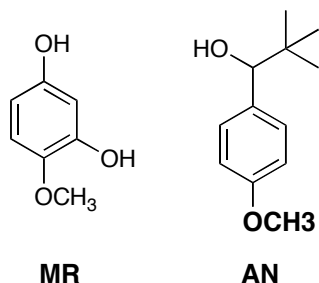
2.0   Experimental

2.1   Materials

All chemicals were obtained from Fisher or Aldrich in the highest purity available and used as received. 4-Methoxyrescorinol (4-methoxybenzene-1,3-diol, **MR**) [17] and *para*-anisyl-1-neopentanol (**AN**) [18,19] were prepared by reported methods. *p*-Anisyl *t*-butyl ketone (**8**) was prepared as described by Smyth [19] and reduced with NaBH$_4$ to produce **AN** [16]. Compounds **9**, **10**, and **11** were commercially available, and compounds obtained from degradation of **MR** were obtained as previously described [15].

p-Hydroxyphenyl *t*-butyl ketone (**12**) was prepared by demethylation of **8** with thiophenol [20]. Yield 16%, unoptimized. ^{1}H-NMR (CDCl$_3$, 300 MHz) δ 1.35 (s, 9H), 6.82 (d, J = 9 Hz, 2H), 7.79 (d, J = 9 Hz, 2H); ^{13}C-NMR (CDCl$_3$, 300 MHz) δ 28, 44, 115, 129, 131, 160, 208; MS (*m/z*) 178 (M$^+$), 121 (100), 95, 77, 65. MS (*m/z*) 178 (M$^+$), 121, 95, 77,

65.

1-*p*-Hydroxyphenyl-1-neopentyl alcohol (6) was prepared by reduction of **12**.
Methanol (10 mL) was charged with 1 mmol ketone and stirred while cooling in an ice bath.
$NaBH_4$ (3 mmol) was slowly added and solution was allowed to warm to room temperature.
The mixture was then heated to 70°C for 5 minutes and allowed to cool to room temperature,
followed by quenching with 10 mL ice water. The mixture was evaporated under reduced
pressure to remove methanol, then extracted with 3 x 15 mL Et_2O, washed with 30 mL brine,
and dried over Na_2SO_4. The solvent was evaporated under reduced pressure and the crude
solid product was collected without further purification. ^{1}H-NMR ($CDCl_3$, 300 MHz) δ 0.88
(s, 9H) 4.33 (d, J = 3 Hz, 1H), 4.72 (s, 1 H), 6.76 (d, J = 8 Hz, 2H), 7.16 (d, J = 8 Hz, 2H);
^{13}C-NMR (CD_3OD, 300 MHz) δ 29, 39, 86, 118, 133, 137, 166; MS (*m/z*) 180 (M$^+$), 123
(100), 95, 77, 65.MS (*m/z*) 180 (M$^+$), 123, 95, 77, 65.

The water had a resistivity of $\geq$ 18 MΩ cm^{-1}. Titania samples were the PC series
from Millenium Chemical and P25 from Degussa.

2.2   *Suspensions and Photolyses*

The standard suspensions for photocatalytic reactions were prepared to result in 100
mg TiO_2 per 100 mL deionized water. A stock 10x TiO_2 suspension was added to
approximately 80 mL water. Sonication for five minutes was used to break up larger
aggregates of TiO_2. As noted, the pH was either not adjusted or set to 2.0 (0.01 M HCl), 8.5
$\pm$ 0.5 (0.1 M NaOH added during the reaction as needed), or 12.0 (0.01 M NaOH).
Unadjusted suspensions had an initial pH of 4.5-5.5, depending on the catalyst. A stock 10x

aqueous solution of the organic material was added to bring the final organic concentration to 0.3 - 1.0 mM, and the total volume was brought to 100 mL as necessary with water. The mixture was then purged with O_2 and stirred for 20 minutes in the dark before the irradiation was started. Both stirring and O_2 purging were continued throughout the reaction. Except as noted, all degradation product identities were confirmed by comparison to authentic samples.

Photocatalytic degradations were carried out with stirring at ambient temperature using a modified Rayonet mini-reactor equipped with a fan and 4-watt broadly-emitting 350 nm "black light" fluorescent tubes. The number of bulbs ranged from two to eight depending on the desired reaction rate. Ferrioxalate actinometry [21,22] was performed to allow semiquantitative comparison of data obtained from reactions using different numbers of bulbs. Reaction times were dependent on the degree of degradation required.

After appropriate irradiation times, samples were removed and acidified with Amberlite IR-120 ion exchange resin. The TiO_2 was separated by centrifugation, followed by filtration through a syringe-mounted 0.2 μm PES filter. Sample sizes were 1 mL for kinetics or 50 mL for product studies. The latter, larger samples were concentrated by rotary evaporation to approximately 2 mL and the residual water was removed by lyophilization.

Dried samples deriving from methoxyresorcinol were exhaustively silylated by treatment with 1 mL anhydrous pyridine, 0.2 mL of 1,1,1,3,3,3-hexamethyldisilazane (HMDS) and 0.1 mL of chlorotrimethylsilane [23]. Samples were vigorously shaken for 1 min, and allowed to stand 5 min at ambient temperature. The resulting pyridinium chloride precipitate was separated by centrifugation prior to chromatographic analysis. Sample deriving from anisyl neopentanol were dissolved in 0.50 mL of a stock solution of methanol containing a known concentration of dodecane as an internal standard and used directly for

chromatographic analysis.

GC-MS work was done with a standard 25 m DB-5 (5% phenyl) column for chromatography, coupled to a time-of-flight mass spectral dedector. The temperature program was 130 ˚C for two minutes, followed by a ramp to 280 ˚C at 20 ˚C/min. Routine work was done on another instrument with an FID detector.

Kinetic data were obtained using HPLC (diode array UV/Vis detection) analysis of 1 mL aliquots that were acidified and centrifuged before injection. A standard C18 reverse-phase column was used. Eluents were 3:7 (v/v) water:acetonitrile for **AN**-derived reactions and 4:1 v/v mixture of a water and methanol that contained 0.15% acetic acid for the **MR** runs. Flow was 1.0 mL/min.

2.3   Adsorption

Adsorption equilibrium measurements of **MR** and **AN** on P25 TiO_2 were obtained. Suspensions were prepared from 20 mL buffer containing 50 mg TiO_2. The pH was held at 2.0, 7.0, 8.5, and 12.0 using 10 mM phosphate buffer. Unbuffered pH was also used. After allowing the desired contact time, an aliquot was removed, centrifuged and filtered (as above) to remove TiO_2. The residual concentrations were determined by HPLC. Kinetic study showed that the extent of adsorption reached a constant value after no more than 2 h for both compounds. For the quantitative adsorption experiments, at least 20 h equilibration was allowed before measurement.

3.0   Results

Two probe molecules, **MR** and **AN**, were used to examine the series of catalysts for
initial rates of decomposition and for product distributions at low conversion. Both **MR** and
AN have previously been documented to show products characteristic of both reactivity
attributable to hydroxyl radical-type chemistry (hereafter referred to as HO•$_{ads}$) and single
electron transfer (SET) chemistry [15,16].   Proposed mechanisms for these reactions are
discussed in these references. **MR** was chosen from among a series of
hydroxylated/methoxylated benzenes because it showed both the HO•$_{ads}$ chemistry
(hydroxylation and demethylation) and SET chemistry (ring opening), and would thus be a
more sensitive reporter molecule than the corresponding trimethoxy- or trihydroxybenzenes,
which gave exclusively HO•$_{ads}$ or SET chemistry, respectively, with P25 [15]. These
products are illustrated in Scheme 1, along with some additional products that clearly show
multiple reaction steps. Because we know that 1,2,4-benzenetriol produces almost
exclusively ring-opened products [24], we can attribute these secondary hydroxylated and
opened products to hydroxylation-first, rather than ring-opening-first sequences. After ring
opening, subsequent oxidations result in compounds that are easily distinguished as being
further downstream by the smaller number of carbon atoms (and hence mass).

AN is expected to have a different binding motif than **MR**, and also shows different
SET chemistry, namely loss of the *t*-butyl group and oxidation to the corresponding
aldehyde, as illustrated in Scheme 1 [16]. These were established by analogy to results with
homogeneous solution-phase SET reagents [25]. Also illustrated are secondary degradation
products, but in this case, it is not as obvious in which order the chemistry occurs.

Scheme 1.
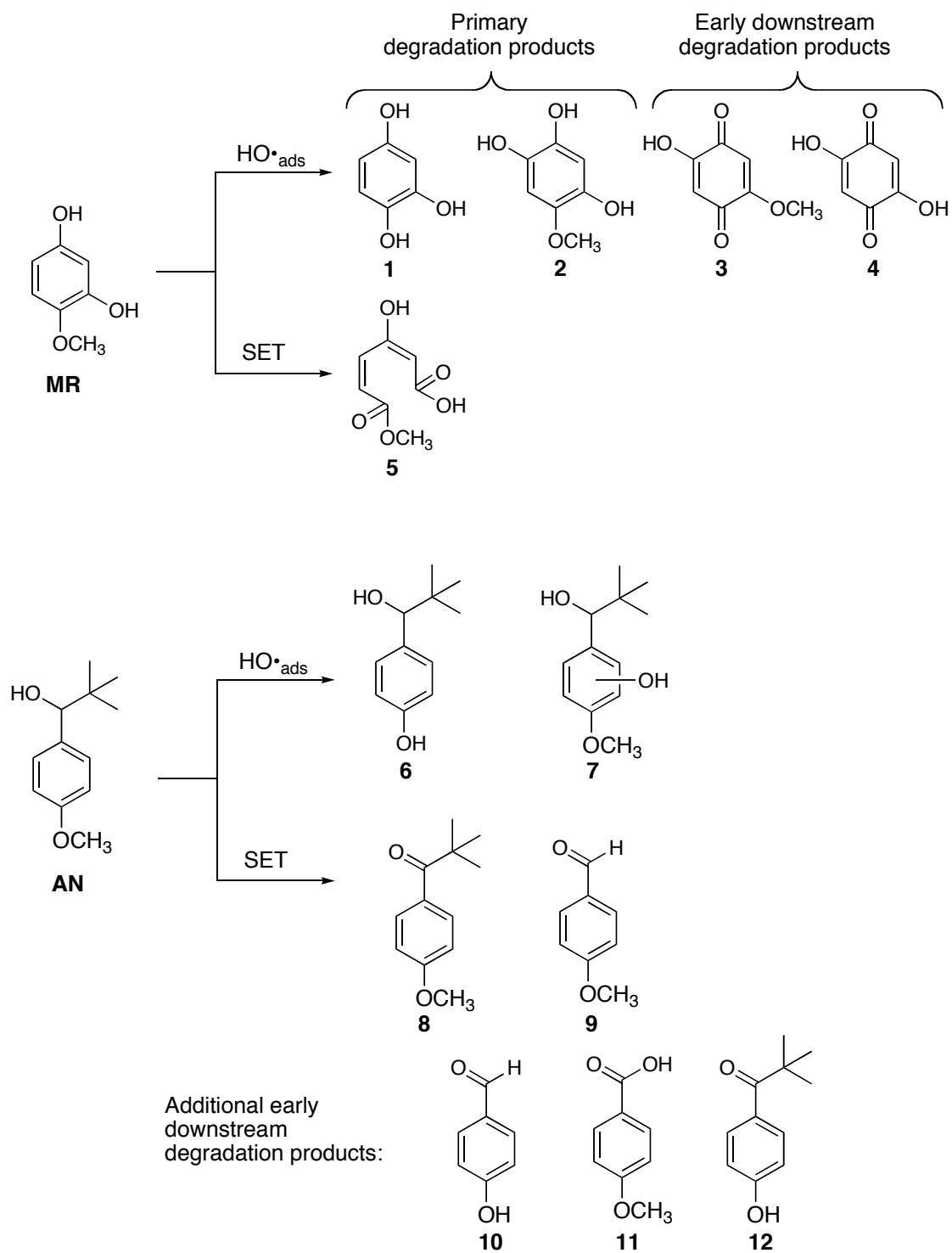
Ideally, the reactions used to determine product distribution are carried out to very low conversion in order to get the best representation of initial products. Degradation of the early intermediates can be very competitive with or faster than that of the starting material. We presume this is because of the more highly oxidized functionality is more adherent to the catalyst, thermodynamically easier to oxidize (e.g., by SET), or both. (The lack of any observed intermediates while degradation is taking place is indicative of this in the extreme limit.) The counterbalance to this desire for low conversion is simply having enough material to characterize. Our experience is that conversion of about 20% of the original material is a good starting point to look for intermediates at reasonable concentrations.

3.1   *Adsorption*

Dark adsorption isotherms for **MR** and **AN** were obtained using P25 at 2.5 g/L. Though the relationship between dark adsorption and the rate of degradation of compounds is certainly not direct, certain functional groups may exhibit different types of binding under different conditions (e.g., pH), which can result in different interactions with the catalyst surface, and potentially differing reactivity.

Figure 1 illustrates dark adsorption isotherms for (a) **MR** and (b) **AN**, obtained at different pH values. It was found that **MR** is not stable in highly basic aqueous solutions so isotherms were obtained at pH 2.0, 7.0, and 8.5. The smooth curve is a least squares fit from the Langmuir-Hinshelwood model (eq 1), where the ordinate is the amount adsorbed per gram of catalyst n_{ads}, the abscissa is the equilibrium dissolved concentration of the organic compound (C_{eq}), and K_L is the adsorption equilibrium constant.

$$n_{ads} = \frac{n_{ads(\max)}K_L C_{eq}}{1 + K_L C_{eq}} \qquad (1)$$

The curves show a higher capacity of binding (saturation) at low pH for **MR**. For **AN**, he data are not as clear, and unfortunately cannot be made much better because 250 μM is nearing the limiting solubility point. Linearization by inversion of equation 1 [26] and fitting the data result in capacities and binding constants given in Table 2. The errors are taken as standard errors of the linear fit propagated through the equations. Despite the variation in the binding constants and adsorption capacities, these data and eq 1 can be used to show that all of the degradation experiments were carried out under conditions where the catalyst is saturated, yet only a relatively small fraction of the **MR** or **AN** is bound to the catalyst surface at any given moment [27].

Table 2. Adsorption isotherm data for MR an AN in the presence of 2.5 g/L P25 TiO$_2$.

Probe molecule	pH	Adsorption capacity, μmol/g (n$_{ads, max}$)	Adsorption capacity, molecules/nm^2	Binding constant (K$_L$, mM^{-1})
MR	2	14.2 ± 0.2	0.156 ± 0.002	205 ± 20
	7.0	8.3 ± 0.6	0.091 ± 0.007	66 ± 15
	8.5	18 ± 2	0.20 ± 0.02	19 ± 2
AN	2	25 ± 5	0.28 ± 0.06	28 ± 22
	5	41 ± 7	0.45 ± 0.08	9 ± 2
	8.5	35 ± 11	0.39 ± 0.12	6 ± 2
	12	25 ± 4	0.28 ± 0.04	16 ± 16

Figure 1. Adsorption isotherms for P25 and (a) **MR** and (b) **AN**.
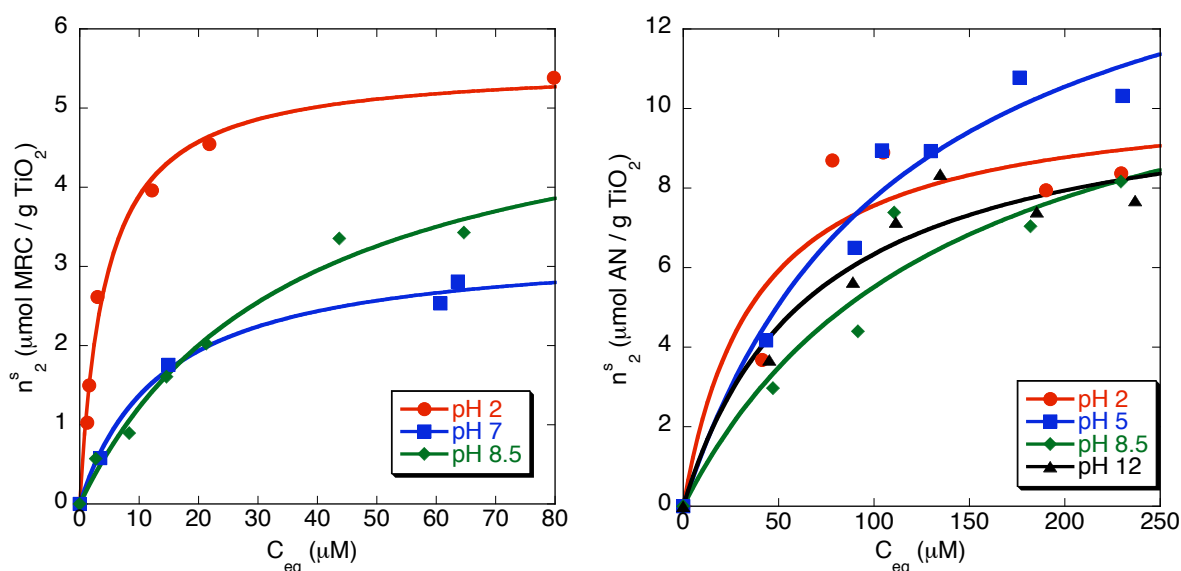
MR, which has easily deprotonated phenolic sites, shows a fairly dramatic change in binding constant with pH. It is well known that carboxylic acids also are stronger binders to TiO_2 at low pH; we take this to be an example of an analogous phenomenon.

By contrast, the binding constants measured for **AN** (which are subject to considerably larger error) were arguably invariant to pH, and certainly do not show a clear trend as do those for **MR**. Though the charge on the TiO_2 surface clearly still varies with pH (its pI being routinely quoted from 4-6, depending on material), the hindered alcohol in **AN** undoubtedly has a pK_a outside the range examined here, probably in the range of 16-18.

3.2   *Initial Degradation Kinetics*

Photocatalytic degradation usually follows apparent first order kinetics. However, the initial kinetics (e.g., to 20-30%) can be reasonably approximated to the more traditional zero-

order kinetics for photochemical reactions. Either approach can be valid, depending on the range of interest. Since we were interested in the initial chemistry, we obtained zero-order rate constants for the early-phase degradation of both probe molecules with the variety of catalysts at several pH values. These are given in Table 3. The absolute rate constants, obtained with initial concentrations of 0.3 mM (**MR**) or 2.0 mM (**AN**) depend on lamp intensity, sample geometry, and so on. However, all these parameters are held constant for the series, so the relative values are meaningful.

All samples were prepared with the same density of catalyst on a weight-to-volume basis. Analyzing the data in this way, the catalyst-to-catalyst variation in rate is not large. Unbuffered PC 500 was slower than the rest for both probe molecules, but otherwise, most rates are within a factor of 3 of one another. At low pH, it is possible that the degradation of **MR** is being artificially lowered by the presence of chloride ions, perhaps by a factor of two, as documented for benzoic acid derivatives [28,29]. However, this does not account for the full variability of the rate, nor for the results with **AN** (below).

Considering the rates as a function of catalyst surface area gives an alternate picture. (Remember that the names of the PC series correspond approximately to the BET surface area in m^2/g. The surface area of P25 is about the same as PC 50.) Notably P25 and PC 50 have fairly similar rates when expressed this way, but it is the larger particles that have the highest rates per surface area on the whole.

Table 3. Initial rates of loss of MR and AN with equal mass catalyst.

Compound	Catalyst	Degradation rate [c]			
		Absolute rate, $\mu M/min^{-1}$ and			
		(Rate normalized for catalyst surface area, nM g/m^2 g)			
		pH 2	Unbuffered[d]	pH 8.5	pH 12
MR[a]	PC 10	1.0	0.6	22	[d]
		(94)	(53)	(2000)	
	PC 50	1.0	1.0	36	
		(20)	(20)	(774)	
	PC 100	0.9	1.1	48	
		(10)	(13)	(554)	
	PC 500	0.3	0.04	12	
		(1)	(<1)	(56)	
	P25	1.2	1.0	28	
		(22)	(18)	(502)	
AN[b]	PC 10	7	13	9	10
		(650)	(1200)	(850)	(900)
	PC 50	16	12	14	16
		(320)	(240)	(270)	(330)
	PC 100	24	6	11	9
		(280)	(73)	(120)	(100)
	PC 500	12	4	5	7
		(36)	(11)	(16)	(20)
	P25	30	30	9	19
		(550)	(540)	(160)	(340)

[a] Initial concentration 0.30 mM. Rates at pH 2 and unbuffered pH were obtained with higher lamp intensity and normalized to the other rate constants by means of ferrioxalate actinometry. [b] Initial concentration 2.0 mM. [c] Standard errors of fits from linear plots were almost all approximately 10% or less. [e] pH approximately 5.0 ± 0.5 [e] Not measured due to base hydrolysis.

The initial degradation rates were sensitive to pH, particularly for **MR**. The rate of degradation was greatest at pH 8.5, which is also the pH at which the most intermediates are generally observed for molecules of this type [15,24]; this may be because ~8.5 is the pH at which the relative rate of degradation of **MR** is greatest, relative to the downstream intermediates, causing their apparent accumulation. No reliable data are available at pH 12 due to decomposition of **MR** in the dark.

For **AN**, there was considerably less pH sensitivity for PC 10 and PC 50, the most annealed catalysts. For the original catalyst PC 500 and for PC 100, there was a somewhat larger variation: a factor of 2-3 across the pH spectrum with the low rates being the unbuffered case. For P25, the minimum degradation rate was observed at pH 8.5, but it was still within a factor of 3 of the fastest degradations. The initial pH of the unbuffered suspensions was 4.5-5.5, depending on the catalyst.

3.3   *Product distributions*

3.3.1   MR degradations
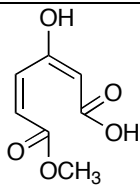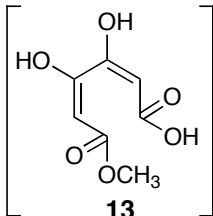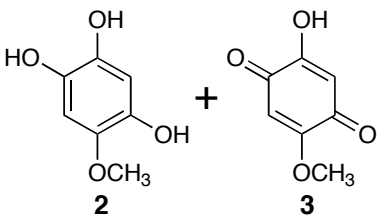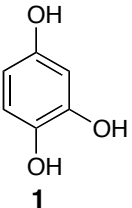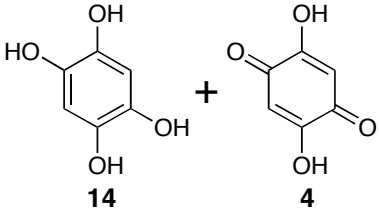
Degradations were carried out at several pH and catalyst combinations. The product distributions obtained using PC 100 are shown in Table 4. As in our previous work [15], the intermediates were silylated before separation and identification by GC-MS. The tabulation is given in order of short to long retention time of the silylated derivatives by GC. The compounds are illustrated in their form before silylation, and are also drawn as the most obvious tautomer, e.g., **5**. In addition to the compounds illustrated in Table 1, another multiply reacted compound, **13**, was observed. Very qualitative observations on the

intensities of the GC peaks are given in the Table, with the largest peaks being a few percent of that of the remaining starting material. Note that pairs of hydroquinones and quinones are given as a single compound, as they are interchangeable by trivial air oxidation or by reduction by TiO_2 [30]. Very small quantities of 3-5 carbon compounds were also observed, indicating that some intermediates were undergoing successive decomposition steps even at fairly low conversion.

The results in Table 4 were obtained with PC100, but they are representative of all the other catalysts tested, including P25; qualitatively identical distributions were obtained at equal conversion of the starting material. Compounds **1**, **2**, **3**, **4**, **5**, and **14** were identified as their silylated derivatives, as previously described [15,24]. Compound **13** is shown in brackets because its structure is only tentative; in fact it is most likely a combination of two or more isomeric structures where **MR** has been hydroxylated twice and the ring opened. The suggestion that it is a mixture comes from the observation that the GC peak was always broad, relative to the others.

The formula and proposed structural assignment is done by analogy to compounds **48** and **51** from Li, et al. [15]. These compounds differ by m/z=88, i.e., a $(CH_3)_3SiO$ substitution as do **13** and **5**. Characteristic losses of CH_3, $CO_2Si(CH_3)_3$, and CO_2CH_3 are noted for each compound. The retention time of **13** was the longest of any of these, also consistent with a more substituted compound.

Table 4. Products observed on photocatalytic degradation of MR using PC100

Compound[a]	Abundance			
	pH 2	pH 5.5[b] (Unbuffered)	pH 8.5	pH 12
5 (OH, O, OH, O, OCH₃)	–	–	low	med
13 [OH, HO, O, OH, O, OCH₃]	–	–	med	high
2 (OH, HO, OH, OCH₃) + **3** (OH, O, O, OCH₃)	low	med	high	–
1 (OH, OH, OH)	med	med	–	–
14 (OH, HO, OH, OH) + **4** (OH, O, O, OH)	–	–	high	high

[a] Compounds are listed in order of GC elution. [b] The initial pH of the unbuffered solution was 5.5 using PC 100 and dropped about 1 pH unit through the photolysis. The pH of the unbuffered solution varied slightly from catalyst to catalyst.

Clearly, multiple steps are required to get to structure **13**. We presume that hydroxylation to **2** is the first step, i.e., MR → **2** →→ **13**. After **2**, the path is more uncertain, and multiple regioisomers are obtained. We speculate that another hydroxylation follows, and ring opening is the third step. The position of the ring opening also could also provide multiple isomers. Again, we speculate that cleavage between two *ortho* hydroxyl groups is favored over other positions on the basis of analogy [24,31]; a few of the potential structures for **13** are illustrated in Scheme 2. (Again, these are illustrated as the most suggestive possible tautomer.)

Scheme 2. Potential isomers for compound **13**.
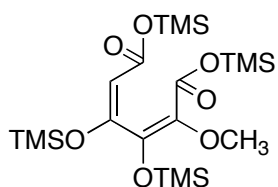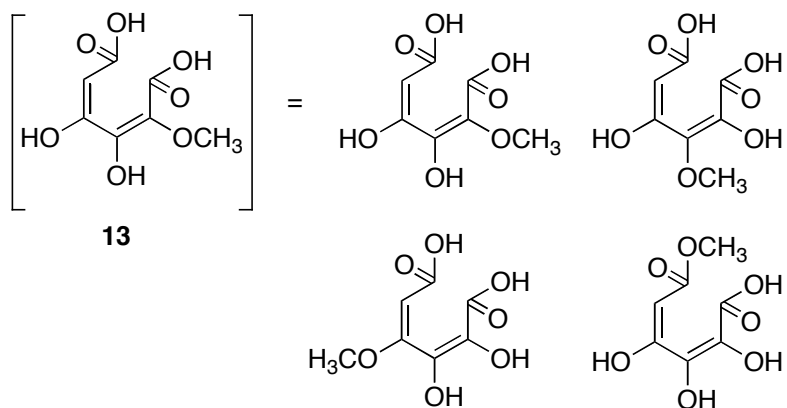
As Detected: MS m/z (intensity) 59 (9), 73 (100), 101 (12), 123 (5), 147 (19), 169 (49), 257 (25), 287(15), 303 (23), 360 (2), 375 (98), 403 (5), 433 (2), 449 (10), 477 (2)

While very similar product distributions were obtained with each catalyst, there was a striking effect of pH on the observed product distributions: under acidic conditions, only

demethylation product **1** and hydroxylation products **2** and **3** are detected. Somewhat higher concentrations of the hydroxylation products are seen at the still-acidic but higher pH extant when the system is not buffered. At the intermediate pH of 8.5 and at pH 12, both SET and HO•$_{ads}$ products are observed.
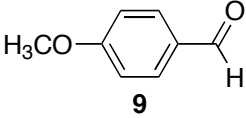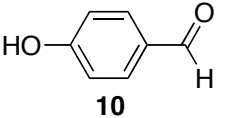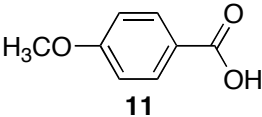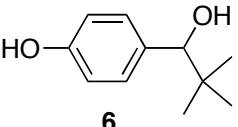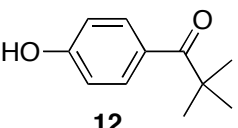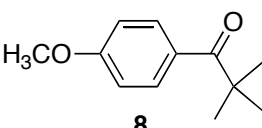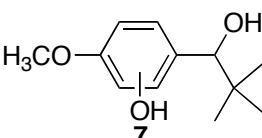
3.3.2 AN Degradations

Degradations of **AN** were carried out in similar fashion, but the products of these reactions did not require silylation for observation by GC. The results of photolysis, using PC 100 at pH 2, are shown in Table 5. It is at this pH at which the greatest number of intermediates is observed. Product distributions under other conditions are discussed below. We made no attempt to observe *t*-BuOH, *t*-BuOOH or other small alkyl products. All compounds were identified by comparison to authentic samples, save for **7**. Its structure is proposed from the mass, and we do not know the position of the hydroxylation, but it would ordinarily be favored *ortho* to the methoxy group over being *ortho* to an alkyl substituent. Hydroxylation of the alkyl group was dismissed due to lack of precedent under related oxidative conditions [32,33].

Treatment of **AN** with chemical SET reagents results in formation of **9** by cleavage of the resulting radical cation [16]. Thus, **9** is taken as a marker for SET chemistry by TiO$_2$. Ketone **8** is a substantial product in conventional SET reactions [34], but it is a minor product in Ranchella's titania-in-acetonitrile work, as it is here. Ranchella showed it also to be a marker for SET reactions for TiO$_2$.

Table 5. Products observed on photocatalytic degradation of **AN** to low conversion at pH 2

using PC 100.

Compound	GC Peak size (s/m/l)	Retention time, min[a]	Principle MS peaks, m/z (rel intensity)[b]
H₃CO—⟨⟩—CHO **9**	small	3.85	77 (25), 92 (15), 107 (30), 135 (100), 136 (68)
HO—⟨⟩—CHO **10**	small	4.47	65 (23), 93 (38), 121 (100), 122 (91)
H₃CO—⟨⟩—COOH **11**	small	4.96	77 (5), 96 (5), 121 (10), 122 (9),135 (12), 151 100), 152 (9)
HO—⟨⟩—C(OH)(CH₃)₂ **6**	medium	6.11	65 (5), 77 (14), 95 (16), 123 (100), 180 (3)
HO—⟨⟩—CO—C(CH₃)₃ **12**	small	6.15	65 (8), 93 (9), 121 (100), 178 (4)
H₃CO—⟨⟩—CO—C(CH₃)₃ **8**	very small	6.30	77 (18), 91 (19)), 121 (13), 135 (100),192 (1)
H₃CO—⟨⟩(OH)—C(OH)(CH₃)₂ **7**	medium	6.86	57 (8), 65 (15), 93 (36), 125 (20), 153 (100), 210 (8)

[a] The temperature program of column was as follows: Initial time of 2 min 130 ˚C; ramp from 130 to 280 ˚C at 20 ˚C/min. [b] EI-TOF as GC detector.

Compound **6** is an example of the demethylation chemistry that we have shown can come about through either stepwise oxidation of the methyl group or *ipso* attack [35]. We attribute this to HO•ₐds. Again, while SET-based mechanisms can be written down, we

attribute hydroxylation of **AN** to form **7** to HO•$_{ads}$ chemistry.

Several of the compounds in Table 5 are clearly secondary products. Demethylation of **AN** to form **6**, followed by SET oxidation to **10** seems a more likely sequence than the opposite, in that the aldehyde is such an easily functionalized position. At modest conversion, **11** is observed (clearly via aldehyde **9**) but not 4-hydroxybenzoic acid. This lends at least circumstantial support for this proposed sequence of **AN** to **6** to **10**. 4-Methoxybenzoic acid (**11**) has been observed previously as a product from **AN** using organic dyes as SET reagents [34], but not from TiO$_2$ oxidations. It could also come about through Bayer-Villager chemistry from peroxides. We believe that **11** is the source of small quantities of anisole that can be observed when the conversion of **AN** is taken as high as 50%. This is attributed to standard photo-Kolbe type chemistry, and is a standard SET reaction of carboxylic acids.

Another secondary product is ketophenol **12**. Whether it is formed via **6** or **8** cannot be determined; both are possible and both may occur.

Ultimately, the data in Table 5 show that similar quantities of SET and hydroxyl-type products are derived from the initial steps of degradation of **AN** at pH 2. This is in distinct contrast to the observations at higher pH values. Unbuffered reactions (pH 4.5-5.5) showed nearly a 10:1 ratio of the hydroxylation to SET oxidation products. At any higher pH (8.5 or 12) the SET products were simply undetectable. Again, while we cannot absolutely rule out that the SET products are degraded more efficiently at high pH, this seems an unlikely explanation. Here, we take into account the ordinary result with carboxylic acid derivatives that their degradation is also faster at low pH. Thus, we at least tentatively conclude that there is a true change in the balance of chemistries, with high pH favoring hydroxylation of

AN over SET-induced cleavage. This is in contrast to the case for **MR**, where more SET-type products are observed at high pH.

4.0   Discussion

Pichat and coworkers have recently published a trio of papers also evaluating this series of catalysts by measuring the relative rates of degradation of a set of probes, but using a much different set of probe molecules: 4-chlorophenol, 2,5-dichlorophenol, 4-chlorobenzoic acid, dichloroacetic acid, phenol, anisol, and pyridine [12-14]. All of their studies were carried out under unbuffered conditions, presumably near pH 5. Compared to our conditions, differences are that they used a modestly higher catalyst suspension "concentration" and lower organic compound concentration, such that our catalyst loading is somewhat higher (within an order of magnitude). Also, we flush with O_2, while the Pichat experiments were carried out under air, so the concentration of O_2 is higher in our experiments. We carried out some control experiments with air bubbling and did not note any discernable differences.

They observed that the phenols, anisole, and 4-chlorobenzoic acid were degraded more rapidly by the catalysts sintered at higher temperature (e.g., PC10 was faster than PC500). For pyridine and dichloroacetic acid, the trend was reversed. (PC10 provided anomalously fast degradation of pyridine.) For most of the compounds, the range of rate constants was within a factor of 4-7, but the rate of degradation of anisole was about 33 times faster using PC10 than using PC500 and the fastest catalyst for pyridine (PC10) was faster by an order of magnitude than the slowest catalyst (PC50).

Their interpretation focused on the balance between reducing defects in the titania anatase crystals (which are thought to lead to more rapid electron-hole recombination and thus photon wastage) and reducing surface area (which might lead to lower catalytic rates because of less adsorbed material). The reduction of surface area with higher temperature sintering is directly documented for these catalysts (Table 1), and the reduction of crystalline defects is of course completely expected by the sintering/annealing process, if not directly quantified.

Pichat et al. concluded that the drop in rates for dichloroacetic acid and pyridine degradation were attributed to the need for direct adsorption of these compounds to the catalyst in order for "hole attack" (SET) to occur. For the other compounds, it was concluded that direct adsorption was not required, and the lower rate of electron-hole recombination dominated the kinetics. The assumption was that hydroxyl-like chemistry (perhaps literally HO• radicals) could occur in the first few layers of solvent surrounding the catalyst.

We have similarly concluded in previous work that SET chemistry required what we called specific adsorption, whereas hydroxyl type chemistry did not – and that the latter might happen in the multilayers around the catalyst [15].

Therefore, a study related to the Pichat work, in which variable chemistry, i.e., products deriving from differing mechanisms (hydroxyl-like vs. SET) was warranted and might serve to confirm the Pichat hypothesis. We chose these two molecules **AN** and **MR**, since both were easily capable of displaying products of both types of chemistry as had been demonstrated in earlier papers. These choices contrast with Pichat's probes, which generally were molecules that had a strong bias for one type of reactivity or the other. Like Pichat, we

chose to work at least initially (i.e., for this paper) with catalysts that would be available and thus completely reproducible to the full community, i.e., the PC series and P25.

At unbuffered pH, we see little systematic effect among the catalysts. However, on an equal weight-to-volume basis, PC 500 was a less efficient catalyst (factor of ~25) for degradation of **MR** than the others. The catalyst with the highest surface area and highest defect concentration was thus the slowest catalyst for **MR**, but the product distribution was not significantly different for this catalyst, compared to the others.

For **AN**, there was a general downward trend in rate from PC 10 to PC 500 in unbuffered suspensions, but it was not dramatic, only a factor of 3. Again, although smaller, the trend is to higher efficiency at this pH with fewer defects and smaller surface area. The products were invariant with catalyst. While the modest effects on observed rate were in line with the results reported by Pichat [13], we thought more specific control of the pH might yield more systematic data.

At acidic pH (2.0), we essentially no difference among the PC series for **MR**, save for a modest decline (factor of 3) for PC 500. For **AN**, the rates go up from PC 10 to PC 100 (factor of 3-4) and then fall again for PC 500 (factor of 2). This latter trend of a modest increase in observed rate that peaks for one of the two "middle" catalysts is reproduced for both **MR** and **AN** at pH 8.5, and 12.

For any given catalyst, we also do not see a dramatic shift in the reaction rates across pH, with a single exception, which is the high pH degradation of **MR**. We believe this is attributable to the fact that the pKa of **MR** is within a couple of units of 8.5 and that the phenolate should be easier to adsorb and degrade than the phenol. By contrast, if there is any significance to the pH dependence of the rate data for **AN**, it is in the direction that

degradation is somewhat faster in more acidic conditions. A speculative interpretation of the acceleration is probably not justified on the basis of the data in hand.

The product distributions as a function of pH, however, are notably different for both probes. For **MR**, more ring opening reactions are observed at low pH. Given that we attribute such ring opening reactions to SET chemistry, and that we believe the SET chemistry requires adsorption, we offer the following interpretation.

The strongest adsorption points in **MR** are clearly the two phenolic groups. However, with the groups positioned *meta* to one another, only one of them may adsorb directly to the TiO$_2$ surface, and the other is necessarily exposed to the aqueous layers. Certainly by pH 12, and probably at least significantly by pH 8.5, a large fraction of the exposed phenolic hydroxyl groups are deprotonated. These adsorbed phenolates certainly have lower oxidation potentials than their protonated counterparts. Although there is certainly enough chemical potential available from a TiO$_2$ h$^+$ to oxidize any of these species, it has been our experience that there is a qualitative correlation between low oxidation potentials and rapid SET-type chemistry [15,24,31].

For **AN**, the distinction between low and high pH products is that at higher pH, no SET products are observed, i.e., none of the compounds in which the *t*-butyl group has been removed are found, but hydoxylation and demethylation products are still obtained. A model that might account for this is based on the formation of hydrogen bonds between the *para* methoxy group of **AN** and the surface of the catalyst, in addition to what we presume is the stronger interaction between the alcohol and the TiO$_2$ (Scheme 3). At high enough pH, the majority of the surface TiOH groups are not protonated and cannot easily interact with the OCH$_3$ group. As a result, there may be a tendency for the phenyl group not to be as closely

held to the surface. When the interaction is stronger due to the ability of the surface to form

hydrogen bonds to the OCH_3 at low pH, oxidation of the phenyl ring by SET is facilitated by

its proximity to the surface, and the SET-induced chemistry, namely loss of the *t*-butyl group,

may occur.

Scheme 3.
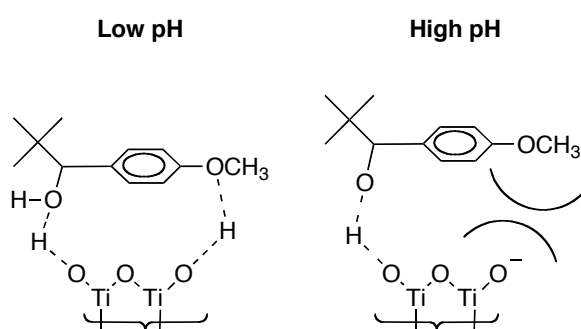
One plausible interpretation of the data presented here is that most of the chemistry,

regardless of the conditions, occurs in solution rather than on the surface, and thus hydroxyl-

type chemistry predominates for all catalysts: all potential variability attributable to the

catalysts is washed out. This may be correct for certain pH conditions, e.g., **AN** degradations

at high pH. However, the very observation of substantial fractions of SET products under

other conditions (e.g., **AN** at low pH and **MR** at higher pH) belies this as a universal

interpretation, as long as it is postulated that SET chemistry demands adsorption. We are not

yet prepared to abandon that hypothesis.

5.0   Conclusions

We draw two conclusions from the observations reported in this paper. If it were the

case that degradation reactions, or even particular forms of degradation chemistry, required adsorption to certain types of defect sites, we would expect a strong inverse correlation between the degree of sintering in these catalysts and formation of that class of compounds. It would be the case that on a per-gram basis, the absolute concentration of available defect sites would decrease dramatically from PC500 to PC10. Thus, product distributions should vary with the catalyst, especially with our relatively high catalyst loading. However, we see no such consistent trend in the data. We can conclude that adsorption to special reactive sites that can be annealed away is not required.

In the second place, we do not find strong evidence to confirm Pichat's hypothesis regarding the effects of sintering on rate. If mutually compensating effects of decreasing surface area and decreasing defect concentration affects the rates of SET-chemistry in one way (lowering it due to the need for adsorption) and $HO\bullet_{ads}$ chemistry the other (raising it, because adsorption is not critical), we would expect to see distinctions in product distributions among the catalysts. Particularly the example of **MR** at pH 8.5 stands out as having both kinds of chemistry observed for all catalysts, and not in significantly different proportion. The same is true of the degradation of **AN** at low pH. We do not argue that these experiments disprove the Pichat hypothesis, but we do not find support here either. From a strictly practical point of view, the effects of differing catalysts among this series are of the same magnitude as those of pH, light intensity, and other experimental parameters, and can be different, even in direction, for different substrates.

Acknowledgments

References

[1]   P.K.J. Robertson, D.W. Bahnemann, J.M.C. Robertson, F. Wood, Handbook of Environmental Chemistry 2 (2005) 367-423.

[2]   D. Bahnemann, J. Cunningham, M.A. Fox, E. Pelizzetti, P. Pichat, N. Serpone In Book, Photocatalytic treatment of waters; G.R. Helz, R.G. Zepp, D.G. Crosby, Eds. 1994, p 261-316.

[3]   W.S. Jenks In Book, The organic chemistry of TiO2 photocatalysis of aromatic hydrocarbons; V.H. Grassian, Ed.; CRC Press: Boca Raton, 2005, p 307-346.

[4]   P. Pichat, Environmental Science and Pollution Control Series 26 (2003) 77-119.

[5]   M.K. Nowotny, L.R. Sheppard, T. Bak, J. Nowotny, J. Phys. Chem. C 112 (2008) 5275-5300.

[6]   T.L. Thompson, J. John T. Yates, J. Phys. Chem. B 109 (2005) 18230-18236.

[7]   M.A. Henderson, W.S. Epling, C.H.F. Peden, C.L. Perkins, J. Phys. Chem. B 107 (2003) 534-545.

[8]   C. Minero, G. Mariella, V. Maurino, E. Pelizzetti, Langmuir 16 (2000) 2632-2641.

[9]   K.I. Hadjiivanov, D.G. Klissurski, Chem. Rev. 25 (1996) 61-69.

[10]   M.R. Hoffmann, S.T. Martin, W. Choi, D.W. Bahnemann, Chem. Rev. 95 (1995) 69-96.

[11]   M.A. Fox, M.T. Dulay, Chem. Rev. 93 (1993) 341-357.

[12]   R. Enriquez, P. Pichat, J. Environ. Sci. Health A 41 (2006) 955-966.

[13]   R. Enriquez, A.G. Agrios, P. Pichat, Catal. Today 120 (2007) 196-202.

[14]   A.G. Agrios, P. Pichat, J. Photochem. Photobiol., A 180 (2006) 130-135.

[15]   X. Li, J.W. Cubbage, W.S. Jenks, J. Photochem. Photobiol. A 143 (2001) 69-85.

[16]   M. Ranchella, C. Rol, G.V. Sebastiani, J. Chem. Soc. Perkin Trans. 2 (2000) 311-315.

[17]   C. Lang'at-Thoruwa, T. Song Tong, J. Hu, L. Simons Andrean, A. Murphy Patricia, J. Nat. Prod. 66 (2003) 149-51.

[18]   C.G.M. Janssen, E.F. Godefroi, J. Org. Chem. 49 (1984) 3600-3603.

[19]   T.P. Smyth, B.W. Corby, J. Org. Chem. 63 (1998) 8946-8951.

[20]   A.K. Chakraborti, L. Sharma, M.K. Nayak, J. Org. Chem. 67 (2002) 6406-6414.

[21]   C.G. Hatchard, C.A. Parker, Proc. Royal. Soc. A 235 (1956) 518-536.

[22]   W.D. Bowman, J.N. Demas, J. Phys. Chem. 80 (1976) 2434-2435.

[23]   C.C. Sweeley, R. Bentley, M. Makita, W.W. Wells, J. Am. Chem. Soc. 85 (1963) 2497-2507.

[24]   X. Li, J.W. Cubbage, T.A. Tetzlaff, W.S. Jenks, J. Org. Chem. 64 (1999) 8509-8524.

[25]   E. Baciocchi, M. Bietti, O. Lanzalunga, Acc. Chem. Res. 33 (2000) 243-251.

[26]   J. Cunningham, G. Al-Sayyed, S. Srijaranal In *Aquat. Surf. Photochem.*; G.R. Helz, Ed.; Lewis, Boca Raton, Fla: 1994, p 317-348.

[27]   The surface area of PC 500 is enough greater than the others that it is possible that this catalyst is not fully saturated under our conditions.

[28]   M. Abdulla, G.K.-C. Low, R.W. Matthews, J. Phys. Chem. 94 (1990) 6820-6825.

[29]   K.H. Wang, Y.H. Hsieh, C.H. Wu, C.Y. Chang, Chemosphere 40 (2000) 389-394.

[30]   C. Richard, New J. Chem. 18 (1994) 443-445.

[31]   X. Li, J.W. Cubbage, W.S. Jenks, J. Org. Chem. 64 (1999) 8525-8536.

[32]   J. Cunningham, B.K. Hodnett, J. Chem. Soc. Faraday 1 77 (1981) 2777-2801.

[33]   E. Papaconstantinou, Chem. Rev. 18 (1989) 1-31.

[34]   I.N. Lykakis, C. Tanielian, M. Orfanopoulos, Org. Lett. 5 (2003) 2875-2878.

[35]   X. Li, W.S. Jenks, J. Am. Chem. Soc. 122 (2000) 11864-11870.

Chapter 3

Photocatalytic degradation using tungsten-modified TiO₂ and visible light: kinetic and mechanistic effects using multiple catalyst doping strategies

Timothy Hathway, Erin M. Rockafellow, Youn-Chul Oh and William S. Jenks

Abstract

Tungsten-modified titanium dioxide catalysts prepared from sol-gel methods and obtained commercially were compared for their photocatalytic activity using mechanistic probes designed to examine chemical pathways of oxidation. No special visible absorbance was noted for the sol-gel catalyts. However, an increase in the single-electron transfer chemistry with the presence of WO_x was noted, and a distinct wavelength dependence on the product ratios.

1.0   Introduction

Titanium dioxide is an excellent photocatalyst for the degradation of organic contaminants in water and air. Most organic compounds are degraded to CO_2, H_2O, and appropriate inorganic ions on exposure to TiO_2 in the presence of light and oxygen [1-7]. A distinct hindrance, however, for more widespread application of TiO_2 as a catalyst for removal of organic pollutants is its lack of absorption in the visible spectrum, as betrayed by its appearance as a white powder. Another is its relatively low efficiency. Modification of TiO_2 is thus an active and important field of research.

Of the three common phases of crystalline TiO_2, it is widely held that anatase (band gap = 3.2 eV, absorption ≤ 385 nm) is the most photocatalytically active, yet rutile (band gap = 3.0 eV, absorption ≤410 nm) absorbs light to the red of the anatase band edge. This poses an obvious advantage, when considering the utility of solar light, but still does not extend far into the visible, where the majority terrestrial solar energy lies. The most commonly used and most effective TiO_2 photocatalyst is probably DeGussa's P25, which contains adjoining anatase and rutile microcrystalline regions. Gray has shown that this extended functionality is due in large part to the extended near-visible absorption of the rutile phase, followed by rapid electron transfer between the phases, leading to enhanced charge separation and reduced energy wastage by electron-hole recombination [8,9].

In this sense, DeGussa P25 and other mixed-phase TiO_2 samples are inherently multicomponent catalysts, but other multi-component strategies for enhancing photocatalysts have emerged as well [10,11]. One approach to building multi-component catalysts to increase physical charge separation and/or visible light absorption include nanodeposits of noble metal pools on the exterior of TiO_2 particles [12-15]. Another, more in the spirit of

P25, is the overt use of additional semiconductors, such as CdS or WO_3, coupled to TiO_2 [16-20]. Kamat has outlined both core-shell and coupled geometries [16,17], but for practical purposes, we are concerned with the coupled case, which may be envisioned as small adjoining nanodomains. Here, both photogenerated holes and electrons are potentially accessible at the particle surface.

In this paper, we examine the photocatalytic chemistry of a series of WO_3-modified titanium dioxide samples [21-24]. The band gap of bulk WO_3 is 2.5 eV, which corresponds to absorption out to approximately 500 nm, well into the visible. Moreover, because of the absolute positions of the bands, conduction bond electrons from TiO_2 can migrate to WO_3, while the complementary migration can occur for valence band holes. With small percentages of tungsten, relative to titanium, it is also possible that simple substitutional doping may occur, with less predictable results.

A key issue, however, is whether the ordinary modes of reactivity for TiO_2 are maintained, enhanced, or destroyed [25]. We and others have generally drawn a distinction between hydroxyl-like ($HO\bullet_{ads}$) and SET-initiated chemistry. (See, for example, ref [26].) Bahnemann has referred to these phenomenologically different reactivities as deriving from "deeply" and "surface" trapped holes, respectively [27]. Others, as summarized by Fujishima [7], argue that the hydroxyl-like chemistry can occur away from the particle surface, indicative of a diffusible intermediate (presumably $HO\bullet$ itself). Regardless of the claims of true action-at-a-distance, we have argued that SET chemistry has a more stringent requirement for pre-adsorption to the catalyst and shown this to be the case for both oxidative and reductive SET reactions [26,28].

In principle, if reactivity in WO_x-modified TiO_2 derives from the oxidative reactivity

of holes residing in TiO_2 alone (surface or "deep"), then both the typical hydroxyl-like and single-electron transfer initiated chemistry ought still occur, assuming the reactivity is still dominated by adsorption on TiO_2 sites. The valence band for WO_3 is at a higher potential than for TiO_2, which could result in hole trapping concentrated on these sites, which might, in turn, be observable in the oxidative behavior. There is also a possibility of true wavelength dependence of the chemistry because of the dopint, depending on the dynamics of hole trapping vs. substrate oxidation.

There are multiple methods of making WO_x-modified TiO_2, including an incipient wetness method, in which TiO_2 is at least partially coated with WO_x from solution deposition, and sol-gel methods, in which the tungsten is coprecipitated with the titanium and is presumably distributed throughout the catalyst. (We will use the term W-TiO_2 below to mean tungsten-modified TiO_2 in the most general sense, and will be more precise when referring to specific preparations.)

We examine the oxidative chemistry of two sets of catalysts. First, we compare two commercial catalysts: PC50 and DT52 from Millenium chemicals. The latter of these is derived by treatment of the former to coat it with WO_x by an incipient wetness method, such as that described by Do [21]. A second series is a set of sol-gel-prepared W-TiO_2 catalysts with 0-5% tungsten, prepared according to the method of Li [23]. Rather than evaluate the chemistry by disappearance of a dye such as methylene blue [29], we use chemical probes originally proposed by Ranchella [30] and Pichat [31,32] that provide more detailed information regarding the chemical mechanisms of oxidation of these catalysts, revealing pathways through product analysis.

2.0   Experimental

2.1   General Materials

1-*p*-Anisylneopentanol (**AN**) and the oxidized products of its degradation were synthesized and characterized as published previously [25]. Quinoline and its major oxidized products were obtained from Aldrich. Distilled water was purified from a Millipore MilliQ UV system and had a resistivity of $\geq 18\ M\Omega\ cm^{-1}$. Commercial titania samples were PC50 and DT52 obtained from Millennium Chemical.

2.2 Preparation of W-TiO$_2$ catalysts

W-TiO$_2$ was prepared by a sol-gel method based closely on that of Li [23]. A TiO$_2$ transparent sol was prepared by combining 17.5 g Ti(O-*n*Bu)$_4$, 120 mL ethanol, 15 mL acetic acid, and 5 mL de-ionized water.   The mixture was aged for 1 day, stirring at room temperature.   To this sol was added dropwise added 60 mL of aqueous solution of containing 4.56 g of ammonium paratungstate ((NH$_4$)$_{10}$W$_{12}$O$_{41}$, F.W.= 3042.55) under vigorous stirring over 2 hours until WO$_x$-TiO$_2$ (3 mol % WO$_x$ to TiO$_2$) gel is formed. Similarly, 0%, 1%, and 5% WO$_x$-TiO$_2$ samples were prepared by using appropriate amounts of ammonium paratungstate. Ammonium tungstate was also used in the same way to prepare a 3% WO$_x$-TiO$_2$ gel with a different W source; no detectable difference was found between materials made from the two precursor.

The W-TiO$_2$ gels were aged two days with vigorous stirring, then one day undisturbed followed by one more day with vigorous stirring. The W-TiO$_2$ gels were then dried with a rotary evaporator at 358 K. As the gels dried, they shrunk and coated the surface of their flasks, eventually forming powders. After drying, the samples were ground for eight

minutes in an agate ball mill.

Sintering was then carried out in porcelain crucibles. The furnace was heated at a moderate rate (10 K/min) to ensure that ejection of the volatiles did not discharge powder from the crucibles. The furnace was allowed to reach 923 K, which then stayed constant for two hours. A calibrated thermocouple was placed in the center of the cluster of crucibles to continuously monitor the temperature at the location of the samples. The furnace was then allowed to cool down over the course of two hours. The cooled powders were immediately transferred to storage vials.

2.3 *Catalyst Characterization*

Powder x-ray diffraction (XRD) measurements were carried out at room temperature using a diffractometer with Cu K_α radiation. An accelerating voltage of 40 kV and an emission current of 30 mA were used.

X-ray photoelectron spectroscopy (XPS) was performed with a multi-technique spectrometer employing monochromatized Al K_α radiation. The instrumental Gaussian full-width at half maximum (GFWHM), which characterizes the resolution, was 0.65 eV for the Al source. The take-off angle was fixed at 45˚ and the x-ray source was run at 14 kV and 250 W. The emitted photoelectrons were sampled from a 1 mm^2 area. The XPS energy scale was calibrated against Au $4f_{7/2}$ and Ag $3d_{5/2}$ peaks at 84.0 and 368.27 eV, respectively. The sample was mounted on an indium foil for XPS analysis and placed in the XPS chamber, whose base pressure was about 3×10^{-10} Torr. Temperature was measured with a Type K thermocouple.

Particles were examined by scanning electron microscopy (SEM) using a variable

pressure scanning electron microscope with 20 kV accelerating voltage and ~0.5 nA of beam current for imaging in 25 mm working distance. SEM-EDX analyses were performed to check for segregation of the tungsten. A high-purity Ge light-element x-ray detector was employed and the take-off angle was fixed at 30°.

2.4   *Suspensions and Photolyses*

Photocatalytic degradations were carried out as described previously [25,33]. Broadly emitting fluorescent lamps centered at 419 nm (roughly 390 – 500 nm total range) or 350 nm (roughly 320-380 nm) were used. The spectral distributions are available in the supporting information. Ferrioxalate actinometry was employed in order to compare the rates between UV and visible reactions [34,35]. Initial conditions were 300 μM **AN** or 150 μM **Q** in water containing 1 g/L catalyst and all solutions were purged with O_2. The pH was controlled throughout the kinetic run reactions by careful addition of aqueous NaOH as necessary. The reported initial degradation rates were normalized for total lamp flux by means of potassium ferrioxalate actinometry.

3.0   Results

3.1   *Catalyst characterization*

Based on SEM analysis, the average particle size of the sintered, tungstated catalysts was in the range of 100 nm to 3 μm, which is much larger than P25 particles (Figure 1d). Ball-milling was used to successfully grind the particles into the 20 nm regime (Figure 2e), yielding both smaller particles and a tighter distribution of sizes.

As was noted by Li [23], addition of WO_x to the sol-gel preparation of TiO_2 inhibited the conversion of anatase to rutile on annealing at 923 K. Studies of similar substitutionally W-doped titania catalysts show that W^{6+} exists in distorted octahedra. These cause long-range distortions that lead to anatase being favored over rutile up to temperatures higher than for undoped catalysts [36].

Figure 1a shows the powder XRD of P25 (anatase and rutile), the undoped catalyst (0% WO_x-TiO_2, mainly rutile), and the doped materials (mainly anatase). Using the Scherrer equation, average particle sizes were found to be 15 nm, 18 nm, 23 nm, 28 nm, and 19 nm for 5% WO_x, 3% WO_x, 1% WO_x, 0% WO_x, and DeGussa P25, respectively.
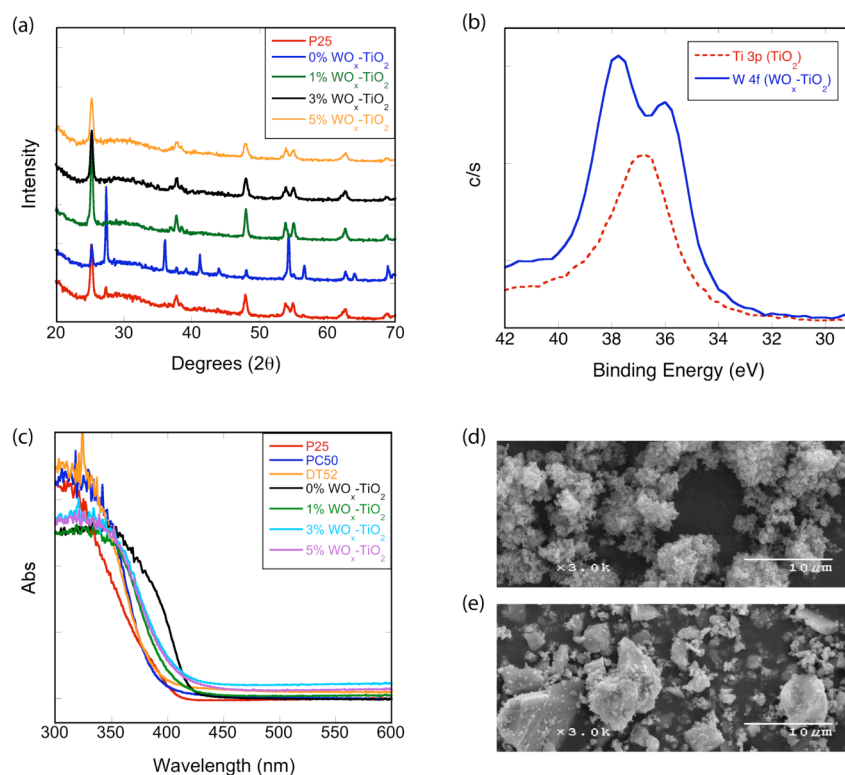
Figure 1. Characterization of sol-gel catalysts. (a) Powder XRD patterns; (b) Detail of XP spectrum of 3% WO_x-TiO_2; (c), Diffuse reflectance UV-vis

XPS was used to determine the oxidation state of W near the surface of the catalysts. Figure 2b shows the underlying Ti 3p signal at 36.6 eV for the undoped sample. For the 3% WO_x-TiO_2 sample, the signal for the W^{6+} $4f_{7/2}$-$4f_{5/2}$ doublet at 36.0 eV is an inherently stronger peak and dominates the spectrum, with the apparent loss of resolution between the double peaks being due to the underlying Ti signal. Small contributions of other states are possible due to broad peaks [37].

Diffuse reflectance UV-visible spectrophotometry (Figure 2c) shows that there was not a dramatic shift in the absorption spectra of the catalysts outside of what is predictable from the XRD data. P25 shows the typical band edge of TiO_2, with a slight tail into the red due to rutile.   DT52 and the PC50 from which it is made had nearly identical spectra. The most red-shifted absorption came from the 0% $WO_x$$TiO_2$. However, this effect can be attributed entirely to the great fraction of rutile in this material. We do not know why these materials exhibit a different result than the materials reported by Li, *et al.* [23].

SEM-EDX was used to check for segregation of WO_3. The data in Figure 2 show an even distribution of W in the 3% W catalyst, though the resolution of the images (ca. 0.2 µm) is not good enough to demonstrate whether there are nano-sized aggregations on the TiO_2 particles, or whether the W is homogeneously dispersed on the atomic scale. The same results were obtained for the 1% and 5% WO_x catalysts. More SEM and SEM-EDX data are available in the Supporting Information.
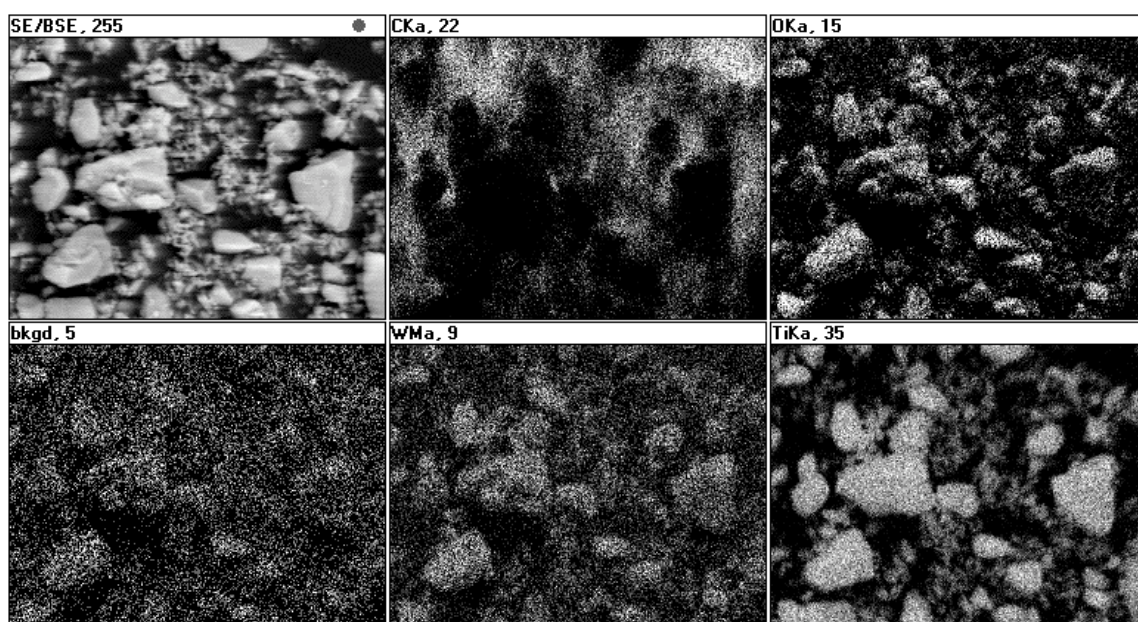
Figure 2. SEM-EDX images of the 3% WO$_x$ catalyst on the same scale as Figure 1d and 1e. Clockwise from the top left: overall SEM, C signal, O signal, background, W signal, Ti signal.

3.2   *Probe Degradations*

Because one of the important questions of modified photocatalysts is whether they are more functional with visible light than undoped TiO$_2$, the experiments described below were carried out with lamps whose irradiation is centered at 419 nm, to the red of the onset of absorption of the bare catalysts as documented in Figure 1. The irradiation frequencies, however, are such that a small amount of light below 380 nm is available. As noted, other irradiations used lamps centered at 350 nm.

Initially, 4-methoxyresorcinol (2,4-dihydroxyanisole), was chosen as a probe because it exhibits a mixture of SET and hydroxyl chemistry with P25 and the PC series of catalysts

[25,26]. However, initial experiments using 420 nm irradiation indicated a high degradation efficiency. Subsequent preliminary experiments using a white light source and a 435 nm high pass cutoff filter suggested that any differences between the catalysts were being overwhelmed by visible-light mediated degradation that could be attributed to the formation of a charge transfer complex between this very electron rich arene and TiO_2, analogous to the reports of Agrios and Gray [38,39]. We therefore resorted to the less electron rich probes shown in Scheme 1.

Scheme 1.
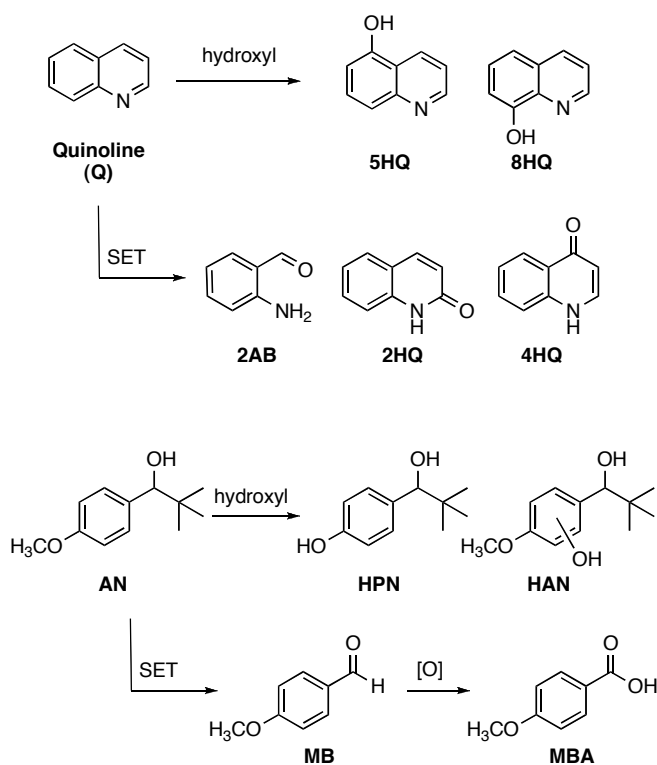
3.2.1 Kinetic Traces

The initial degradative steps of probe molecules quinoline (**Q**) and 1-*p*-

anisylneopentanol (**AN**) have been discussed at length previously [25,30,31]; the essentials are illustrated in Scheme 1 and can be summarized by noting the differing products predominant for single electron transfer (SET) chemistry and hydroxyl-type chemistry. These two probes were chosen for their lack of strong adsorption to the TiO_2 and for their well-defined partial degradation chemistry. Conditions were chosen on the basis of previous work [25] under which both SET and hydroxyl products would normally be observed.

Kinetic traces were obtained. As seen in Figure 3, which illustrates the data obtained at 419 nm, the traces could be acceptably fit to zero order decays for degradation of up to approximately 25%. The results are given numerically in Table 1, and the values were reproducible within a 5% standard deviation. Immediately striking is the two order of magnitude increase in rate at 350 nm, relative to 419 nm.
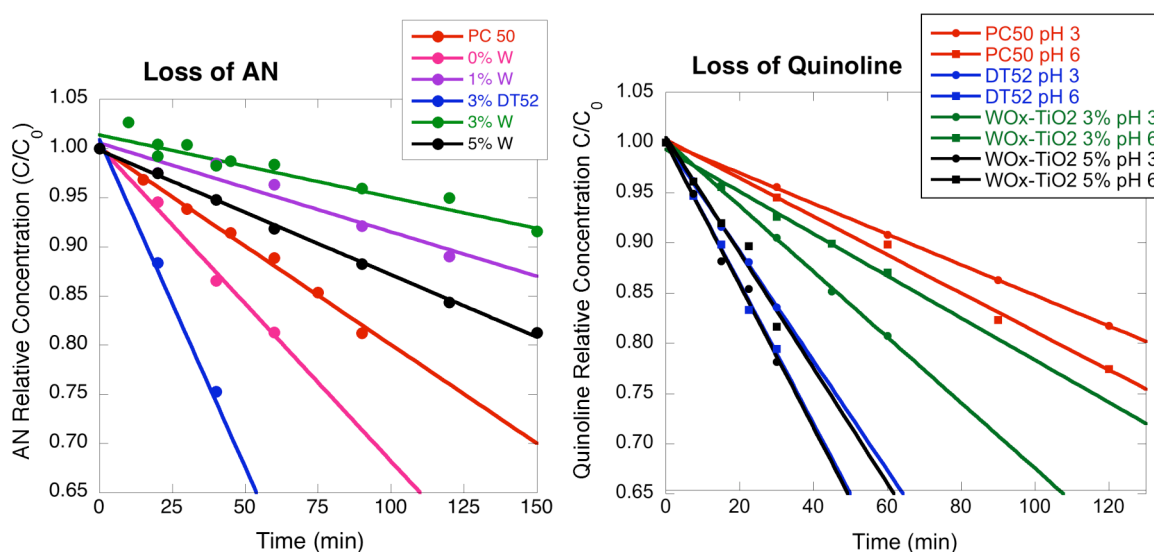
Figure 3. Kinetic traces for degradation of **AN** (pH 2) and **Q** (pH 3 or 6) by various photocatalysts using irradiation centered at 419 nm.

Table 1. Degradation rates of **AN** and **Q** with various catalysts.

	Rate (µM/min) [a]					
Catalyst	**AN** pH 2 420 nm	**Q** pH 3 420 nm	**Q** pH 6 420 nm	**AN** pH 2 350 nm	**Q** pH 3 350 nm	**Q** pH 6 350 nm
PC50	2.00	1.52	1.91	354	154	287
3% DT52	6.70	5.45	6.99		597	616
0% WO_x–TiO_2	3.20					
1% WO_x–TiO_2	0.90					
3% WO_x–TiO_2	0.63	3.27	2.10		145	329
5% WO_x–TiO_2	1.27	7.09	5.75	179	605	228

[a] All rages were reproducible to standard deviations of ≤5%

For **AN**, the clearly superior catalyst is DT52, with the others varying without a discernable pattern. The rate of degradation of quinoline is not especially pH sensitive, despite its pKa being between 4.5 and 5, such that the protonated and deprotonated forms are predominant at pH 3 and 6, respectively. Adsorption is difficult to measure quantitatively, but it is expected that quinolinium, due to its greater water solubility and positive charge, would be less adsorbed to the catalyst, which is also positively charged at pH 3. At pH 6, adsorption of quinoline through the nitrogen lone pair is expected. The rate of degradation does not vary much, however, suggesting that adsorption to the catalyst is not rate-determining for this compound.

3.2.2   Product Studies

The sole product obtained for low conversion of **AN** with the 419 nm bulbs was *p*-methoxybenzoic acid (**MBA**). This is clearly the result of a two-step oxidation whose initial product is *p*-methoxybenzaldehyde (**MB**). The second oxidation step may be photochemical or a result of the formation of hydrogen peroxide and either autoxidation or Bayer-Villager chemistry. In any case, it is clear that **MB** is oxidized more rapidly than it is formed and thus does not accumulate. For the 5% WO$_x$-TO$_2$ catalyst, both the usual **MBA** and hydroxylated products (Scheme 1) were observed, though the total accumulated intensity of the products was only about 10% of that of the other catalysts. The simplest explanation for the lower accumulation of intermediates is that they are degraded faster than they are formed, implying that the 5% WO$_x$-TiO$_2$ catalyst was superior from this perspective.

The 350 nm bulbs were also used to determine product ratios under UV irradiation. In distinct contrast to the 419 nm irradiations, all four products (**MB**, **MBA**, **HPN**, and **HAN**) were found in very comparable amounts for low conversion.

For degradation of **Q**, both HO•$_{ads}$-type products (**5HQ** and **8HQ**) and SET products (**2AB, 2HQ**, and **4HQ**) are observed on 419 nm irradiation. At low pH, where quinoline is protonated, the hydroxyl type products predominate, whereas the SET products are found at higher concentration at pH 6. The ratios of initially formed (SET products)/(HO•$_{ads}$-type products) are given in Table 2. With 350 nm irradiation at pH 3, the hydroxyl products still predominate; at pH 6, the dominance of SET products declines, relative to the 419 nm values.

Table 2. Ratio of initial SET products to hydroxyl-type products[a] in quinoline degradations.

Catalyst	pH 3 420 nm	pH 6 420 nm	pH 3 350 nm	pH 6 350 nm
PC50	0.08	9.5	0.11	0.63
3% DT52	0.54	11	0.13	1.2
3% WO_x–TiO_2	0.15	15	0.43	4.3
5% WO_x–TiO_2	0.25	4.2	<0.01	0.89

[a] See Scheme 1.

4.0   Discussion

In keeping with other publications examining the efficacy of tungstated titanium dioxide catalysts, we find DT52, the tungsten-treated PC50 derivative is more active than its parent material. The same cannot be directly concluded for the sol-gel samples examined here, because the crystal composition of the undoped sol-gel sample is a qualitatively different mix of anatase and rutile nanodomains than the others, as demonstrated in Figure 1a. From this point of view, it appears that incipient wetness tungsten-coating of otherwise optimized TiO_2 photocatalysts may be an important empirical parameter for use in achieving the most active catalyst possible. Empirically, we are unaware of any evidence suggesting that the presumably homogeneous distribution of WO_x throughout the particle by the sol gel (or other related) methods presents any special advantage in photocatalytic degradations besides stabilizing the anatase crystal structure (the more active titania polymorph) at high temperatures during catalyst preparation.

Two causes for increased reactivity of WO_x-modified TiO_2 have been proposed: the ability of the WO_3 to trap electrons (and thus preserve holes), and an increase of surface acidity, which is thought to improve the binding of Lewis bases [40]. There is not a consistent pattern of rates among the sol-gel prepared samples, but there is a consistent increase in both rate and proportion of SET products, comparing DT52 to PC50. This latter result suggests that enhanced surface binding may be important.

The materials we prepared (and DT52) do not have extensive absorption into the visible. Nonetheless, the 419 nm lamps we used overemphasize irradiation at the very red edge; only a modest percentage of the lamps' output is below 400 nm, and very little below 380 nm. The two order of magnitude change in rates of photolysis comparing 350 to 419 nm bulbs is at least in very large part due to the much smaller absorption of light by our catalysts in the latter case, since the actinometer counts all of the photons, absorbed by catalyst or not.

In our previously published work [25], partial degradation of **AN** with PC50 (or related catalysts) and 350 nm irradiation at pH 2 yielded a product mixture containing similar amounts of SET and $HO\bullet_{ads}$ products. The present data, with the tungstated catalysts, give the same result. However, we find that only the electron transfer products are observed when irradiating at the red edge of the absorption band, with one exception (5% WO_x-TiO_2). A much smaller total sum of products and some hydroxyl chemistry was observed for the 5% WO_x-TiO. This result is probably due to more efficient degradation of **MBA** by 5% WO_x-TiO_2. The observation of a small amount of **HAB** and **HPN** is consistent with the idea that the **MB** and **MBA**, out-compete the **AN** for the specific adsorption locations that lead to SET reactivity (and get degraded in the process). However, it is not obvious why the phenomenon of the more efficient degradation of **MB** and **MBA** is limited to the 5% WO_x sample.

The red edge irradiation used with quinoline as a probe at pH 6 also shows a relative increase for SET products for every catalyst. At pH 3, the effect is less dramatic. In that the relative increase of SET chemistry at 419 nm is observed for PC50 and the undoped sol-gel TiO_2, it is clearly not a special feature due to the tungsten; rather it is an inherent feature of the interaction between the probes and TiO_2. The two simplest explanations are (1) there is a wavelength dependence on TiO_2 photocatalysis at the red edge of absorption that is generally unnoticed because it represents such a small portion of the excitation spectrum; (2) there is a charge-transfer band or other specific interaction between the small population of adsorbed probes and TiO_2 whose light absorption may extend further into the visible than the classic red edge of the catalyst absorption. Charge transfer interactions between arenes and TiO_2 are well documented in more functionalized cases [39,41]. We cannot be definitive here, but prefer the second explanation, given that the effect is much smaller for quinolinium ion at pH 3 than for the other two cases. Quinolinium's positively charged nature presumably inhibits binding to the positively charged TiO_2, and acts as a control – in combination with **AN** at pH 2 – for the effect being mitigated solely by the protonation state of the catalyst under acidic conditions.

5.0 Conclusions

The results reported here add to the literature that suggests that tungstated TiO_2 can be a catalyst that is functionally superior to its unmodified parent in terms of the speed of degradation for photocatalytic applications. No special advantage was found for sol-gel preparations that presumably disperse WO_x throughout the catalyst over comparable surface-

modified species.

As documented by the diffuse reflectance spectra, surface coating of WO_x (e.g., DT52) does not have a significant effect on the light absorbed by the bare photocatalyst. Any effects on the absorption of the photocatalysts made by the sol gel method may easily derive more from subtly different ratios of anatase and rutile in the annealed catalysts, since WO_x inhibits the conversion to rutile.

Product distributions for partial degradation are affected by the modification of the TiO_2. With surface modification (DT52 vs. PC50), the tendency was for the added tungsten to increase the fraction of SET-derived products, which accompanied an acceleration of overall reaction. This might be explained either by greater adsorption of the organic to the modified catalyst or by a longer lifetime of the SET-active "hole" before findint an alternative trap site that results in hydroxyl chemistry. Of these, the former, simpler explanation is more appealing, but more evidence would be required to be certain.

Also, a wavelength dependence was found. Irradiation at the red edge of TiO_2 absorption (and beyond) favored the cleavage reactions that have been attributed to SET chemistry for **AN** and the regiochemistry of hydroxylation that indicates SET chemistry for **Q**. In the absence of evidence to the contrary, the simplest explanation is a previously unknown charge transfer band formed on adsorption to the catalyst by almost any arene.

obtain diffuse reflection spectra on his instrumentation. We also gratefully acknowledge the assistance of Jim Anderegg with the XPS data.

References

[1]   P.K.J. Robertson, D.W. Bahnemann, J.M.C. Robertson, F. Wood, Handbook of Environmental Chemistry 2 (2005) 367-423.

[2]   D. Bahnemann, J. Cunningham, M.A. Fox, E. Pelizzetti, P. Pichat, N. Serpone In Book, Photocatalytic treatment of waters; G.R. Helz, R.G. Zepp, D.G. Crosby, Eds. 1994, p 261-316.

[3]   P. Pichat, Environmental Science and Pollution Control Series 26 (2003) 77-119.

[4]   W.S. Jenks In Book, The Organic chemistry of TiO_2 photocatalysis of aromatic hydrocarbons; V.H. Grassian, Ed.; CRC Press: Boca Raton, 2005, p 307-346.

[5]   D.F. Ollis, E. Pelizzettti, N. Serpone In Book, Heterogeneous Photocatalysis in the Environment: Application to Water Purification; N. Serpone, E. Pelizzetti, Eds.; John Wiley & Sons: New York, 1989, p 603-637.

[6]   Photocatalysis: Fundamentals and Applications; N. Serpone, E. Pelizzetti, Eds.; John Wiley & Sons: New York, 1989.

[7]   A. Fujishima, X. Zhang, D.A. Tryk, Surface Science Reports 63 (2008) 515-582.

[8]   D.C. Hurum, A.G. Agrios, K.A. Gray, T. Rajh, M.C. Thurnauer, J. Phys. Chem. B 107 (2003) 4545-4549.

[9]   D.C. Hurum, K.A. Gray, J. Phys. Chem. B 109 (2005) 977-980.

[10]   A.G. Agrios, P. Pichat, J. Appl. Electrochem. 35 (2005) 655-663.

[11]   A.G. Agrios, K.A. Gray In Book, Beyond Photocatalytic Environmental Remediation: Novel TiO_2 Materials and Applications; V.H. Grassian, Ed.; Taylor and Francis: Boca Raton, 2005, p 369-390.

[12]   I. Izumi, W.W. Dunn, K.O. Wilbourn, F.-R.F. Fan, A.J. Bard, J. Phys. Chem. 84 (1980) 3207-10.

[13]   Z. Goren, I. Willner, A.J. Nelson, A.J. Frank, J. Phys. Chem. 94 (1990) 3784-90.

[14]   Y.M. Gao, W. Lee, R. Trehan, R. Kershaw, K. Dwight, A. Wold, Mater. Res. Bull. 26 (1991) 1247-54.

[15]   J.M. Herrmann, J. Disdier, P. Pichat, A. Fernandez, A. Gonzalez-Elipe, G. Munuera, C. Leclercq, J. Catal. 132 (1991) 490-7.

[16]   D. Liu, P. Kamat, J. Phys. Chem. 97 (1993) 10769-10773.

[17]   C. Nasr, P.V. Kamat, S. Hotchandani, J. Electroanal. Chem. 420 (1997) 201-207.

[18]   S. Hotchandani, P.V. Kamat, Chem. Phys. Lett. 191 (1992) 320-6.

[19]   K. Vinodgopal, I. Bedja, P.V. Kamat, Chem. Mater. 8 (1996) 2180-2187.

[20]   C. Nasr, S. Hotchandani, P.V. Kamat, Proceedings - Electrochemical Society 97-20 (1997) 130-140.

[21]   Y.R. Do, W. Lee, K. Dwight, A. Wold, J. Solid State Chem. 108 (1994) 198-201.

[22]   G. Ramis, G. Busca, C. Cristiani, L. Lietti, P. Forzatti, F. Bregani, Langmuir 8 (1992) 1744-9.

[23]   X.Z. Li, F.B. Li, C.L. Yang, W.K. Ge, J. Photochem. Photobiol., A 141 (2001) 209-217.

[24]   J. Papp, S. Soled, K. Dwight, A. Wold, Chem. Mater. 6 (1994) 496-500.

[25]   T. Hathway, W.S. Jenks, J. Photochem. Photobiol. A 200 (2008) 216-224.

[26]   X. Li, J.W. Cubbage, W.S. Jenks, J. Photochem. Photobiol. A 143 (2001) 69-85.

[27]   D. Bahnemann In Book, Photocatalytic detoxification of polluted waters; P. Boule, Ed.; Springer: Berlin, Germany, 1999; Vol. 2 L, p 285-351.

[28]   Y.-C. Oh, X. Li, J.W. Cubbage, S. Jenks William, Appl. Catal. B: Environmental 54 (2004) 105-114.

[29]   X. Yan, T. Ohno, K. Nishijima, R. Abe, B. Ohtani, Chem. Phys. Lett. 429 (2006) 606-610.

[30]   M. Ranchella, C. Rol, G.V. Sebastiani, J. Chem. Soc. Perkin Trans. 2 (2000) 311-315.

[31]   L. Cermenati, P. Pichat, C. Guillard, A. Albini, J. Phys. Chem. B 101 (1997) 2650-2658.

[32]   L. Cermenati, A. Albini, P. Pichat, C. Guillard, Res. Chem. Intermed. 26 (2000) 221-234.

[33]   E.M. Rockafellow, X. Fang, B.G. Trewyn, K. Schmidt-Rohr, W.S. Jenks, Chem.

Mater. Revision submitted (2009).

[34]   A.K. Chakraborti, L. Sharma, M.K. Nayak, J. Org. Chem. 67 (2002) 6406-6414.

[35]   C.G. Hatchard, C.A. Parker, Proc. Royal. Soc. A 235 (1956) 518-536.

[36]   M. Fernandez-Garcia, A. Martinez-Arias, A. Fuerte, J.C. Conesa, J. Phys. Chem. B 109 (2005) 6075-6083.

[37]   J.F. Moulder, W.F. Stickle, P.E. Sobol, K.D. Bomben, Handbook of X-Ray Photoelectron Spectroscopy; Perkin-Elmer Corporation (Physical Electronics): Eden Prairie, MN, 1992.

[38]   A.G. Agrios, K.A. Gray, E. Weitz, Langmuir 19 (2003) 5178.

[39]   A.G. Agrios, K.A. Gray, E. Weitz, Langmuir 20 (2004) 5911-5917.

[40]   K. Tennakone, O.A. Ileperuma, J.M.S. Bandara, W.C.B. Kiridena, Semicond. Sci. Technol. 7 (1992) 423-424.

[41]   A.G. Agrios, K.A. Gray, E. Weitz, Langmuir 19 (2003) 1402-1409.

Chapter 4

Titanium dioxide photocatalysis: modifying the electronics of substituted biphenyls for use as mechanistic probe molecules

Timothy Hathway and William S. Jenks

1.0 Introduction

The benzene ring has been used extensively as a prototype for degradable probe molecules in titanium dioxide photocatalysis for fundamental reasons (environmental toxicity) and practical reasons. It is straightforward to functionalize and its oxidative chemistry is well established in the literature. The oxidative degradation of benzene-based compounds is often described as a competition between hydroxyl-like ($HO^{\bullet}_{ads}$) and single electron transfer (SET) chemistries.[1-11] Comparison of the product ratios of a given probe molecule, for example the ring-opened and hydroxylated products of 4-methoxyresorcinol, is one method for studying this competition.[12,13] The reactivity of such molecules can be correlated with both the electronics and the ability of the substrate to adsorb to the TiO_2 surface.[14,15] By changing these properties of the probe molecules, the balance of SET versus hydroxyl-like chemistry can be

shifted, allowing the finer mechanistic points of oxidative photocatalysis to be determined through chemical means.

In an effort to add to the list of useful photocatalyst probe molecules, we report the exploration of substituted biphenyls such that each benzene ring is functionalized to undergo either SET or hydroxyl-like chemistry. The major goal of this work is to characterize the chemistry of these probes. This will be accomplished by looking at kinetics and product formations using the well-known catalyst P25. Once the chemistry of these probes is clearly defined, we plan to use these biphenyl compounds in future work to help characterize and categorize new photocatalysts based on their reactivity with these probes.

To this end, we have chosen three similar biphenyl-based probe molecules (Figure 1): 4-biphenylcarboxylic acid (**1**), 4-phenylsalicylic acid (**2**), and 5-phenylsalicylic acid (**3**). All three molecules contain a carboxylic acid moiety, which is known to bind well to the TiO_2 surface and undergo decarboxylation after SET.[1] Each molecule also contains an unsubstituted phenyl ring. Hydroxylation of this ring is predicted to occur preferentially over the acid-bearing ring, in that the acid-bearing ring is electron deficient in comparsion.[16] The possibility also exists that the carboxyl-bearing ring will hydroxylate preferentially, since it is physically closer to the catalyst surface than the unsubstituted (more electron rich) ring.
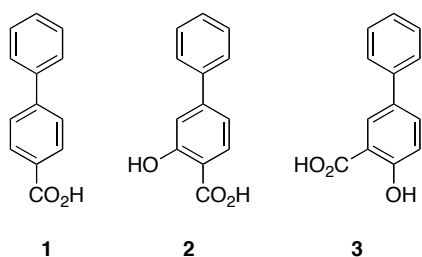
Figure 1. Biphenyl probe compounds used in this study

4-Biphenylcarboxylic acid (**1**) is used as the prototype, since it contains only the benzoic acid and benzene moieties. The reason for usng two salicylic acids, **2** and **3**, is two-fold. First, the electronics of the system change based on the relative positions of the carboxyl and hydroxyl substituents. Second, based on product studies with benzoic acid,[17] **2** is a probable hydroxylation product of **1**, and therefore the kinetics of its degradation and the favored products it forms tell us something about the secondary photocatalytic products of **1**.

The chosen biphenyl compounds can be hydroxylated in at least five unique positions when one or both ends of the molecule are functionalized. We have performed *ab initio* calculations to determine the lowest energy hydroxyl adduct, in order to correlate this with the experimental results. These computational data can be compared with experimental data to test their predictive value, which has been tried with other aromatic molecules.[18] These computations are modeled on the principle that the first step of hydroxyl radical attack leads to formation of the radical adduct. When comparing the energies of addition at each carbon on an aromatic molecule, the lowest energy product would be the kinetically favored product. Should these computed values match experimental data with some accuracy, this method would be a computationally cheap way to predict products for other molecules that would be degraded by photocatalysis (or other oxidative degradation methods).

2.0 Experimental

Materials. Compounds **1**, **1c** (Scheme 1), 4-iodobenzoic acid, 5-iodosalicylic acid, and phenylboronic acid were used as obtained from Sigma-Aldrich. 4-Iodosalicylic acid was used as obtained from Trans World Chemicals. The 2-, 3-, and 4-formylphenylboronic acids were used as obtained from Frontier Scientific.

Preparation of 2 and 3. Scheme 1 shows the general Suzuki-Miyaura coupling scheme used to form the compounds in Chart 1, with **3** used as an example.[19] To a vial, 1 equiv. (2 mmol) of aryl iodide, 1.3 equiv. of aryl boronic acid, 3.4 equiv. of $KHCO_3$ and 0.02 equiv. of $PdCl_2$ were added and dissolved in 10 mL of 4:1 DMF/H_2O. After purging with Ar for 5 min, the mixture was heated and stirred at 85°C for 24 h (or longer based on TLC). Completed reactions were acidified with 10% HCl, washed with thiosulfate to remove iodides, and then extracted into EtOAc. The organic layer was then washed with water three times to remove DMF, followed by a final washing with saturated aqueous NaCl. The organic layer was then dried over Na_2SO_4 before removal of the solvent *in vacuo*. Crude ^{1}H-NMR spectroscopy was used to look for a clean product. If little or no starting materials were present, the product was recrystallized from $EtOH/H_2O$. If aryl boronic acids persisted, column chromatography with 1:1 hexanes:EtOAc was used to remove them. The products were then eluted with 10% MeOH in EtOAc, followed by MeOH.
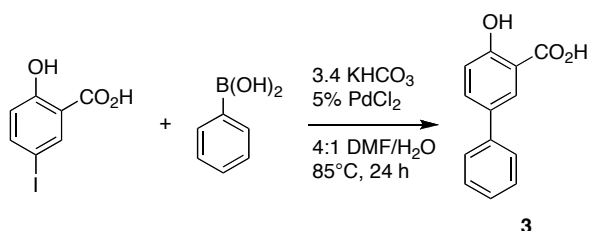
Scheme 1. Suzuki-Miyaura coupling to prepare **3**.

4-Phenylsalicylic acid (2): 238 mg (43%), unoptimized; ^{1}H-NMR (CD$_3$OD, 400 MHz) δ 7.14 (d, J = 8.4 Hz, 1H), 7.16 (s, 1H), 7.37 (t, J = 7.2 Hz, 1H), 7.44 (t, J = 7.2 Hz, 2H), 7.62 (d, J = 7.2 Hz, 2H) 7.90 (d, J = 8.4 Hz, 1 H); ^{13}C-NMR (CD$_3$OD, 400 MHz) δ 112.8, 116.3, 119.0, 128.3, 129.6, 130.1, 132.2, 141.2, 149.8, 163.6, 173.6. HRMS (M+1) 215.0708 calcd, 215.0699 observed.

5-Phenylsalicylic acid (3): 479 mg (86%), unoptimized; ^{1}H-NMR (CD$_3$OD, 400 MHz) δ 7.01 (d, J = 8.8 Hz, 1H), 7.29 (t, J = 7.6 Hz, 1H), 7.40 (t, J = 7.2 Hz, 2H), 7.53 (d, J = 7.6 Hz, 2H), 7.72 (dd, J = 8.4, 2.4 Hz, 1H) 8.08 (d, J = 2.4 Hz, 1 H); ^{13}C-NMR (CD$_3$OD, 400 MHz) δ 114.2, 118.9, 127.6, 128.2, 129.7, 130.1, 133.7, 135.3, 141.4, 162.8, 173.6. HRMS (M+1) 215.0708 calcd, 215.0704 observed.
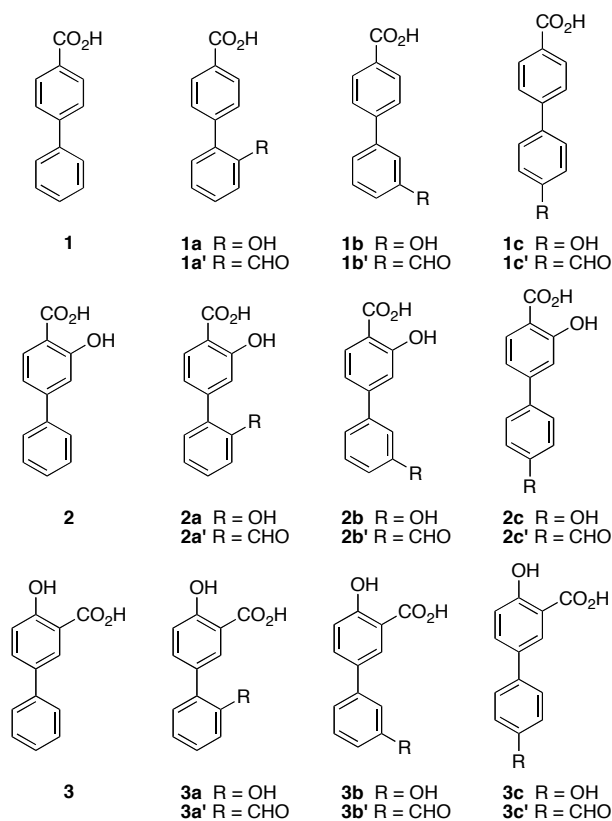
Chart 1. Compounds synthesized and/or used in this study.
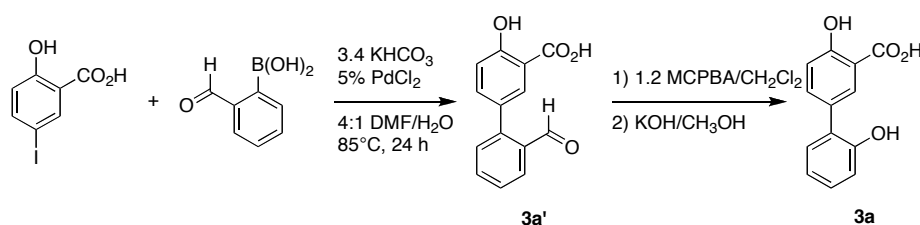
Scheme 2. Preparation of hydroxylated compounds (**3a** shown)

Preparation of hydroxylated biphenyls (1a, 1b, 2a-c, and 3a-3c). Each hydroxylated biphenyl was prepared in two steps using the appropriate formylboronic acid using the above procedure, followed by a Baeyer-Villiger oxidation of the resulting biphenyl aldehyde. The preparation of **3a** is shown as an example in Scheme 2.[20] For the oxidation, 1 equiv. (100 mg) of aldehyde, 1.2 equiv. of MCPBA and dry CH_2Cl_2 (5 mL for each mmol aldehyde) were added to a flame-dried flask and then stirred under Ar overnight. If the oxidation was not complete by TLC, it was heated to reflux for 30 min. MeOH (10 mL) and 10% KOH (10 mL) were then added and stirred for 1 h to hydrolyze the ester, and then the methanol was removed by rotary evaporation. The mixture was then acidified and extracted with ethyl acetate, followed by washes with water and saturated aqueous NaCl. The solvent was completely removed by rotary evaporation. Column chromatography was employed using 19:1 hexanes:EtOAc to remove *meta*-chlorobenzoic acid, followed by 10% MeOH in EtOAc and MeOH to elute the product, which was then recrystallized from $MeOH/H_2O$.

The ^{1}H-NMR, and ^{13}C-NMR spectra are available in Appendix 3. Two step percent yields are given, and each preparation was unoptimized. Crude ^{1}H-NMR spectral data for the aldehydes are given at the end of each entry.

2'-Hydroxybiphenyl-4-carboxylic acid (1a): 56 mg (8%); ^{1}H-NMR (CD$_3$OD, 400 MHz) δ 7.39 (d, J = 7.2 Hz, 1H), 7.42 (d, J = 8.4 Hz, 2H), 7.48 (t, J = 7.2 Hz, 1H), 7.59 (t, J = 7.6 Hz, 1H), 7.87 (d, J = 8.0 Hz, 1H), 8.04 (d, J = 8.4 Hz, 2H); ^{13}C-NMR (CD$_3$OD, 400 MHz) δ 129.0, 129.9, 130.6, 130.7, 131.1, 131.9, 132.6, 132.9, 143.0, 147.9, 169.9, 171.8; HRMS (M+1) 215.0708 calcd, 215.0720 observed. **1a'** ^{1}H-NMR (CD$_3$OD, 300 MHz) δ 7.48 (d, J = 7.0 Hz, 1H), 7.50 (d, J = 8.4 Hz, 2H), 7.56 (t, J = 7.5 Hz, 1H), 7.59 (td, J = 7.5, 1.2 Hz, 1H), 7.98 (dd, J = 7.8, 1.2 Hz, 1H), 8.11 (d, J = 8.4 Hz, 2H), 9.90 (s, 1H).

3'-Hydroxybiphenyl-4-carboxylic acid (1b): 28 mg (2%); ^{1}H-NMR (CD$_3$OD, 300 MHz) δ 7.59 (t, J = 7.2 Hz, 1H), 7.77 (d, J = 8.4 Hz, 2H), 7.92 (d, J = 7.5 Hz, 1H), 8.05 (d, J = 7.5 Hz, 1H), 8.14 (d, J = 8.7 Hz, 2H) 8.32 (s, 1H); ^{13}C-NMR (CD$_3$OD, 400 MHz) δ 126.7, 127.9, 128.9, 129.0, 130.1, 131.2, 131.8, 140.2, 144.4, 168.4; HRMS (M+1) 215.0708 calcd, 215.0710 observed. **1b'** ^{1}H-NMR (CD$_3$OD, 300 MHz) δ 7.68 (t, J = 7.2 Hz, 1H), 7.80 (d, J = 8.4 Hz, 2H), 7.94 (d, J = 7.5 Hz, 1H), 7.99 (d, J = 7.5 Hz, 1H), 8.12 (d, J = 8.7 Hz, 2H) 8.20 (s, 1H), 10.07 (s, 1H).

2',3-Dihydroxybiphenyl-4-carboxylic acid (2a): 352 mg (51%); ^{1}H-NMR (CD$_3$OD, 400 MHz) δ 6.90 (t, J = 7.2 Hz, 2H), 7.11 (d, J = 8.4 Hz, 1H), 7.14 (s, 1H), 7.18 (t, J = 7.6 Hz, 1H), 7.27 (d, J = 7.6 Hz, 1H) 7.85 (d, J = 8.4 Hz, 1H); ^{13}C-NMR (CD$_3$OD, 400 MHz) δ 112.1, 117.2, 118.8, 121.1, 121.6, 128.5, 130.5, 131.1, 131.5, 148.1, 155.6, 162.8, 173.6; HRMS (M+1) 231.0657 calcd, 231.0656. observed. **2a'** ^{1}H-NMR (CD$_3$OD, 300 MHz) δ 6.87 (t, J = 7.2 Hz, 2H), 7.24 (m, 1H), 7.37 (m, 2H), 7.62 (d, J = 7.6 Hz, 1H) 7.89 (d, J = 8.4 Hz, 1H), 9.94 (s, 1H).

3,3'-Dihydroxybiphenyl-4-carboxylic acid (2b): 15 mg (1%); ^{1}H-NMR (CD$_3$OD, 400 MHz) δ 7.17 (s, 2H), 7.58 (t, J = 8.4 Hz, 1H), 7.88 (d, J = 8.0 Hz, 1H), 7.95 (d, J = 7.6 Hz,

1H), 8.04 (d, J = 7.2 Hz, 1H), 8.28 (s, 1H); HRMS (M+1) HRMS (M+1) 231.0657 calcd, 231.0660 observed. ^{13}C-NMR (CD$_3$OD, 400 MHz) δ 116.3, 118.9, 129.4, 130.4, 130.6, 132.5, 132.8, 132.9, 141.7, 142.0, 148.1, 163.6, 169.8; **2b'** ^{1}H-NMR (CD$_3$OD, 300 MHz) δ 7.17 (s, 2H), 7.68 (t, J = 7.8 Hz, 1H), 7.96 (m, 3H), 8.19 (s, 1H), 10.07 (s, 1H).

3,4'-Dihydroxybiphenyl-4-carboxylic acid (2c): 62 mg (18%); ^{1}H-NMR (CD$_3$OD, 400 MHz) δ 6.86 (d, J = 8.4 Hz, 2H), 7.07 (d, J = 8.4 Hz, 1H), 7.09 (s, 1H), 7.48 (d, J = 8.8 Hz, 2H), 7.84 (d, J = 8.8 Hz, 1 H); ^{13}C-NMR (CD$_3$OD, 400 MHz) δ 111.9, 115.3, 116.9, 118.4, 129.4, 132.0, 132.2, 149.7, 159.3. 163.5, 173.6; HRMS (M+1) 231.0657 calcd, 231.0652 observed. **2c'** ^{1}H-NMR (CD$_3$OD, 300 MHz) δ 7.20 (m, 2H), 7.85 (d, J = 8.4 Hz, 2H), 7.93 (m, 1H) 7.98 (d, J = 8.4 Hz, 2H), 10.02 (s, 1H).

2',4-Dihydroxybiphenyl-3-carboxylic acid (3a): 217 mg (31%); ^{1}H-NMR (CD$_3$OD, 400 MHz) δ 6.83 (d, J = 8.1 Hz, 1H), 6.85 (t, J = 6.6 Hz, 1H), 6.91 (d, J = 8.7 Hz, 1H), 7.09 (t, J = 7.5 Hz, 1H), 7.18 (d, J = 8.1 Hz, 2H), 7.66 (d, J = 8.7 Hz, 1H), 8.01 (s, 1H); ^{13}C-NMR (CD$_3$OD, 400 MHz) δ 113.5, 117.0, 117.8, 121.1, 128.8, 129.5, 131.4, 131.4, 132.2, 138.0, 155.5, 162.1, 173.8; HRMS (M+1) 231.0657 calcd, 231.0654 observed. **3a'** ^{1}H-NMR (CD$_3$OD, 300 MHz) δ 7.03 (d, J = 8.4 Hz, 1H), 7.49 (m, 2H), 7.67 (t, J = 7.5 Hz, 2H), 7.82 (d, J = 2.4 Hz, 1H), 7.93 (d, 8.4 Hz, 1H), 9.91 (s, 1H).

3',4-Dihydroxybiphenyl-3-carboxylic acid (3b): 44 mg (4%); ^{1}H-NMR (CD$_3$OD, 400 MHz) δ 7.02 (d, J = 8.4 Hz, 1H), 7.53 (t, J = 8.0, 1H), 7.56 (dd, J = 8.4, 2.4 Hz, 1H), 7.82 (d, J = 7.6 Hz, 1H), 7.96 (d, J = 7.6 Hz, 1H), 8.15 (d, J = 2.4 Hz, 1 H), 8.23 (s, 1H); ^{13}C-NMR (CD$_3$OD, 400 MHz) δ 112.9, 113.5, 117.3, 127.2, 127.7, 128.4, 128.8, 130.6, 130.7, 133.0, 140.5, 161.6, 168.5; HRMS (M+1) 231.0657 calcd, 231.0648 observed. **3b'** ^{1}H-NMR

(CD$_3$OD, 400 MHz) δ 7.16 (d, J = 8.4 Hz, 1H), 7.67 (t, J = 8.0 1H), 7.95 (m, 3H), 8.00 (s, 1H), 8.19 (s, 1H), 10.05 (s, 1H).

4,4'-Dihydroxybiphenyl-3-carboxylic acid (3c): 101 mg (25%); ^{1}H-NMR (CD$_3$OD, 400 MHz) δ 6.84 (d, J = 8.8 Hz, 2H), 6.96 (d, J = 8.8 Hz, 1H), 7.39 (t, J = 8.8 Hz, 2H), 7.66 (dd, J = 2.4, 8.4 Hz, 1H), 8.01 (d, J = 2.4 Hz, 1H); ^{13}C-NMR (CD$_3$OD, 400 MHz) δ 114.7, 116.8, 118.6, 128.7, 129.0, 133.0, 133.7, 134.6, 158.1, 162.1, 173.9; HRMS (M+1) 231.0657 calcd, 231.0648 observed. **3c'** ^{1}H-NMR (CD$_3$OD, 300 MHz) δ 7.00 (d, J = 8.7 Hz, 1H), 7.46 (d, J = 6.9 Hz, 2H), 7.57 (d, J = 6.6 Hz, 2H), 7.75 (dd, J = 2.4, 8.7 Hz, 1H), 8.09 (d, J = 2.4 Hz, 1H), 9.99, (s, 1H).

Photolyses. The standard suspensions for photocatalytic reactions were prepared to result in 100 mg of TiO$_2$ per 100 mL of deionized water. To 75 mL of water was added 100 mg of P25 TiO$_2$. Sonication for five minutes was used to break up larger aggregates of TiO$_2$. As noted, the pH was adjusted to 12.0 ± 0.5 or 8.5 ± 0.5 by adding 0.1 M NaOH at the start of the reaction, then during the reaction as needed. The substrate was then added as a 25 mL aliquot from a 1 mM solution in 1% NaOH v/v in water to give a final concentration of 250 μm starting material. The mixture was then purged with O$_2$ and stirred for 30 min in the dark before the irradiation was started. Both stirring and O$_2$ purging were continued throughout the reaction.

Photolyses were carried out with stirring at ambient temperature using a modified Rayonet mini-reactor equipped with a fan and 2 x 4-watt broadly-emitting 350 nm "black light" fluorescent tubes unless otherwise noted. Reaction times were dependent on the degree of degradation required, although 25 minutes was used for kinetic runs.

After appropriate irradiation times, samples were removed and acidified by addition of Amberlite IR-120 ion exchange resin. The TiO_2 and resin were separated by centrifugation, followed by filtration through a syringe-mounted 0.2 μm PES filter. Sample sizes were 1 mL for kinetics or 50 mL for product studies. The latter, larger samples were concentrated by rotary evaporation to approximately 2 mL and the residual water was removed by lyophilization.

For GC-MS product studies, lyophilized 50 mL samples were exhaustively silylated by treatment with 1 mL of anhydrous pyridine, 0.2 mL of 1,1,1,3,3,3-hexamethyldisilazane (HMDS) and 0.1 mL of chlorotrimethylsilane.[21] Samples were vigorously shaken for 1 min, and allowed to stand 5 min at ambient temperature. The resulting pyridinium chloride precipitate was separated by centrifugation prior to chromatographic analysis.

GC-MS work was done with a standard 25 m DB-5 (5% phenyl) column for chromatography, coupled to a time-of-flight mass spectral detector. The temperature program was 130 ˚C for 2 min, followed by a ramp to 280 ˚C at 20 ˚C/min. Routine work was done on another instrument with an FID detector.

Kinetic data were obtained using HPLC (diode array UV/Vis detection) analysis of 1 mL aliquots that were acidified with Amberlite and centrifuged before injection. A standard C18 reverse-phase column was used. The eluent was a 50:50 mixture of water and acetonitrile that contained 0.1% acetic acid. The flow was 1.0 mL/min.

Photo-Fenton reactions were set up as 100 mL solutions using 25 mL of the organic probe from a 1 mM stock solution, 10 mL of a solution containing 0.05 mM Fe^{3+} (as 0.0277 g $Fe_2(SO_4)_3$ in dilute H_2SO_4), and 1 mL (92 mM) of 30% H_2O_2. A rayonet lamp using 2 x 350 nm lamps was employed for photolysis. Aliquots were taken at regular time points with a

crystal of sodium thiosulfate added to quench excess H_2O_2. These samples were directly injected into the HPLC for identification and quantification.

Computational Chemistry. All stationary state and energy calculations were performed using the GAMESS *ab initio* computational package.[22] Optimized geometries and final energies of the biphenyl, benzene, and quinoline compounds were calculated at the R(O)HF/6-31G(d) level, with ZPE and free energy corrections (at 298.15 K) added to the final energies. The optimized geometries and final energies of the quinoline compounds were also calculated at the MP2/6-31G(d)//R(O)HF/6-31G(d) level with and without using PCM for solvation in water, at the R(O)HF/6-31G(d) level and B3LYP/6-31G(d) level with PCM for water, and at the B3LYP/6-31G(d) level. The optimized energies and coordinates are available in Appendix 2.

3.0 Results and Discussion

3.1 Degradation of biphenyl compounds under TiO₂/UV conditions

Photocatalytic degradation usually follows apparent first order kinetics. However, the initial kinetics (to 20-30%) can be approximately fit to the more traditional zero-order kinetics for photochemical reactions. Since the initial chemistry is of interest, zero-order rates were obtained for the early-phase degradation of all three probe molecules (and **1c**, explained below) with photo-Fenton conditions and P25 at pH 12 and 8.5. These data are given in Table 1. Each kinetic run was duplicated, and the data was averaged. The error limits shown are standard deviations of the linear fits of these averaged data points.

The absolute rate constants, obtained with initial concentrations of 0.25 mM, depend on several parameters, including lamp intensity, sample geometry, etc. However, all physical parameters were held constant for the TiO_2 reactions, so the relative rates are meaningful. The rates from the photo-Fenton reactions can also be directly compared to one another, but there is no meaning to their absolute values in comparison to the TiO_2 reactions. The photo-Fenton reaction was used as a control reaction for hydroxylation products, since free hydroxyl radicals are presumed to be the reactive species present in this solution phase reaction.[23-25]

Table 1. Initial rates of degradation of **1**, **2**, and **3** using titanium dioxide at pH 12 and 8.5 and the photo-Fenton reaction

probe	rate of degradation (μM/min)		
	TiO_2 pH 12	TiO_2 pH 8.5	Fenton
1	15.1 ± 0.9	13.1 ± 0.7	1.4 ± 0.5
2	15.9 ± 1.0	10.7 ± 0.9	15.3 ± 1.0
3	17.2 ± 1.6	15.6 ± 0.6	14.2 ± 1.4

The rates of degradation of each probe (**1**, **2**, **3**) with P25 were relatively insensitive to pH, with a modest increase in rate going from pH 8.5 to 12. Moreover, the rate of disappearance of each substrate is very similar. The contrasting result comes from the photo-Fenton reaction of **1**, which was an order of magnitude slower, relative to those for **2** and **3**. The different patterns of observed rates for **1**, **2**, and **3** under the two sets of reaction conditions demand a

mechanistic exploration in order to explain the trends in degradation rates. To this end, the product formations of each probe must first be examined.

Three products of single hydroxylation of the distal phenyl (**a**, **b**, **c**) for each compound were synthesized and characterized both for identification and quantification. Figure 2 shows the distributions of each of these three distal hydroxylation products, interpolated from actual data to correspond to values at 10% conversion of starting material. The relative error of each product yield is confirmed to be less than 10% for each value, based on zeroth-order growth kinetics calculated in the same way as those of the rates of degradation of the biphenyl probes. The only proximal (carboxyl-bearing ring) hydroxylated product synthesized in the current work was molecule **2**, which is a possible product of **1**. No singly hydroxylated products of **2** or **3** other than the **a**, **b**, and **c** derivatives were observed based on exploratory GC-MS data after silylation of the final reaction mixture.
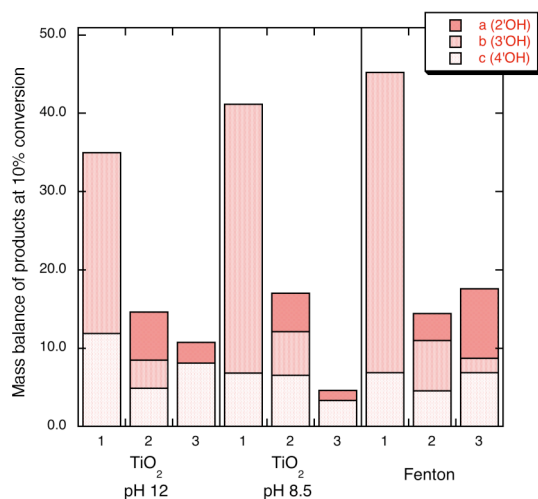
Figure 2. Mass balance of singly hydroxylated products for degradation of **1**, **2**, and **3** for photo-Fenton reactions and TiO$_2$ reactions at pH 12 and 8.5 at 10% conversion of starting material. The initial concentration of **1**, **2**, or **3** was 250 μm.

In the Fenton control reactions, the reactive species is a homogeneously dispersed hydroxyl radical. Here, compound **1b** was the predominant product formed from the degradation of **1**, although the mass balance only approaches 50%. Conspicuously missing from the products of **1** was molecule **2**, which implies that the position next to the carboxylic acid is not favorable for hydroxyl addition. When looking at the mass balance in this reaction, only 40% of the lost starting material is accounted for (within error) by **1b** and **1c** at 10% degradation. Moreover, the distal hydroxylated products of **2** and **3** were obtained in much lower concentrations for treatment of **2** and **3**, leading to an even lower mass balance for **2** and **3** (<20%). It should be noted that the HPLC traces corresponding to 10% and greater conversion yielded peaks of shorter retention times than the **a**-**c** products. Since it was a reverse-phase column, it is likely that these peaks correspond to highly polar compounds, which should be more hydroxylated than the **a**-**c** compounds. This is evidence that primary product degradation is faster than their formations. If this were true, a quantification of downstream (2° and later) products would be needed in order to attain a quantitative mass balance. The ten-fold degradation rate increase of **2** and **3** versus **1** is consistent with fast product degradation and the generally accepted notion that HO• and related species are electrophilic.

To further explore this, compound **1c** was degraded using the Fenton reaction in order to compare its degradation rate to that of **2** and **1**. Eight bulbs (instead of the normal two) were employed, and the rate of **1c** loss was $4.7 \pm 0.6 \ \mu$M/min. When this value is corrected to the light flux of two bulbs using ferrioxalate actinometry, the value drops to 0.8 μM/min. This is near the rate of **1**, but about fifty times slower than **2**. This is a surprising result considering

the reasoning above, and shows that the rate of degradation is obviously sensitive to the position of hydroxylation. As shown in Scheme 3, it is possible that **2** is formed from **1**, but degrades before it can be seen in HPLC traces of **1**. The low rate of **1c** degradation may also explain why **1b** and **1c** build up in solution compared to the products of **2** and **3.**
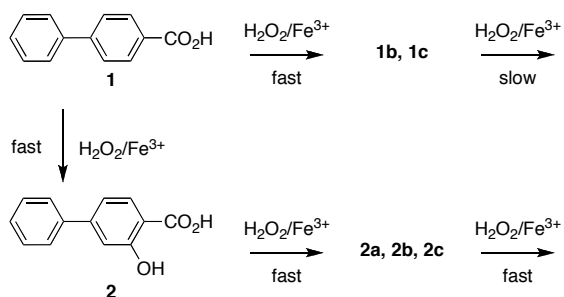
Scheme 3. Proposed Fenton degradation pathway of **1** and **2**

Regarding the ratios of **a:b:c** in the photo-Fenton reaction, it is notable that the reactivity of each probe roughly parallels that of electrophilic aromatic substitution, or other reactions where benzene is the nucleophile. This is sensible given the electrophilic nature of HO$^{\bullet}$. If **1** is considered as a benzene ring substituted by a 4-carboxylphenyl group, then the electron withdrawing nature of the distant carboxyl group would deactivate the *ortho* and *para* positions, leaving the *meta* position as the least electron poor (Figure 3). This would explain the prevalence of **1b** over **1c**, although the absence of **1a** was unexpected. For **2**, the added hydroxyl group likely counteracts the electron withdrawing properties of the carboxyl group, making the *ortho* and *para* positions (leading to **2a** and **2c)** more reactive toward hydroxyl radicals. For **3**, the two substituents switch places, and the *ortho* and *para* positions are even more activated, leading **3a** and **3c** to predominate over **3b**, if only slightly. The use of

electrophilic substitution as a model for hydroxyl radical addition has been used before to compare singly substituted benzenes with varying electronic properties that were partially degraded by titanium dioxide.[26]
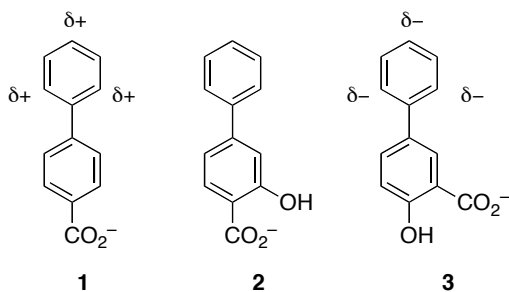
Figure 3. Electronic effects of the proximal substitution on the electronics of the distal ring for **1**-**3**. The protonation states for each molecule at pH 8.5 are shown, with the carboxyl group (pK_a ~4) dissociated, and the hydroxyl group (pK_a ~14) still intact.

The product ratios of **1-3** for titanium dioxide photocatalysis at high pH values (8.5 and 12) yielded similar results as the photo-Fenton reaction. In fact, product **3b** was not observed in measurable amounts in the TiO_2 reactions. However, the degradation rates of **1**, **2**, and **3** were not differentiated substantially. The ratios of hydroxylated products were very similar to that of the Fenton reactions, and **2** still does not appear as a product of the degradation of **1**. When **1c** was degraded with TiO_2 at pH 12, the rate was 8.4 ± 0.7 μM/min. Again, it is apparent that the degradation rate **1c** is less than that of **2** (as shown for the Fenton reaction in Scheme 3), although only by a factor of two, showing that the products of **1** likely don't degrade as quickly as those of **2** and **3**. Much like the Fenton results, it appears that **2a-c** and **3a-c** degrade more quickly than **1b-c**.

Downstream products from **1** at 50% degradation using TiO_2 (Figure 4) were identified (but not quantified) by GC-MS and include benzoic acid, phenol, 2-phenylmalonic acid, and at least one hydroxybenzoic acid (as compared with standards), as well as **1b** and **1c**. Compound **2** was also identified in a minute concentration compared to **1**, **1b**, and **1c**. Multiple lines of evidence are available to explain these product mixtures.

Biphenyl was considered as a possible product of degradation of **1**. In studies of benzoic acid (which can be considered a model for **1**) and hydroxylated derivatives, benzene has yet to be identified as a product of direct or indirect oxidation.[1,6,27] We were not surprised when biphenyl was not observed in the product mixture of **1**, so biphenyl was ruled out as a possible product. In many of these studies, benzoic acid was hydroxylated up to three times (to form 2,4,6-trihydroxybenzoic acid), and no other benzene ring-based products were detected or identified, so it was presumed that ring-opening occurred next.[27,28] Since all biphenylcarboxylic acids (**1**-**3** and the **a**-**c** products of each) in the present study contain a benzoic acid moiety, ring-opening reactions from these would lead to products containing the non-carboxylated ring plus additional oxidized carbons (like phenylmalonic acid).[29] We infer that the benzoic (and hydroxybenzoic) acid formed in the current study was produced from decarboxylation of **1**-**3**, followed by ring-opening and subsequent degradation of the carboxyl-bearing ring, and that secondary steps are faster than distal hydroxylation[1]. Earlier (less degraded) ring-opened products (Scheme 3) were not identified in the mixture. This is unfortunate, as these products would give a more detailed picture of the initial mechanism of the degradation of the carboxyl-bearing end of the biphenyl probes.
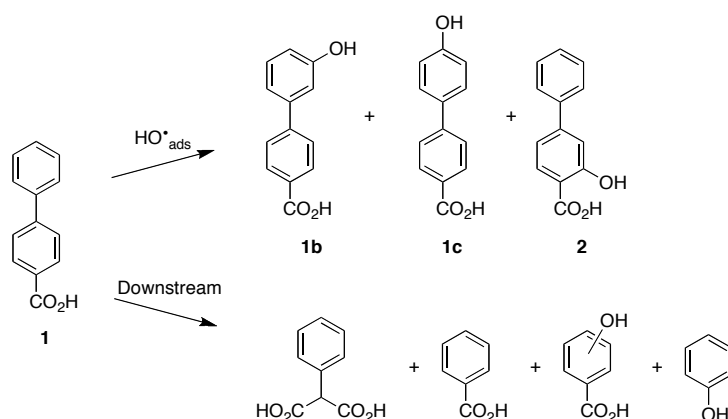
Figure 4. Products of the degradation of **1** at pH 12 as identified by GC-MS

To summarize, the rates of TiO_2-induced degradation of **1**-**3** are very similar, but in the photo-Fenton results, **1** degrades an order of magnitude more slowly than **2** and **3**. Product yields and the degradation rate of **1c** show that the products of **1** exist in higher concentration than those of **2** and **3**. In addition, downstream product studies of the TiO_2 degradation show that ring-opening products of **1** are being formed in addition to hydroxylated products. In order to explain these trends, a discussion of TiO_2 surface reactions needs is warranted, since heterogeneous (TiO_2) and homogenous (Fenton) catalysis operate fundamentally differently.

The primary reactive species in the Fenton reaction is a homogenously dispersed hydroxyl radical. Titanium dioxide is well-known throughout the literature as a source of hydroxyl radical or a related species, but it is either created at or adsorbed to the surface of the photocatalyst.[7,30] In addition to HO• addition, another mechanism is at work on the TiO_2 surface that is not established in Fenton reactions, single electron transfer (SET) from the organic molecule to the photocatalyst.[31] In reactions involving catechol derivatives, there is evidence that the addition of dissolved oxygen to the reaction mixture leads to the aromatic ring-opening after SET occurs.[12] *Ortho*-dihydroxylated rings are apparently susceptible to

C=C cleavage by an oxidative pathway presumably via oxetane formation and ring-opening.[12]

Although molecules **1**-**3** do not contain *ortho*-dihydroxylated rings, it is plausible that they are able to undergo an analogous SET-induced ring-opening aided by oxygen, as shown in Scheme 5. Electron transfer from aromatic rings is thought to require a moiety that can adsorb to the TiO_2 surface, and molecules like benzoic and salicylic acid are known to bind to the surface, much like the catechols.[15,32,33] Surface-bound substituted biphenyls (including **1**) have been studied specifically for their ability to inject electrons into the TiO_2,[32,34,35] which is solid evidence that SET is occurring for **1**-**3**.

Decarboxylation of **1** and related derivatives is likely to occur, which eventually leads to downstream products like phenylmalonic acid through a mechanism resembling the early steps of a Photo-Kolbe reaction (Scheme 6).[1] The resulting biphenyl radical then reacts with O_2 (which is purged throughout the reaction) before a suitable hydrogen donor is available to form biphenyl.
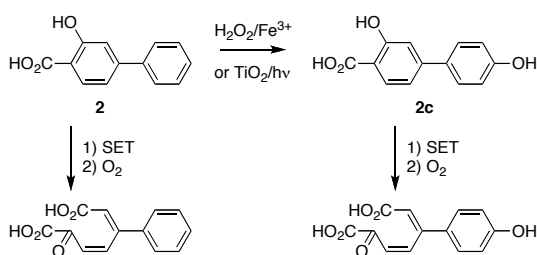
Scheme 5. Reaction cascade for **2** and **2c** leading to proposed ring-opened products
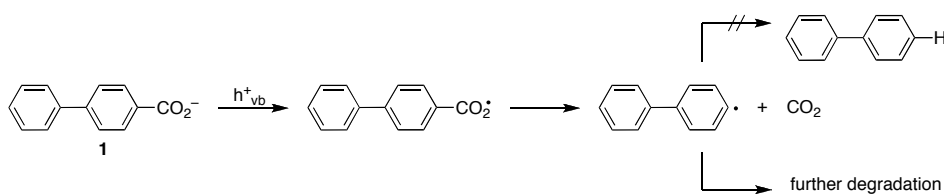
Scheme 6. Photo-Kolbe decarboxylation of **1**.

The Fenton reaction of **1** yields hydroxylated products that accumulate compared to those products of **2** and **3**. When titanium dioxide photocatalysis is utilized instead, the rates of conversion for all of these compounds become similar. This is due to the involvement of SET–initiated chemistry (Schemes 5 and 6) at the titania surface, which opens another pathway in which the recalcitrant molecules can react. This SET mechanism is also supported by the occurrence of products obtained from ring-opening of the carboxyl-bearing ring of **1**.

These relatively clear mechanistic trends, especially for **1**, indicate that these biphenyl probe molecules are selectively oxidized based on the moiety attached to each ring. The proximal carboxyl-bearing ring tends to undergo SET and degrade by ring opening, and the unsubstituted distal ring undergoes hydroxylation at positions determined by the electronics of the entire system. By slightly tweaking the electronics of **1** to make **2** and **3**, the hydroxylation rates and product ratios change markedly.

3.2 Computational Work

Of interest to chemists is the ability to predict and help explain the reactivity of molecules using computational chemistry. To this end, we hope to predict which addition products will

be the most prevalent in the TiO_2-photocatalyzed degradation of the biphenyl probes. Computational studies were performed in order to compare the relative addition energies of HO[.] for each addition point among the three biphenyl molecules.

Quinoline was used as a test case in order to compare computational results to experimental data, such as that from a γ-radiolysis study performed by Wiest and Kamat in which HO[.] formed from water directly attacked dissolved quinoline and the rate of formation of each hydroxylated product was determined.[36] The same group performed computations on this quinoline system that invoked both solvation and transition state calculations.[37] Their computational method was more rigorous than the current method, since the activation barrier derived from a transition state calculation would better describe which addition point would be most favorable, especially if an intermediate is involved between the starting material and hydroxylated adduct and not just a single transition state. However, searching for transition state structures is not trivial, and can be both computationally expensive and time intensive. Our method instead requires calculations of minima only for quinoline and each radical adduct.

The HO[.] addition energies were calculated at each carbon of quinoline using an isodesmic reaction like the one shown in Equation 1 in order to minimize systematic errors. In Table 2, addition energies (ΔE of HO[.] addition, defined as the electronic energy plus the zero point correction) are tabulated along with the point charges of each carbon in quinoline. The experimental rank shown in the table is defined as the comparative rate of formation of each compound, where the highest rank is the hydroxylated product with the highest relative rate of formation. These rankings are taken from the γ-radiolysis experimental data of Wiest and Kamat.[36] The absolute values of the addition energies are meaningless in terms of

comparison to experimental values, but the relative energies are regarded as the valuable information. In addition, the Mulliken charges of each carbon in quinoline were used as point charges in order to estimate the electron density at each addition point.

As an extension, electron correlation and solvent effects were taken into account as shown in Table 2. The PCM, B3LYP, and PCM+MP2 were re-optimized (from the R(O)HF geometries) for water solvation (PCM & PCM+MP2) or DFT (B3YLP). The R(O)HF+MP2 and PCM+MP2 columns involve MP2 single point energies of each optimized structure in order to recover some electron correlation.
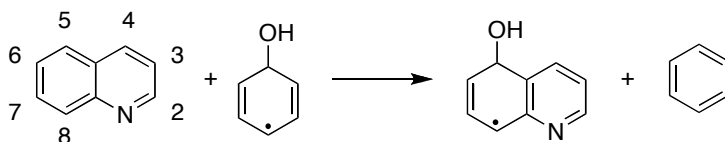
Equation 1. Isodesmic reaction involving the transfer of HO$^{\bullet}$ from benzene to quinoline. The C5-addition adduct of quinoline is shown as an example.

Based on the calculations, 5- and 8-hydroxyquinoline would form the most favorably: large negative point charges are found at these positions in quinoline, and the adduct formation is also the most favorable. This turns out to parallel the experimental result. The formation of 2-hydroxyquinoline was not detected in the radiolysis studies, and, looking at computed values, this makes sense since that carbon is slightly positive, which would not be favorable for an electrophile like HO$^{\bullet}$ to attack. The other positions seem to follow this trend as well.[36] These results also correlate well with Fenton reactions of quinoline.[23]

Table 2. Calculated energies of HO• addition (in kcal/mol) and point charges for each carbon of quinoline, including a ranking of the experimental rates of formation of each product derived from attack at that point.

addition point	ΔE of HO• addition (kcal/mol)					point charge		expt. rank[36]
	R(O)HF	PCM	B3LYP	MP2	PCM +MP2	quinoline	[quinoline•+]	
2	-5.4	-5.3	-2.7	3.1	3.5	0.01	0.12	-
3	-5.5	-5.9	-2.8	-1.1	-1.1	-0.20	-0.26	3
4	-6.3	-6.5	-5.9	-4.5	-4.7	-0.15	-0.08	5
5	-9.4	-7.5	-7.7	-8.3	-9.4	-0.19	-0.09	2
6	-6.3	-6.4	-3.0	-1.5	-1.4	-0.17	-0.18	4
7	-6.0	-6.3	-2.4	-0.4	-0.5	-0.18	-0.18	4
8	-8.4	-7.4	-8.4	-9.8	-9.7	-0.15	-0.07	1

In order to attempt to improve upon the accuracy of the R(O)HF calculations without greatly increasing the computational cost, MP2 single point energies were calculated at the R(O)HF geometries. The MP2 calculations show a more direct correlation between addition energy and experimental rank. For example, the energy difference between the 2 and the 5 and 8 positions are much larger in the MP2 calculations, with a 13 kcal/mol difference versus the 3 kcal/mol difference calculated by simple R(O)HF. Since both the RHF and MP2 energies are relatively cheap computationally, both levels of theory can be considered acceptable for this method. The PCM calculations shown in Table 2 include solvent interactions of the quinoline molecule with water. On top of the MP2 calculations, this

solvation method made little difference (0.1 – 0.4 kcal/mol) on the calculated ΔE, so it was deemed unnecessary.

Although solution-phase hydroxylation by γ-radiolysis or Fenton chemistry is qualitatively predicted by the current method, heterogeneous catalysis is another matter. The effect of quinoline binding to the titanium dioxide surface changes the electronics of the molecule. Below the pK_a of the quinoline (pH 4.5), quinolinium$^+$ (protonated quinoline) is the dominant quinoline species in aqueous solution of quinoline. In titanium dioxide photocatalysis at pH 6, quinoline is thought to bind to the surface specifically through a surface to N bond, yielding an electronic structure that is formally quinolinium$^+$.[23] Table 3 shows the HO$^•$ addition energies and point charges for quinolinium$^+$, as well as an experimental ranking based on results obtained for TiO_2 photocatalysis at pH 6 by the Pichat group.[23] Compared to quinoline, the main difference is that the 2 position has an addition energy comparable to the 5 and 8 positions, even though the point charge of the 2 carbon is still comparatively positive. The computational results do not agree as well with the experimental data in this case, since the C4 position has neither the most exothermic ΔE nor the most negative point charge. It is likely that quinolinium$^+$ is not the correct model for HO$^•$ addition calculations.
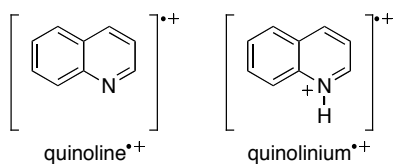
Scheme 7. Structures of quinoline and quinolinium radical cations

Table 3. Calculated energies of HO˙ addition (in kcal/mol) and point charges for each carbon of quinolinium at the MP2/6-31G(d)//RHF/6-31G(d) level, including a ranking of the experimental rates of formation of each product derived from attack at that point from TiO_2 photocatalysis at pH 6.

addition point	ΔE of HO˙ addition	point charge quinolinium$^+$	[quinolinium$^{˙+2}$]	expt. rank[23]
2	-9.7	0.10	0.23	2
3	7.0	-0.20	-0.29	-
4	-1.4	-0.11	0.00	1
5	-8.9	-0.18	-0.06	3
6	1.2	-0.14	-0.09	-
7	0.0	-0.18	-0.20	-
8	-9.5	-0.16	-0.08	-

With the hydroxyl reactivity predicted successfully by computations, the SET reactivity of quinoline should be considered in more depth. After injecting an electron into the titanium dioxide surface, the quinoline radical cation can react with a nearby species. The positive charge could attract nucleophiles, especially at the 2 and 4 positions based on the data in the quinoline$^{˙+}$ and quinolinium$^{˙+2}$ columns of Tables 2 and 3 respectively. The structures of quinoline$^{˙+}$ and quinolinium$^{˙+2}$ are shown in Scheme 7. In aqueous TiO_2 photocatalysis at pH 6, it has been proposed that the 2- and 4-quinolinone products present in product mixtures are mainly due to superoxide addition and subsequent oxygen loss.[23] Since SET from quinoline (or any aromatic) normally requires binding to the TiO_2 surface, the proposed quinolinium$^+$

model would best represent a surface-bound quinolinium that has been oxidized, and awaits reaction from a nucleophile like water. The relative lack of hydroxyl addition products in TiO$_2$ reactions at pH 6 (2.5 nmol) compared to pH 3 (26 nmol) or Fenton reactions confirms that the positive charge of the radical cation lowers the incidence of electrophilic radical attack, at least in part.[23] Therefore, the computations better explains SET reactivity in this case, where both the C2 and C4 positions are calculated to have positive point charges (especially for quinolinium[•+]), which would favor nucleophilic attack by water.

It is clear that this proposed computational method is adequate in order to shed light on the experimental ratios of quinoline products, if only qualitatively. This method was therefore extended in order to verify the assumptions made earlier about the reactivity of hydroxyl radical with the biphenyl probes, where the electronics of each system are dependent on the placement of the acid and the hydroxyl group.
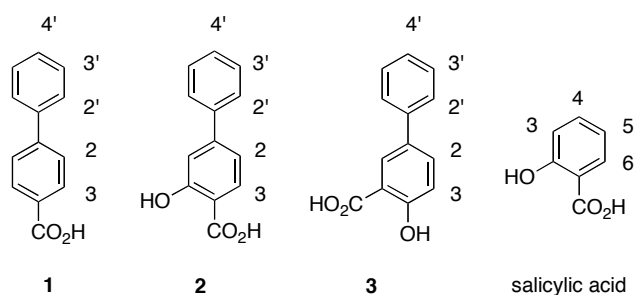
Scheme 8. Addition points for each biphenyl molecule and salicylic acid.

Table 4 shows the calculated addition energies and point charges for each hydroxyl adduct of the biphenyl compounds illustrated in Scheme 8. Equation 2 shows an example of an isodesmic reaction used to calculate the addition point energies in Table 4. The addition

points are numbered in relation to the biphenyl tether, as noted in Scheme 8. The numbering is based on the C1 and C1' positions being the two linking carbons in the biphenyl system. Based on the calculated addition energy values, the C4' ("**c**") position on all three probes appears to be the most feasible position of attack for HO$^{\bullet}$. The C3 positions on **2** and **3** are also exothermic, which is similar to results from previous studies with salicylic acid degradation by TiO$_2$.[6] For salicylic acid, the hydroxylations experimentally occurred at the 4 and 6 positions (C3, C2' and C4' on **2** and **3**), as well as 4,6-dihydroxylation. The C2' ("**a**") and C3' ("**b**") products follow, and the C2 adduct is the least likely to be hydroxylated, since it has the most positive addition energy for each of the three probes. Based on the point charges, we predict that the C3 position is less likely to be attacked by an electrophile (with the exception of **3**, which has reversed electron demand compared to **1** and **2**).
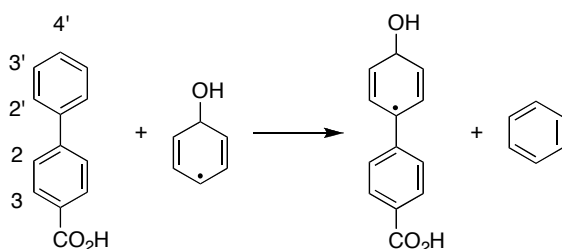
Equation 2. Isodesmic reaction involving the transfer of HO$^{\bullet}$ from benzene to **1**. The C4'-addition adduct of **1** is shown as an example.

Table 4. Calculated energies of HO• addition (in kcal/mol) and point charges for each carbon of **1**, **2**, and **3** in both neutral and radical cation forms. All structures and energies were calculated at the R(O)HF/6-31G(d) level. Illustrations of the addition points are shown in Scheme 8.

addition point	molecule	ΔE of HO• addition	point charge
C3	**1**	0.22	-0.17
	2	-1.40	-0.17
	3	-2.19	-0.24
C2	**1**	1.47	-0.23
	2	1.57	-0.24
	3	0.60	-0.18
C2'	**1**	0.39	-0.21
	2	0.44	-0.21
	3	0.16	-0.22
C3'	**1**	0.38	-0.20
	2	0.37	-0.20
	3	0.55	-0.20
C4'	**1**	-1.39	-0.20
	2	-1.44	-0.20
	3	-1.00	-0.22

It is interesting to note that, relative to quinoline, most of the addition energies on the biphenyl compounds are relatively endothermic. The point charges for all of the carbons are very similar, suggesting that selective hydroxylation will more likely be determined by

thermodynamics, and not by electronics. Also, the average energy difference between addition points at R(O)HF/6-31G(d) (~1 kcal/mol) is comparable to the quinoline calculations, which means that results may be more clear if MP2 single point energies had been used, much like in the quinoline case.

Taking all of the R(O)HF calculation data into account, it appears that the addition energies don't adequately predict the experimental trends of Fenton or TiO_2 reactions for **1a**-**1c** (Figure 2), since the calculated addition energy of **1c** (C4' adduct) has the most exothermic energy.

The results for **2** and **3** are more in line with the experimental data, since **2c** and **3c** are the most common intermediates. For **2a** and **2b**, the addition energies are very similar (0.44 and 0.37 kcal/mol), and experimentally they show up in equal concentrations. For **3a** (0.16 kcal/mol) and **3b** (0.55 kcal/mol), the experimental result that **3b** shows up in the lowest concentration is verified by the most endothermic addition energy.

It should be again stressed that these calculations are very simple, and therefore more rigorous methods (like MP2 for single point energies) may be useful in order to yield more directly predictive values, since the computational trends for the biphenyls are not as clear as the trends for quinoline. Although this computational method is reasonably fast, more work must be done to successfully extend this method to other systems in order to confirm or deny its predictive value.

4.0 Conclusions

Based on these product and kinetic studies, molecules **1**-**3** present a rich mechanistic chemistry. Especially for **1**, the ability of the proximal ring to preferentially degrade by SET and the ability of the distal ring to primarily degrade by hydroxylation allows for clear identification of which processes are occurring when a given photocatalyst is employed. Therefore, these probes can be used in order to chemically characterize titania or other photocatalysts where reactivity of the catalyst is unknown or under question, which is important with the plethora of new catalysts being presented in journals every year.

In addition, the computational method proposed in this paper contains some predictive value for the hydroxylation of simple aromatic systems like quinoline. The verification of experimental biphenyl hydroxylation data was not as successful though, so more work refining this method must ensue before it can be widely applied.

References

(1)   Izumi, I.; Fan, F.-R. F.; Bard, A. J. *J. Phys. Chem.* **1981**, *85*, 218-223.

(2)   Okamato, K.-i.; Yamamoto, Y.; Tanaka, H.; Tanaka, M.; Itaya, A. *Bull. Chem. Soc. Japan* **1985**, *58*, 2015.

(3)   Fox, M. A. *Chem. Rev.* **1993**, *93*, 341-357.

(4)   Legrini, O.; Oliveros, E.; Braun, A. M. *Chem. Rev.* **1993**, *93*, 671-698.

(5)   Mallard-Dupuy, C.; Guillard, C.; Courbon, H.; Pichat, P. *Environ. Sci. Technol.* **1994**, *28*, 2176-2183.

(6)   Mills, A.; Holland, C. E.; Davies, R. H.; Worsley, D. *J. Photochem. Photobiol. A* **1994**, *83*, 257-263.

(7)   Hoffmann, M. R.; Martin, S. T.; Choi, W.; Bahnemann, D. W. *Chem. Rev.* **1995**, *95*, 69-96.

(8)   Linsebigler, A. L.; Lu, G.; Yates Jr., J. T. *Chem. Rev.* **1995**, *95*, 735-758.

(9)   Sun, Y.; Pignatello, J. J. *Environ. Sci. Technol.* **1995**, *29*, 2065-2072.

(10)   Li, X.; Cubbage, J. W.; Jenks, W. S. *J. Org. Chem.* **1999**, *64*, 8525-8536.

(11)   Li, X.; Cubbage, J. W.; Tetzlaff, T. A.; Jenks, W. S. *J. Org. Chem.* **1999**, *64*, 8509-8524.

(12)   Li, X.; Cubbage, J. W.; Jenks, W. S. *J. Photochem. Photobiol. A* **2001**, *143*, 69-85.

(13)   Hathway, T.; Jenks, W. S. *J. Photochem. Photobiol. A* **2008**, *200*, 216-224.

(14)   Cunningham, J.; Al-Sayyed, G.; Srijaranai, S. In *Aquatic and Surface Photochemistry*; Helz, G. R., Zepp, R. G., Crosby, D. G., Eds.; Lewis Publishers: Boca Raton, 1994, p 317-348.

(15)   Tunesi, S.; Anderson, M. *J. Phys. Chem.* **1991**, *95*, 3399-3405.

(16)   Witte, F.; Urbanik, E.; Zetsch, C. *J. Phys. Chem.* **1986**, *90*, 3251-3259.

(17)   Matthews, R. W. *J. Chem. Soc.* **1984**, *80*, 457-471.

(18)   DeMatteo, M.; Poole, J.; Shi, X.; Sachdeva, R.; Hatcher, P.; Hadad, C.; Platz, M. *J. Am. Chem. Soc* **2005**, *127*, 7094-7109.

(19)   Waldo, J. P.; Larock, R. C. *Org. Lett.* **2005**, *7*, 5203-5205.

(20)   Fujishiro, K.; Mitamura, S. *Bull. Chem. Soc. Japan* **1988**, *61*, 4464-4466.

(21)   Sweeley, C. C.; Bentley, R.; Makita, M.; Wells, W. W. *J. Am. Chem. Soc.* **1963**, *85*, 2497-2507.

(22)   Gordon, M. S.; Schmidt, M. W. In *Theory and Applications of Computational Chemistry, the first forty years*; Elsevier: 2005.

(23)   Cermenati, L.; Pichat, P.; Guillard, C.; Albini, A. *J. Phys. Chem. B* **1997**, *101*, 2650-2658.

(24)   De Laat, J.; Gallard, H. *Environ. Sci. Technol* **1999**, *33*, 2726-2732.

(25)   Pignatello, J. *Environ. Sci. Technol.* **1992**, *26*, 944-951.

(26)   Palmisano, G.; Addamo, M.; Augugliaro, V.; Caronna, T.; Dipaola, A.; Lopez, E.; Loddo, V.; Marci, G.; Palmisano, L.; Schiavello, M. *Catal. Today* **2007**, *122*, 118-127.

(27)   Velegraki, T.; Mantzavinos, D. *Chem. Eng. J.* **2008**, *140*, 15-21.

(28)   Benoit-Marquie, F.; Puech-Costes, E.; Braun, A. M.; Oliveros, E.; Maurette, M. T. *J. Photochem. Photobiol. A* **1997**, *108*, 65-71.

(29)   At least one salicylic acid isomer was detected by GC-MS, leading us to believe that hydroxylation of the distal ring is possible before ring-opening occurs.

(30)   Li, X.; Jenks, W. S. *J. Am. Chem. Soc.* **2000**, *122*, 11864-11870.

(31)   Goldstein, S.; Czapski, G.; Rabani, J. *J. Phys. Chem.* **1994**, *98*, 6586-6591.

(32)   Tachikawa, T.; Tojo, S.; Fujitsuka, M.; Majima, T. *Langmuir* **2004**, *20*, 2753-2759.

(33)   Tunesi, S.; Anderson, M. A. *Langmuir* **1992**, *8*, 487-495.

(34)   Tachikawa, T.; Tojo, S.; Fujitsuka, M.; Majima, T. *Chem. Phys. Lett.* **2004**, *392*, 50-54.

(35)   Tachikawa, T.; Fujitsuka, M.; Majima, T. *J. Phys. Chem. C* **2007**, *111*, 5259-5275.

(36)   Nicolaescu, A. R.; Wiest, O.; Kamat, P. V. *J. Phys. Chem. A* **2005**, *109*, 2822-2828.

(37)   Nicolaescu, A. R.; Wiest, O.; Kamat, P. V. *J. Phys. Chem. A* **2005**, *109*, 2829-2835.

Chapter 5

General Conclusions

1.0 Conclusions

The photocatalytic degradation of organic molecules using titanium dioxide was investigated in this work. More specifically, the initial mechanistic steps of these degradations were studied in order to characterize the reactivity of the titanium dioxide catalyst, and to study the chemistry of the probes themselves. Using both kinetic rates of degradation and the ratios of products formed, the mechanistic details of hydroxyl-like chemistry and single electron transfer (SET) chemistry could be explained.

In Chapter 2, *para*-anisyl-1-neopentanol (AN) and 4-methoxyresorcinol (MR) were employed in order to determine the effect of photocatalyst particle size on the degradation of organic molecules. Using the Millennium PC series of anatase catalysts that ranged from 5 to 100 nm in primary particle size, the kinetic rates of degradation, product ratios, and adsorption properties of AN and MR were compared. These data were compared to data obtained with Degussa P25, a well-understood commercial catalyst. It was determined that the degree of sintering that led the 5 nm catalyst to be transformed into the other three larger catalysts (10, 50, and 100 nm) had no significant effect on the reactivity or adsorption properties of the molecules. The data itself showed no meaningful trends in reactivity among the series of catalysts, where only slight differences in reaction rate were observed. The

product ratios obtained from all five tested catalysts were the same, showing that the reactivity of anatase catalysts between 5 and 100 nm was not significantly different from that of P25, which has a primary particle size of ~35 nm. The major takeaway from this work was that supposed particle size effects in this regime were insignificant, but on the positive side, the probe molecule AN was characterized for its SET and hydroxyl-like chemistries. The stark differences in the product mixtures of AN for these two mechanisms led us to believe that this probe molecule would be ideal as a probe molecule for later studies.

In Chapter 3, the reactivity of tungsten-modified titanium dioxide catalysts was investigated. The modification of titania in order to produce visible light absorption, as well as other forms of increased activity is a very active area of current research. Lacking in many of the current catalyst studies are careful investigations of the organic chemistry induced by these catalysts, since the real utility of these catalysts is determined by whether or not they can degrade organic molecules as efficiently as unmodified TiO_2, which mineralizes most compounds in UV light. Tungstated catalysts were prepared as directed from a recent paper that proposed a sol-gel based W-doping that led to strong visible light activity and otherwise superior degradative ability. Using a combination of quinoline (Q), AN, and careful physical characterizations (XPS, DRS, XRD), we determined that W-doping was only of value when the WO_x was coated on the surface of the catalyst, based on studies with a commercial surface-doped catalyst (DT52). In the sol-gel doping method, the tungsten centers was evenly dispersed throughout the catalyst and offered no special increase in reactivity compared to pristine TiO_2. In addition, the visible-light-absorbing effects mentioned in the original paper could not be reproduced in either type of catalyst, which led to the belief that any visible light absorption was an artifact of catalyst preparation, and not an intrinsic property of the mixed

photocatalyst. In effect, this study emphasized the need for careful physical organic studies of new photocatalyst formulations, so that successful catalysts are further pursued. In addition, failed catalysts need to be studied so that considerations for why they failed are taken when newer generations of catalysts are planned.

Finally, the aim in Chapter 4 is shifted from characterizing new photocatalysts to that of new molecular probes. In order for new catalysts to be tested as completely as possible, a large bank of probe molecules with differing structural and electronic properties is needed. Chapter 4 proposes the use of biphenylcarboxylic acids (referred to as biphenyl probes) to add to the ranks of molecules like MR, AN, and Q. The perceived advantage of these probes is an extension of the reactivity of Q, where hydroxyl-like chemistry led to substitution on the non-N-bearing ring, whereas the SET-derived products were those involving substitution on the N-bearing ring. The biphenyl probes were hypothesized to yield hydroxylation products primarily on the unsubstituted ring, whereas SET products were derived from reactivity of the carboxyl-bearing ring. Indeed, the identification of both primary hydroxylation products and downstream SET ring-opened products confirmed these hypotheses. 4-Biphenylcarboxylic acid (**1**) was especially sensitive to oxidative conditions, and compared to the more electron rich compounds. Molecule **1** showed a marked decrease in reactivity rate under Fenton conditions, where SET-initiated reactions are not known to occur. The sensitivity of these molecules to their oxidative environment makes them ideal when trying to study the degradative capabilities of new photocatalysts and other oxidative methods.

This study also proposed the use of a cheap, but rigorous, computational method that could be used to predict the product ratios of both hydroxyl-like and SET chemistries for any given

molecule. This method consisted of calculating the energies of hydroxyl-radical adducts and point charges of a given molecule, and then determining which positions were the most reactive. This method successfully verified the hydroxylation chemistry and SET-initiated chemistry of quinoline, as well as yielding the same qualitative answer as more rigorous but time-consuming calculations. This method was then applied to the biphenyl probes, whose reactivities were not as well explained by this method, especially for **1**, which means more work needs to be done before this method can be extended to a wider variety of systems.

Appendix 1: Supporting Information for Chapter 2

Degradation of organic molecules using tungsten-doped titanium dioxide catalysts with visible light: kinetic and mechanistic effects using multiple catalyst doping strategies

Timothy Hathway, Erin M. Rockafellow, Youn Chul-Oh and William S. Jenks

Table of Contents

SEM Images

SEM data (Figures S1-S5) were collected as mentioned in the experimental section. The homemade W-TiO$_2$ samples were imaged after annealing and ball-milling. The pictures shown below were chosen as "average" representations of each catalyst, taken at 3,000 times magnification.

Figure S1. SEM image of the 0% WO$_x$ catalyst.
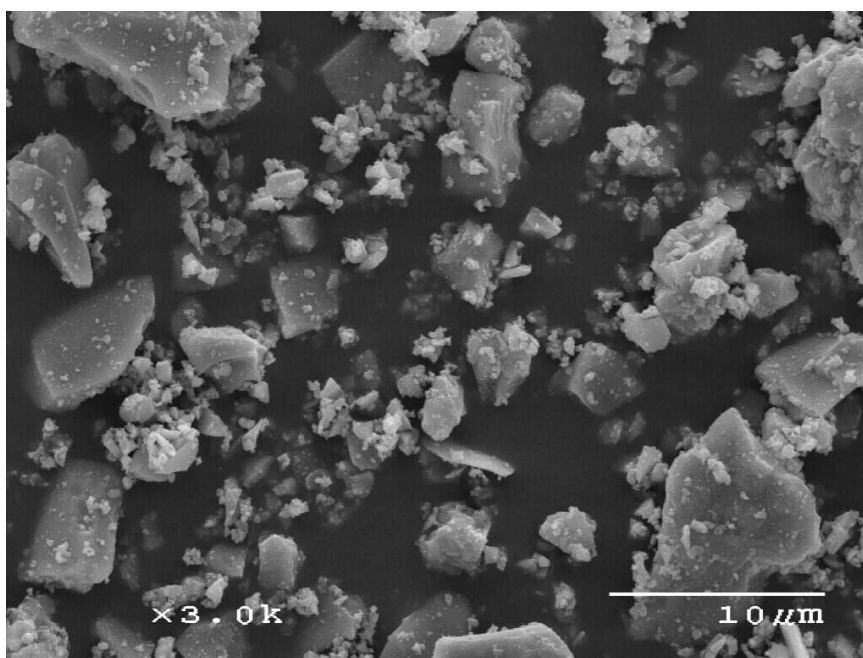
Figure S2. SEM image of the 1% WO$_x$ catalyst.
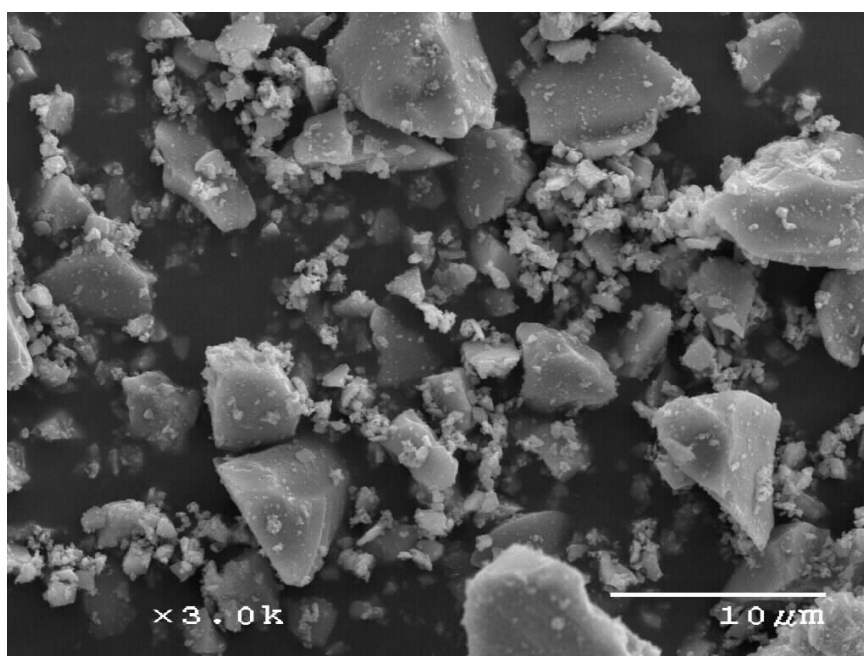
Figure S3. SEM image of the 3% WO$_x$ catalyst.
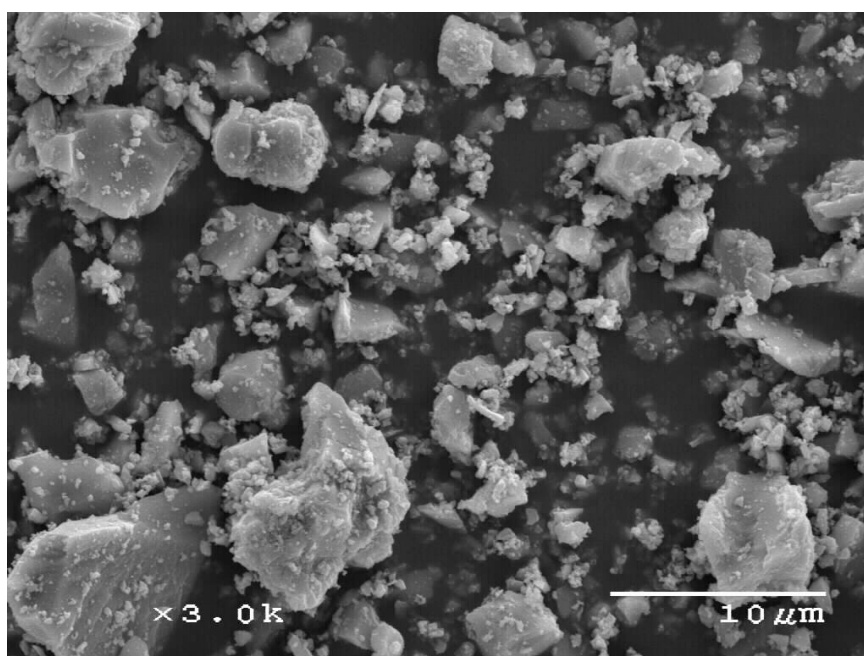
Figure S4. SEM image of the 5% WO$_x$ catalyst.
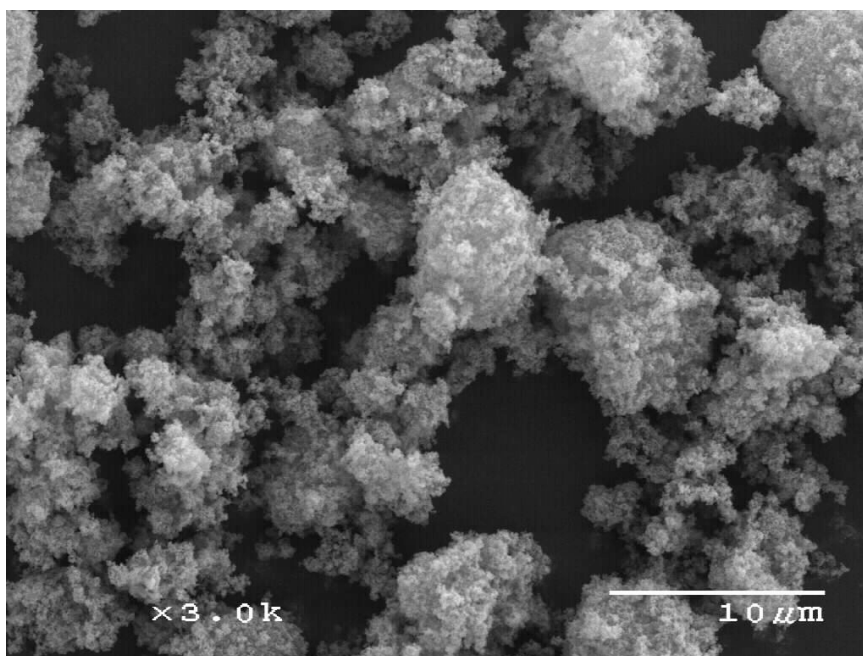
Figure S5. SEM image of the P25 catalyst.

SEM-EDX Maps

SEM-EDX data (Figures S6-S10) were collected as mentioned in the experimental section. The homemade W-TiO$_2$ samples were imaged after annealing and ball-milling. The maps contain six panels: (clockwise from the top left) total SEM, carbon channel, oxygen channel, titanium channel, tungsten channel, and background channel. Each map is shown at 2,000 times magnification, except DT52, which is shown at 10,000 times magnification.
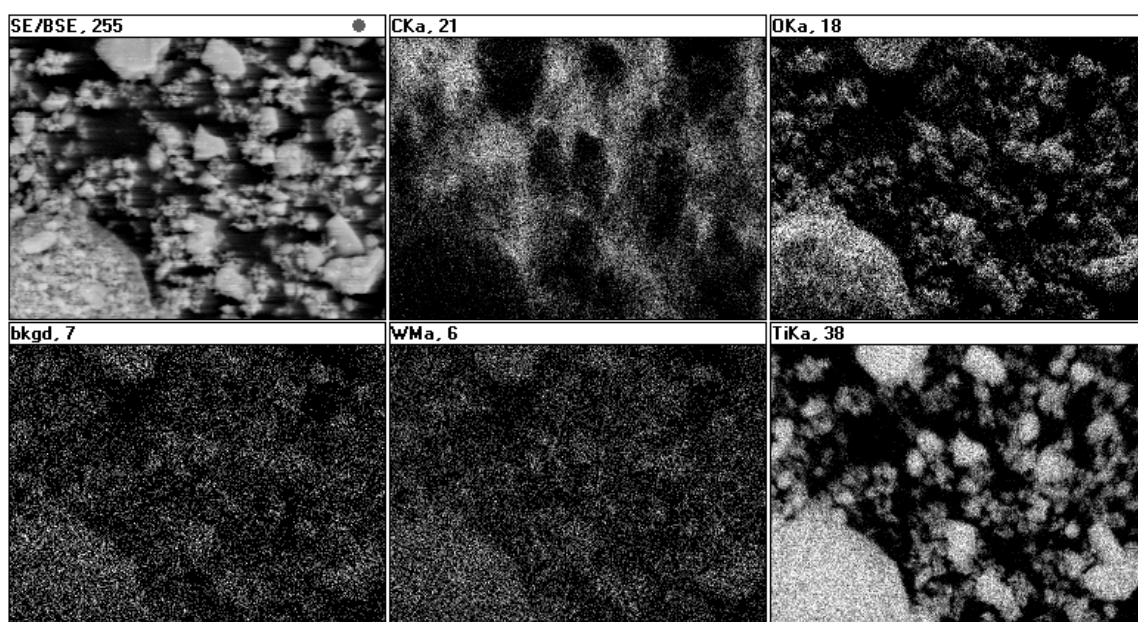
Figure S6. SEM-EDX map of the 0% WO$_x$ catalyst.
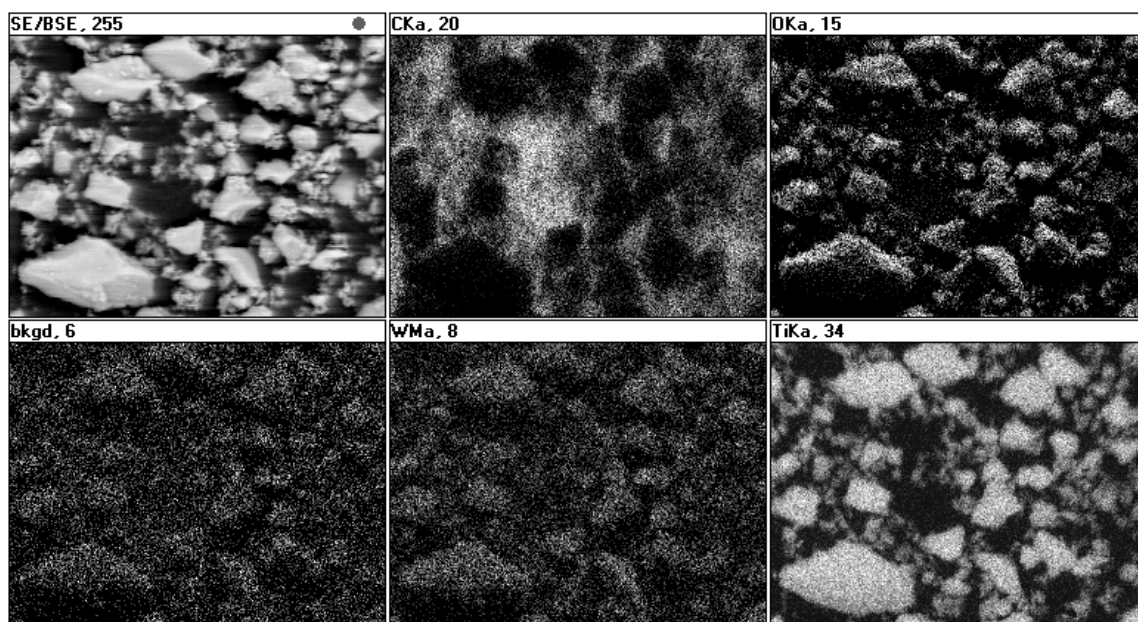
Figure S7. SEM-EDX map of the 1% WO$_x$ catalyst.
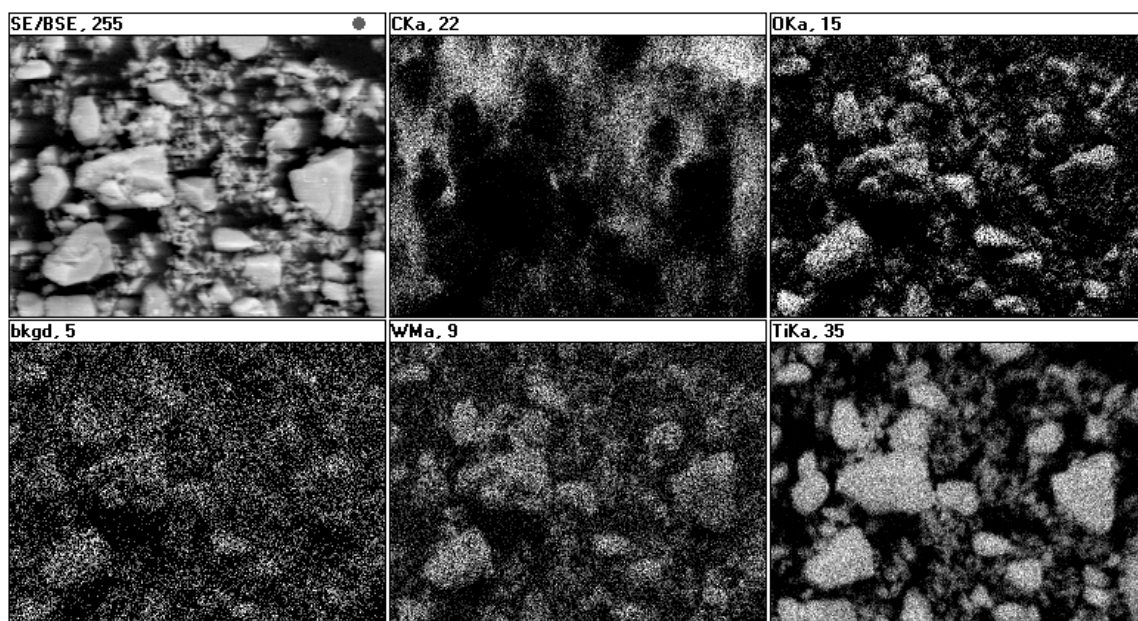
Figure S8. SEM-EDX map of the 3% WO$_x$ catalyst.
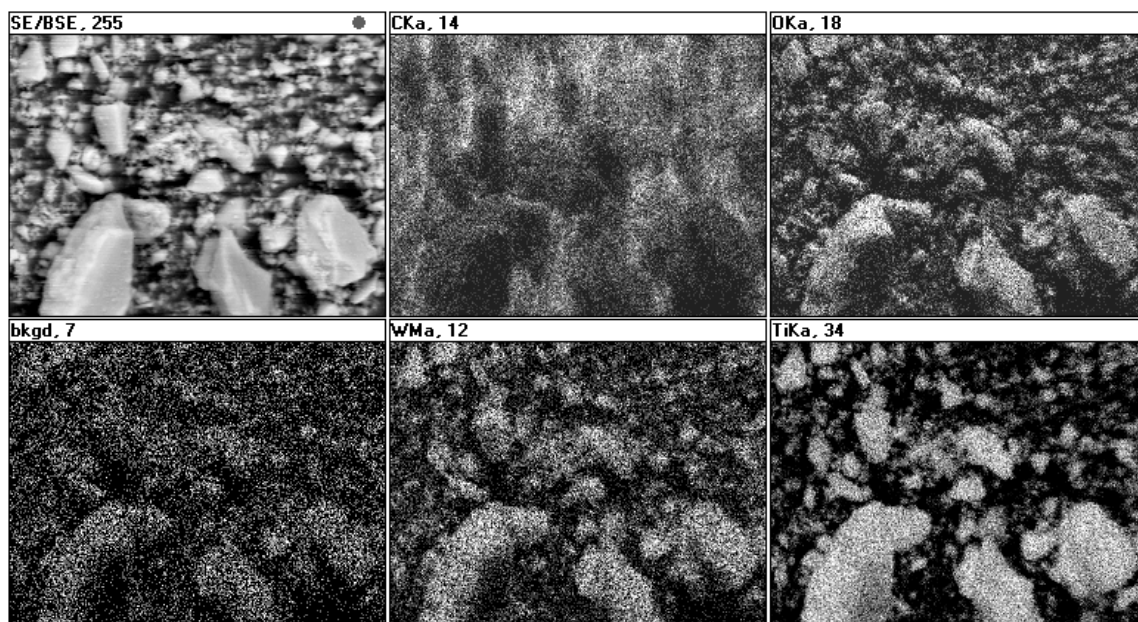
Figure S9. SEM-EDX map of the 5% WO$_x$ catalyst.
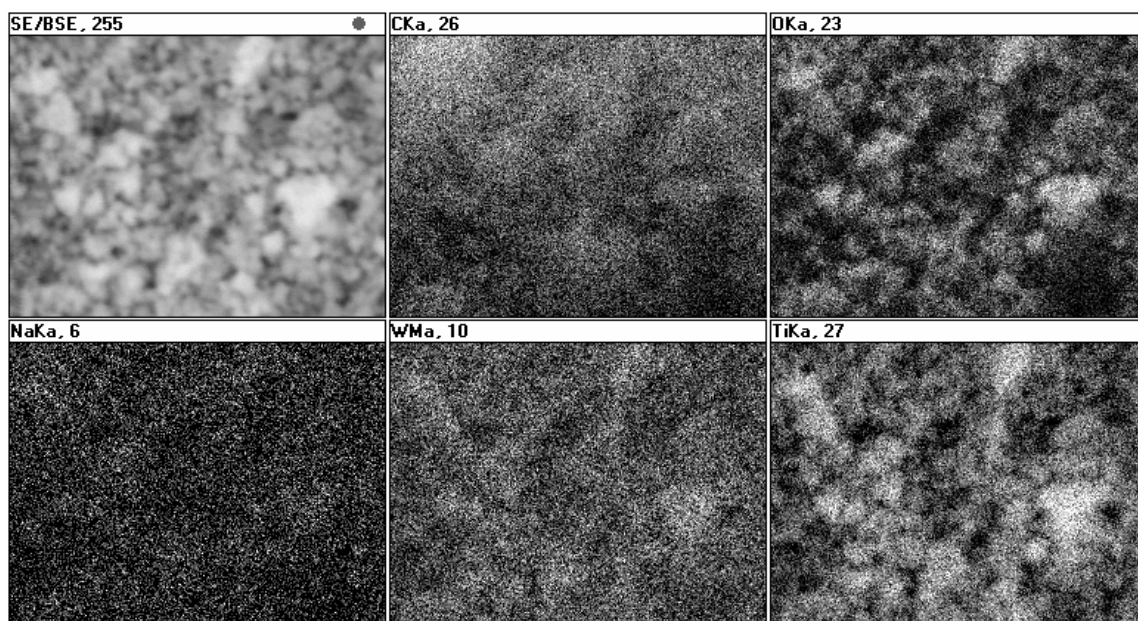
Figure S10. SEM-EDX map of the DT52 catalyst.
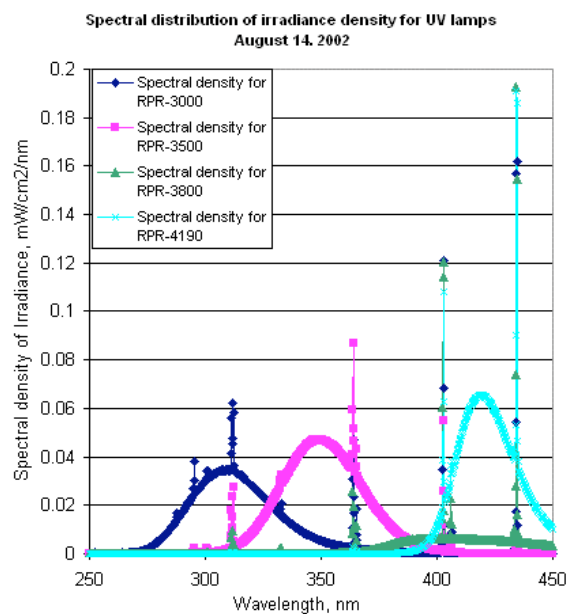
Figure S11. Linear spectral distributions of Rayonet lamps (obtained from

http://www.rayonet.org/spectral-graphs.htm, accessed 11/11/2008)
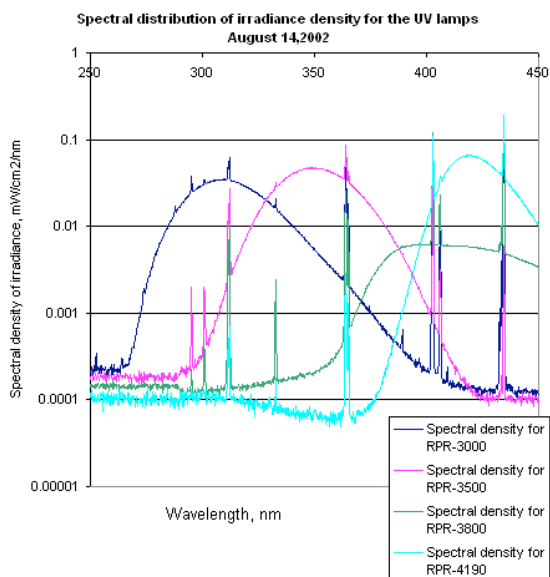
Figure S12. Logarithmic spectral distributions of Rayonet lamps (obtained from

http://www.rayonet.org/spectral-graphs.htm, accessed 11/11/2008)

Appendix 2: Computational Chemistry

Coordinates and absolute energies of optimized structures

4-biphenyl carboxylic acid (**1**)

RHF/6-31G(d)

```
C        6.0  -2.4747211999   1.0798885238  -0.3774878887
C        6.0  -1.0950236714   1.0988920018  -0.4258416568
C        6.0  -0.3522385335  -0.0121569244  -0.0282584617
C        6.0  -1.0332859693  -1.1418302295   0.4203109139
C        6.0  -2.4146021090  -1.1649757280   0.4690271143
C        6.0  -3.1444387688  -0.0525576939   0.0694244432
H        1.0  -3.0442762415   1.9337422621  -0.6913056508
H        1.0  -0.5897990886   1.9724700528  -0.7947348730
H        1.0  -0.4787078763  -2.0001809046   0.7523080922
H        1.0  -2.9232257088  -2.0408692046   0.8227645464
C        6.0   1.8520548518   1.1118044047   0.3724571895
C        6.0   3.2354476824   1.1298702422   0.3203371548
C        6.0   3.9280707452   0.0448705267  -0.1916931811
C        6.0   3.2273098410  -1.0588345305  -0.6497254833
C        6.0   1.8440755310  -1.0776942893  -0.5948636149
C        6.0   1.1367001340   0.0075291176  -0.0837624783
H        1.0   1.3256904033   1.9517628455   0.7886681026
H        1.0   3.7709308449   1.9883629616   0.6845691721
H        1.0   3.7556871631  -1.9028992607  -1.0557073985
H        1.0   1.3096057690  -1.9313585631  -0.9709157024
C        6.0  -4.6286983622  -0.0269373196   0.1001233842
O        8.0  -5.2970810611   0.9023817277  -0.2275882295
O        8.0  -5.1705149596  -1.1618411841   0.5362001738
H        1.0  -6.1163195248  -1.0548161757   0.5214979252
H        1.0   5.0023852993   0.0594179316  -0.2336083931
```

```
Energy                              -406548.021 KCAL/MOL
ZPE Correction                 132.655 KCAL/MOL
298.15K Temperature Correction    139.547 KCAL/MOL
```

```
TOTAL MULLIKEN AND LOWDIN ATOMIC POPULATIONS
  ATOM            MULL.POP.  CHARGE          LOW.POP.   CHARGE
   1 C            6.171259  -0.171259        6.118161  -0.118161
   2 C            6.228728  -0.228728        6.179300  -0.179300
   3 C            5.969607   0.030393        5.975157   0.024843
```

```
 4 C              6.229451   -0.229451         6.180851   -0.180851
 5 C              6.173378   -0.173378         6.128100   -0.128100
 6 C              6.157347   -0.157347         6.080268   -0.080268
 7 H              0.749646    0.250354         0.810370    0.189630
 8 H              0.782441    0.217559         0.827622    0.172378
 9 H              0.783742    0.216258         0.828121    0.171879
10 H              0.755684    0.244316         0.815351    0.184649
11 C              6.213149   -0.213149         6.166106   -0.166106
12 C              6.199467   -0.199467         6.160634   -0.160634
13 C              6.199751   -0.199751         6.159069   -0.159069
14 C              6.199461   -0.199461         6.160885   -0.160885
15 C              6.213038   -0.213038         6.166270   -0.166270
16 C              5.992604    0.007396         6.009052   -0.009052
17 H              0.787810    0.212190         0.830173    0.169827
18 H              0.794444    0.205556         0.831984    0.168016
19 H              0.794739    0.205261         0.832004    0.167996
20 H              0.788637    0.211363         0.830656    0.169344
21 C              5.203516    0.796484         5.711188    0.288812
22 O              8.571710   -0.571710         8.337527   -0.337527
23 O              8.715112   -0.715112         8.410900   -0.410900
24 H              0.530185    0.469815         0.614849    0.385151
25 H              0.795094    0.204906         0.835403    0.164597
```

3-hydroxy-4-biphenyl carboxylic acid radical adduct

ROHF/6-31G(d)

```
C       6.0   -2.5429938473    1.1108289836   -0.5235138344
C       6.0   -1.1207378386    1.1269225633   -0.5459150598
C       6.0   -0.3767131628    0.0181507614    0.0029016917
C       6.0   -1.0424414549   -1.0098678658    0.5400856781
C       6.0   -2.5387953957   -1.1100868720    0.6246390330
C       6.0   -3.2284721563    0.0888990302    0.0125977362
H       1.0   -3.0836640858    1.9374173578   -0.9461686239
H       1.0   -0.6041666809    1.9439132176   -1.0100863673
C       6.0    1.8197865414    1.1798351297    0.3364272459
C       6.0    3.2035002858    1.2035585508    0.2945211534
C       6.0    3.9060573677    0.0929833915   -0.1445115874
C       6.0    3.2147235282   -1.0396061262   -0.5415640257
C       6.0    1.8305100584   -1.0628006733   -0.4992596054
C       6.0    1.1148354300    0.0447295743   -0.0549052964
H       1.0    1.2860652756    2.0431973834    0.6928804234
H       1.0    3.7313430209    2.0863622894    0.6085816975
H       1.0    3.7509469413   -1.9033019539   -0.8924042592
H       1.0    1.3005665306   -1.9381137183   -0.8284949396
C       6.0   -4.7039552499    0.1680393856    0.0082739699
```

```
O      8.0   -5.3582058192    1.0499187724   -0.4519427252
O      8.0   -5.2800951624   -0.8849185037    0.6042883285
H      1.0   -6.2234396930   -0.7573728377    0.5708655272
H      1.0    4.9806144280    0.1115811084   -0.1794702938
H      1.0   -0.5111780472   -1.8479433053    0.9532343448
H      1.0   -2.8112111709   -1.1678958936    1.6782781750
O      8.0   -2.8997626099   -2.3218868932    0.0024823118
H      1.0   -3.8056730432   -2.5084316464    0.2110050816
```

Energy   -453844.002 KCAL/MOL
ZPE Correction   142.358 KCAL/MOL
298.15K Temperature Correction   150.242 KCAL/MOL

TOTAL MULLIKEN AND LOWDIN ATOMIC POPULATIONS

ATOM	MULL.POP.	CHARGE	LOW.POP.	CHARGE
1 C	6.145939	-0.145939	6.102030	-0.102030
2 C	6.207727	-0.207727	6.133579	-0.133579
3 C	5.975595	0.024405	6.020014	-0.020014
4 C	6.203625	-0.203625	6.146173	-0.146173
5 C	5.855972	0.144028	5.960083	0.039917
6 C	6.166682	-0.166682	6.102720	-0.102720
7 H	0.745395	0.254605	0.807278	0.192722
8 H	0.770448	0.229552	0.820443	0.179557
9 C	6.216816	-0.216816	6.171332	-0.171332
10 C	6.198749	-0.198749	6.160753	-0.160753
11 C	6.201095	-0.201095	6.161241	-0.161241
12 C	6.198880	-0.198880	6.160229	-0.160229
13 C	6.213947	-0.213947	6.165313	-0.165313
14 C	5.990508	0.009492	6.005725	-0.005725
15 H	0.793981	0.206019	0.833806	0.166194
16 H	0.796193	0.203807	0.833104	0.166896
17 H	0.794916	0.205084	0.832208	0.167792
18 H	0.781902	0.218098	0.827554	0.172446
19 C	5.207271	0.792729	5.711983	0.288017
20 O	8.573922	-0.573922	8.337679	-0.337679
21 O	8.742447	-0.742447	8.426139	-0.426139
22 H	0.527071	0.472929	0.613665	0.386335
23 H	0.796418	0.203582	0.836072	0.163928
24 H	0.780430	0.219570	0.822200	0.177800
25 H	0.823697	0.176303	0.857892	0.142108
26 O	8.754127	-0.754127	8.515243	-0.515243
27 H	0.536249	0.463751	0.635544	0.364456

2-hydroxy-4-biphenyl carboxylic acid radical adduct

ROHF/6-31G(d)

C	6.0	-2.4924904880	1.0719314806	-0.5256520740
C	6.0	-1.0720951545	1.0346482229	-0.6021785198
C	6.0	-0.3415079251	-0.0077101300	-0.1592140669
C	6.0	-1.0400292075	-1.2677679519	0.3196407169
C	6.0	-2.5191455618	-1.0889381169	0.5355931335
C	6.0	-3.1894485390	-0.0169581554	0.1011167272
H	1.0	-3.0446699595	1.9111991191	-0.8954521977
H	1.0	-0.5762225975	1.8936013559	-1.0167190139
H	1.0	-3.0303093681	-1.9109912607	0.9988073373
C	6.0	1.8004893165	1.2461002775	0.1458800041
C	6.0	3.1808606637	1.3156970570	0.1913498499
C	6.0	3.9434310521	0.1768589211	-0.0122962656
C	6.0	3.3091409183	-1.0290778105	-0.2555674227
C	6.0	1.9265829706	-1.1008021013	-0.3042024074
C	6.0	1.1451877646	0.0405090085	-0.1160593417
H	1.0	1.2264729894	2.1325704991	0.3427949607
H	1.0	3.6590467473	2.2563423024	0.3993253622
H	1.0	3.8896815495	-1.9209173585	-0.4118071724
H	1.0	1.4535253420	-2.0415952744	-0.5040512391
C	6.0	-4.6674097292	0.1031587663	0.2439511242
O	8.0	-5.3017007480	1.0266474971	-0.1563567653
O	8.0	-5.2327864964	-0.9262970212	0.8654132675
H	1.0	-6.1695077968	-0.7616466917	0.9080490016
H	1.0	5.0168348446	0.2284887870	0.0265156908
H	1.0	-0.5819812746	-1.6020885926	1.2425446105
O	8.0	-0.8498743391	-2.3560850980	-0.5693006574
H	1.0	-1.2009465234	-2.1186086011	-1.4186183825

```
Energy                                  -453842.747 KCAL/MOL
ZPE Correction                  142.477 KCAL/MOL
298.15K Temperature Correction       150.399 KCAL/MOL
```

TOTAL MULLIKEN AND LOWDIN ATOMIC POPULATIONS

ATOM		MULL.POP.	CHARGE	LOW.POP.	CHARGE
1	C	6.193997	-0.193997	6.136550	-0.136550
2	C	6.211334	-0.211334	6.180038	-0.180038
3	C	6.009511	-0.009511	6.024163	-0.024163
4	C	5.891791	0.108209	5.966699	0.033301
5	C	6.202779	-0.202779	6.132153	-0.132153
6	C	6.115193	-0.115193	6.080305	-0.080305
7	H	0.748072	0.251928	0.807946	0.192054
8	H	0.785304	0.214696	0.827703	0.172297
9	H	0.751561	0.248439	0.809449	0.190551
10	C	6.215994	-0.215994	6.166137	-0.166137
11	C	6.201832	-0.201832	6.164930	-0.164930
12	C	6.198597	-0.198597	6.158544	-0.158544

13 C	6.200646	-0.200646	6.164044	-0.164044
14 C	6.233286	-0.233286	6.170186	-0.170186
15 C	6.004344	-0.004344	6.013677	-0.013677
16 H	0.794122	0.205878	0.833315	0.166685
17 H	0.798088	0.201912	0.834590	0.165410
18 H	0.796897	0.203103	0.833768	0.166232
19 H	0.746256	0.253744	0.815304	0.184696
20 C	5.202459	0.797541	5.710536	0.289464
21 O	8.563402	-0.563402	8.329815	-0.329815
22 O	8.711338	-0.711338	8.405981	-0.405981
23 H	0.528429	0.471571	0.613122	0.386878
24 H	0.797496	0.202504	0.836793	0.163207
25 H	0.800170	0.199830	0.838646	0.161354
26 O	8.736851	-0.736851	8.507629	-0.507629
27 H	0.560253	0.439747	0.637975	0.362025

2'-hydroxy-4-biphenyl carboxylic acid radical adduct

ROHF/6-31G(d)

C	6.0	-2.4710748315	1.1034124642	-0.3204654377
C	6.0	-1.0922684256	1.0905348351	-0.3414323804
C	6.0	-0.3745034788	-0.0592017768	0.0033523271
C	6.0	-1.0940904588	-1.2084912102	0.3348038482
C	6.0	-2.4773018566	-1.1960395057	0.3564349824
C	6.0	-3.1756811147	-0.0398141230	0.0367155169
H	1.0	-3.0128845652	1.9904354200	-0.5880124877
H	1.0	-0.5664846392	1.9738144651	-0.6517203351
H	1.0	-0.5704906027	-2.1064443460	0.5930544889
H	1.0	-3.0114857637	-2.0859626059	0.6281926921
C	6.0	1.7911199911	1.0694885711	0.3576868980
C	6.0	3.2104646350	1.1700769287	0.2542486641
C	6.0	3.9524249210	0.0819352115	-0.3092990522
C	6.0	3.3331462397	-1.0425662846	-0.6720315938
C	6.0	1.8654838053	-1.2844537017	-0.4401159956
C	6.0	1.1138463741	-0.0359540582	-0.0056264004
H	1.0	1.2550795286	1.9237795234	0.7305474727
H	1.0	3.7099299969	2.0645794104	0.5724725758
H	1.0	3.8815731165	-1.8687718723	-1.0886216793
C	6.0	-4.6587718433	0.0239086270	0.0575391171
O	8.0	-5.2994886553	0.9880412649	-0.2227120867
O	8.0	-5.2350228436	-1.1163803579	0.4305361302
H	1.0	-6.1771609516	-0.9809190468	0.4185436499
H	1.0	5.0151474989	0.1867399604	-0.4396530760
H	1.0	1.4121395067	-1.6715780664	-1.3450248849
O	8.0	1.7171735002	-2.3444628856	0.4920112276

```
 H              1.0    2.1374584265   -2.0901283709    1.3040235587
```

```
Energy                                  -453844.002 KCAL/MOL
ZPE Correction                  142.509 KCAL/MOL
298.15K Temperature Correction      150.419 KCAL/MOL
```

TOTAL MULLIKEN AND LOWDIN ATOMIC POPULATIONS

ATOM	MULL.POP.	CHARGE	LOW.POP.	CHARGE
1 C	6.174540	-0.174540	6.123701	-0.123701
2 C	6.231196	-0.231196	6.178728	-0.178728
3 C	5.989266	0.010734	5.983249	0.016751
4 C	6.243986	-0.243986	6.181994	-0.181994
5 C	6.175912	-0.175912	6.131131	-0.131131
6 C	6.154457	-0.154457	6.078294	-0.078294
7 H	0.752260	0.247740	0.811935	0.188065
8 H	0.787730	0.212270	0.830123	0.169877
9 H	0.737510	0.262490	0.810382	0.189618
10 H	0.756632	0.243368	0.816218	0.183782
11 C	6.204903	-0.204903	6.174081	-0.174081
12 C	6.207821	-0.207821	6.147449	-0.147449
13 C	6.179065	-0.179065	6.172082	-0.172082
14 C	6.216705	-0.216705	6.179355	-0.179355
15 C	5.883063	0.116937	5.966158	0.033842
16 C	6.014114	-0.014114	6.029589	-0.029589
17 H	0.787096	0.212904	0.828906	0.171094
18 H	0.786365	0.213635	0.827175	0.172825
19 H	0.792871	0.207129	0.827572	0.172428
20 C	5.204019	0.795981	5.711741	0.288259
21 O	8.573165	-0.573165	8.338859	-0.338859
22 O	8.714160	-0.714160	8.410307	-0.410307
23 H	0.530854	0.469146	0.615156	0.384844
24 H	0.793793	0.206207	0.833306	0.166694
25 H	0.805426	0.194574	0.841428	0.158572
26 O	8.740395	-0.740395	8.512001	-0.512001
27 H	0.562697	0.437303	0.639079	0.360921

3'-hydroxy-4-biphenyl carboxylic acid radical adduct

ROHF/6-31G(d)

```
 C              6.0   -2.4766700575    1.0744325050   -0.3680236449
 C              6.0   -1.0966737897    1.0879172259   -0.4024211696
 C              6.0   -0.3634296575   -0.0309084258   -0.0092665484
 C              6.0   -1.0513245740   -1.1582466649    0.4304829398
 C              6.0   -2.4337996494   -1.1754803957    0.4667029783
 C              6.0   -3.1547276177   -0.0580683009    0.0666490163
```

H	1.0	-3.0400144253	1.9331203560	-0.6797802763
H	1.0	-0.5851951636	1.9651017845	-0.7545993932
H	1.0	-0.5014862198	-2.0196151327	0.7614246598
H	1.0	-2.9493252156	-2.0508218723	0.8116032209
C	6.0	1.8380274689	1.1327747102	0.4440995790
C	6.0	3.2685388139	1.1804499282	0.3513263271
C	6.0	3.9666736103	0.1671428535	-0.1640315751
C	6.0	3.3173969138	-1.0889524082	-0.6753898172
C	6.0	1.8154965759	-1.0424688188	-0.5852711067
C	6.0	1.1280445163	-0.0178947834	-0.0638475210
H	1.0	1.2995339731	1.9378291672	0.9041375498
H	1.0	3.7746130800	2.0590703649	0.7116035779
H	1.0	1.3017826004	-1.8916696937	-1.0004216772
C	6.0	-4.6395468030	-0.0246950885	0.0876616227
O	8.0	-5.2998142989	0.9100133349	-0.2408674288
O	8.0	-5.1898548764	-1.1580942678	0.5156940560
H	1.0	-6.1351166432	-1.0469591751	0.4952938224
H	1.0	5.0388745516	0.2117707787	-0.2388942350
O	8.0	3.7363677790	-1.3844692146	-1.9915874374
H	1.0	3.6783080997	-1.9352486456	-0.0971222496
H	1.0	3.4540776589	-0.6825349609	-2.5641133995

Energy		-453843.374 KCAL/MOL
ZPE Correction	142.166 KCAL/MOL	
298.15K Temperature Correction	150.147 KCAL/MOL	

TOTAL MULLIKEN AND LOWDIN ATOMIC POPULATIONS

ATOM		MULL.POP.	CHARGE	LOW.POP.	CHARGE
1	C	6.171362	-0.171362	6.118490	-0.118490
2	C	6.229383	-0.229383	6.180432	-0.180432
3	C	5.968294	0.031706	5.975920	0.024080
4	C	6.226862	-0.226862	6.177756	-0.177756
5	C	6.173378	-0.173378	6.127816	-0.127816
6	C	6.156286	-0.156286	6.078629	-0.078629
7	H	0.748981	0.251019	0.810101	0.189899
8	H	0.784487	0.215513	0.829063	0.170937
9	H	0.782758	0.217242	0.827060	0.172940
10	H	0.754340	0.245660	0.814629	0.185371
11	C	6.218329	-0.218329	6.151608	-0.151608
12	C	6.174438	-0.174438	6.172436	-0.172436
13	C	6.229811	-0.229811	6.179634	-0.179634
14	C	5.861946	0.138054	5.966538	0.033462
15	C	6.263714	-0.263714	6.187018	-0.187018
16	C	5.964550	0.035450	6.019654	-0.019654
17	H	0.779599	0.220401	0.824630	0.175370
18	H	0.793817	0.206183	0.830925	0.169075
19	H	0.786544	0.213456	0.826572	0.173428

20 C		5.203047	0.796953	5.711278	0.288722
21 O		8.570844	-0.570844	8.336661	-0.336661
22 O		8.714518	-0.714518	8.410052	-0.410052
23 H		0.529609	0.470391	0.614407	0.385593
24 H		0.793269	0.206731	0.831276	0.168724
25 O		8.743705	-0.743705	8.514596	-0.514596
26 H		0.810535	0.189465	0.842664	0.157336
27 H		0.565595	0.434405	0.640154	0.359846

4'-hydroxy-4-biphenyl carboxylic acid radical adduct

ROHF/6-31G(d)

```
C       6.0   -2.4988194447    1.1212490470   -0.2405157189
C       6.0   -1.1214475744    1.1535732146   -0.3061609504
C       6.0   -0.3617542080    0.0082130480   -0.0460409534
C       6.0   -1.0402690087   -1.1675369928    0.2871865324
C       6.0   -2.4189352028   -1.2000225815    0.3580394362
C       6.0   -3.1598069379   -0.0550822365    0.0924445326
H       1.0   -3.0750675268    2.0015113179   -0.4527128661
H       1.0   -0.6342593943    2.0680651154   -0.5879607503
H       1.0   -0.4859805488   -2.0575312879    0.5191727142
H       1.0   -2.9184200545   -2.1110431957    0.6254955206
C       6.0    1.8616487086    1.2199937054    0.2159070934
C       6.0    3.1945934213    1.2448331312    0.1804122745
C       6.0    4.0345721277    0.0630744081   -0.2169325921
C       6.0    3.1914530737   -1.1183832239   -0.6078321017
C       6.0    1.8591701166   -1.1202874045   -0.5515412534
C       6.0    1.1073037675    0.0351687929   -0.1203242779
H       1.0    1.3272280807    2.0968710526    0.5333093914
H       1.0    3.7317618865    2.1381386215    0.4468848653
H       1.0    3.7251556156   -1.9826714580   -0.9624265839
H       1.0    1.3189655410   -1.9937824905   -0.8688659621
C       6.0   -4.6428182424   -0.0395236126    0.1494973548
O       8.0   -5.3191864449    0.9141743503   -0.0759564345
O       8.0   -5.1731019850   -1.2139084873    0.4828541434
H       1.0   -6.1194805855   -1.1113930686    0.4949614905
O       8.0    4.9501048763    0.3999721174   -1.2377294571
H       1.0    4.6716117325   -0.2145479730    0.6182595335
H       1.0    4.4624256308    0.6596476906   -2.0091085812
```

Energy	-453845.884 KCAL/MOL	
ZPE Correction	142.639 KCAL/MOL	
298.15K Temperature Correction	150.578 KCAL/MOL	

TOTAL MULLIKEN AND LOWDIN ATOMIC POPULATIONS
ATOM   MULL.POP. CHARGE   LOW.POP.   CHARGE

```
 1 C           6.170290   -0.170290       6.116813   -0.116813
 2 C           6.232346   -0.232346       6.181033   -0.181033
 3 C           5.964652    0.035348       5.981242    0.018758
 4 C           6.233319   -0.233319       6.182091   -0.182091
 5 C           6.171970   -0.171970       6.126507   -0.126507
 6 C           6.159736   -0.159736       6.080197   -0.080197
 7 H           0.748462    0.251538       0.810030    0.189970
 8 H           0.783589    0.216411       0.829043    0.170957
 9 H           0.783389    0.216611       0.828600    0.171400
10 H           0.754264    0.245736       0.815001    0.184999
11 C           6.173816   -0.173816       6.174810   -0.174810
12 C           6.237942   -0.237942       6.178835   -0.178835
13 C           5.862104    0.137896       5.969644    0.030356
14 C           6.236900   -0.236900       6.179156   -0.179156
15 C           6.176098   -0.176098       6.175725   -0.175725
16 C           6.014862   -0.014862       5.990396    0.009604
17 H           0.787882    0.212118       0.829079    0.170921
18 H           0.791781    0.208219       0.827745    0.172255
19 H           0.791903    0.208097       0.827463    0.172537
20 H           0.788441    0.211559       0.829388    0.170612
21 C           5.202588    0.797412       5.711551    0.288449
22 O           8.571244   -0.571244       8.337048   -0.337048
23 O           8.715226   -0.715226       8.410841   -0.410841
24 H           0.529628    0.470372       0.614485    0.385515
25 O           8.743577   -0.743577       8.511646   -0.511646
26 H           0.808733    0.191267       0.841535    0.158465
27 H           0.565258    0.434742       0.640095    0.359905
```

3-hydroxybiphenyl-4-carboxylic acid (**2**)

RHF/6-31G(d)

```
C         6.0   -2.4495103409    1.1659064161   -0.3956399224
C         6.0   -1.0557562864    1.1486467320   -0.4313860321
C         6.0   -0.3456293686    0.0288030968   -0.0462360531
C         6.0   -1.0427105347   -1.1106933189    0.3873140961
C         6.0   -2.4122183130   -1.1008043588    0.4223801815
C         6.0   -3.1442100469    0.0284523363    0.0337369150
H         1.0   -0.5568127866    2.0278236984   -0.7916750094
H         1.0   -0.5030031876   -1.9792258190    0.7140023051
H         1.0   -2.9441392832   -1.9687653680    0.7609045218
C         6.0    1.8704480000    1.1259572580    0.3655453234
C         6.0    3.2542918331    1.1236174566    0.3240043149
C         6.0    3.9347594643    0.0264225683   -0.1779916879
C         6.0    3.2222450723   -1.0698376843   -0.6358234145
C         6.0    1.8387102546   -1.0696088072   -0.5893525647
```

```
C       6.0    1.1438864288    0.0291283492   -0.0902505570
H       1.0    1.3526768233    1.9755940539    0.7719718121
H       1.0    3.7991864938    1.9762730664    0.6877638964
H       1.0    3.7416451225   -1.9232699203   -1.0335509371
H       1.0    1.2952984543   -1.9185434530   -0.9628131502
C       6.0   -4.6128567117    0.0370199880    0.0684851657
O       8.0   -5.3000513640    0.9708362948   -0.2510268712
O       8.0   -5.1587464475   -1.0938814503    0.4897033274
H       1.0   -6.1046619747   -0.9846644516    0.4740245394
H       1.0    5.0094675727    0.0255294436   -0.2120385050
O       8.0   -3.0447081635    2.2880691787   -0.7892728954
H       1.0   -3.9941583104    2.1944124243   -0.7331978687
```

```
Energy                                  -453526.482 KCAL/MOL
ZPE Correction                   136.144 KCAL/MOL
298.15K Temperature Correction      143.500 KCAL/MOL
```

```
TOTAL MULLIKEN AND LOWDIN ATOMIC POPULATIONS
  ATOM            MULL.POP.   CHARGE        LOW.POP.   CHARGE
   1 C            5.548762    0.451238      5.810150   0.189850
   2 C            6.289636   -0.289636      6.223589  -0.223589
   3 C            5.944338    0.055662      5.947132   0.052868
   4 C            6.252962   -0.252962      6.219517  -0.219517
   5 C            6.150904   -0.150904      6.103085  -0.103085
   6 C            6.253452   -0.253452      6.154936  -0.154936
   7 H            0.768955    0.231045      0.817156   0.182844
   8 H            0.786000    0.214000      0.828297   0.171703
   9 H            0.753334    0.246666      0.813947   0.186053
  10 C            6.209494   -0.209494      6.162246  -0.162246
  11 C            6.200744   -0.200744      6.161214  -0.161214
  12 C            6.197994   -0.197994      6.156896  -0.156896
  13 C            6.200593   -0.200593      6.161684  -0.161684
  14 C            6.211187   -0.211187      6.164029  -0.164029
  15 C            5.998109    0.001891      6.010290  -0.010290
  16 H            0.783412    0.216588      0.828032   0.171968
  17 H            0.793598    0.206402      0.831481   0.168519
  18 H            0.794527    0.205473      0.831960   0.168040
  19 H            0.787107    0.212893      0.829862   0.170138
  20 C            5.158858    0.841142      5.697108   0.302892
  21 O            8.637204   -0.637204      8.373652  -0.373652
  22 O            8.707073   -0.707073      8.397126  -0.397126
  23 H            0.525341    0.474659      0.611603   0.388397
  24 H            0.794632    0.205368      0.835205   0.164795
  25 O            8.770287   -0.770287      8.421350  -0.421350
  26 H            0.481497    0.518503      0.608453   0.391547
```

3,5-dihydroxybiphenyl-4-carboxylic acid radical adduct

ROHF/6-31G(d)

```
C        6.0    -2.5128667471     1.1112843621    -0.3746762581
C        6.0    -1.0620428712     1.0957986053    -0.4242843223
C        6.0    -0.3601680891     0.0248457120     0.0029105622
C        6.0    -1.0572849117    -1.1121291034     0.5021381214
C        6.0    -2.5507548622    -1.2276006080     0.5138039419
C        6.0    -3.2324512855     0.0467347818     0.0691123645
H        1.0    -0.5866684258     1.9659942054    -0.8327962059
C        6.0     1.8628223954     1.1137041948     0.3901610395
C        6.0     3.2466844104     1.1011280974     0.3452080533
C        6.0     3.9179947238    -0.0137779808    -0.1290438332
C        6.0     3.1974363086    -1.1177737922    -0.5556695013
C        6.0     1.8141546803    -1.1079358754    -0.5057591668
C        6.0     1.1299634408     0.0102343309    -0.0365972837
H        1.0     1.3498521625     1.9762823046     0.7748491895
H        1.0     3.7984753795     1.9590527940     0.6854906368
H        1.0     3.7106391668    -1.9850827513    -0.9305428528
H        1.0     1.2643085915    -1.9642119942    -0.8526932408
C        6.0    -4.6777347422     0.1346528418     0.0971433924
O        8.0    -5.3422606141     1.0874289354    -0.2324916937
O        8.0    -5.2775858666    -0.9739914425     0.5374947170
H        1.0    -6.2173111756    -0.8187372725     0.5272789618
H        1.0     4.9925825187    -0.0234380993    -0.1644278996
O        8.0    -3.0357590067     2.2490158223    -0.7900724926
H        1.0    -3.9929018178     2.2063188413    -0.7390781696
H        1.0    -0.5116120475    -1.9673299766     0.8495205763
O        8.0    -2.8690675249    -2.3397915862    -0.2977343775
H        1.0    -2.8592888488    -1.4557827448     1.5324211695
H        1.0    -3.7865882513    -2.5448290217    -0.1738956783
```

Energy   -500823.718 KCAL/MOL
ZPE Correction   145.772 KCAL/MOL
298.15K Temperature Correction   154.148 KCAL/MOL

TOTAL MULLIKEN AND LOWDIN ATOMIC POPULATIONS

ATOM		MULL.POP.	CHARGE	LOW.POP.	CHARGE
1	C	5.513244	0.486756	5.777671	0.222329
2	C	6.288010	-0.288010	6.213049	-0.213049
3	C	5.930965	0.069035	5.966110	0.033890
4	C	6.184316	-0.184316	6.119187	-0.119187
5	C	5.840061	0.159939	5.955904	0.044096
6	C	6.302101	-0.302101	6.224955	-0.224955
7	H	0.761186	0.238814	0.813170	0.186830
8	C	6.208036	-0.208036	6.161940	-0.161940

9 C	6.200917	-0.200917	6.161165	-0.161165
10 C	6.196935	-0.196935	6.155309	-0.155309
11 C	6.200723	-0.200723	6.160462	-0.160462
12 C	6.213016	-0.213016	6.163076	-0.163076
13 C	5.999429	0.000571	6.011400	-0.011400
14 H	0.784298	0.215702	0.828483	0.171517
15 H	0.792674	0.207326	0.831034	0.168966
16 H	0.792061	0.207939	0.830846	0.169154
17 H	0.778601	0.221399	0.826787	0.173213
18 C	5.168370	0.831630	5.699305	0.300695
19 O	8.660630	-0.660630	8.394220	-0.394220
20 O	8.737146	-0.737146	8.417272	-0.417272
21 H	0.525517	0.474483	0.612613	0.387387
22 H	0.793245	0.206755	0.834507	0.165493
23 O	8.759020	-0.759020	8.402568	-0.402568
24 H	0.475369	0.524631	0.603905	0.396095
25 H	0.773808	0.226192	0.818708	0.181292
26 O	8.753990	-0.753990	8.520293	-0.520293
27 H	0.825357	0.174643	0.858524	0.141476
28 H	0.540977	0.459023	0.637536	0.362464

3,6-dihydroxybiphenyl-4-carboxylic acid radical adduct

ROHF/6-31G(d)

C	6.0	-2.4818698001	1.0422945953	-0.4188968772
C	6.0	-1.0274375141	1.0132028171	-0.4738804168
C	6.0	-0.3108200745	-0.0597803462	-0.1306703447
C	6.0	-1.0167676549	-1.3654313794	0.2079540104
C	6.0	-2.4586369791	-1.1661297818	0.5522539308
C	6.0	-3.1842234664	-0.0142027505	0.0871063450
H	1.0	-0.5610431364	1.9236113799	-0.7998102489
H	1.0	-2.9898515049	-2.0036130994	0.9556896181
C	6.0	1.8346668820	1.1363571125	0.3258605134
C	6.0	3.2160719640	1.1921175356	0.3717743345
C	6.0	3.9689030248	0.0888775830	0.0036140629
C	6.0	3.3284445156	-1.0694972182	-0.4033243935
C	6.0	1.9456260847	-1.1291565293	-0.4472951092
C	6.0	1.1766129147	-0.0203028612	-0.0934736183
H	1.0	1.2636399596	1.9894871291	0.6426893007
H	1.0	3.7018394769	2.0919938951	0.7042609978
H	1.0	3.9044864210	-1.9311752194	-0.6897751801
H	1.0	1.4623594977	-2.0287552854	-0.7737938013
C	6.0	-4.6393181556	0.0789289678	0.1849071411
O	8.0	-5.2950025955	1.0234536889	-0.1807990632
O	8.0	-5.2222969379	-0.9812491053	0.7222382328

```
H      1.0   -6.1603562747   -0.8187645205    0.7444972715
H      1.0    5.0428168039    0.1300104581    0.0404467865
O      8.0   -3.0097818009    2.1637498059   -0.8714079997
H      1.0   -3.9644163941    2.1304944674   -0.7830604087
O      8.0   -0.8672543304   -2.2925988034   -0.8581702461
H      1.0   -1.3585449498   -1.9797605526   -1.6072370063
H      1.0   -0.5051823253   -1.8382538632    1.0353830483
```

Energy   -500821.208 KCAL/MOL
ZPE Correction   145.929 KCAL/MOL
298.15K Temperature Correction   154.392 KCAL/MOL

TOTAL MULLIKEN AND LOWDIN ATOMIC POPULATIONS

ATOM		MULL.POP.	CHARGE	LOW.POP.	CHARGE
1	C	5.554416	0.445584	5.797179	0.202821
2	C	6.268602	-0.268602	6.210827	-0.210827
3	C	5.954025	0.045975	5.972907	0.027093
4	C	5.892549	0.107451	5.969741	0.030259
5	C	6.203923	-0.203923	6.175423	-0.175423
6	C	6.246547	-0.246547	6.187731	-0.187731
7	H	0.764247	0.235753	0.815381	0.184619
8	H	0.769152	0.230848	0.815074	0.184926
9	C	6.208919	-0.208919	6.159977	-0.159977
10	C	6.204341	-0.204341	6.165810	-0.165810
11	C	6.193924	-0.193924	6.152360	-0.152360
12	C	6.203229	-0.203229	6.164907	-0.164907
13	C	6.223495	-0.223495	6.161905	-0.161905
14	C	6.021303	-0.021303	6.019873	-0.019873
15	H	0.787667	0.212333	0.830037	0.169963
16	H	0.794717	0.205283	0.832431	0.167569
17	H	0.793790	0.206210	0.831890	0.168110
18	H	0.740801	0.259199	0.812081	0.187919
19	C	5.167569	0.832431	5.697399	0.302601
20	O	8.653460	-0.653460	8.389680	-0.389680
21	O	8.703440	-0.703440	8.394908	-0.394908
22	H	0.526965	0.473035	0.612438	0.387562
23	H	0.794479	0.205521	0.835317	0.164683
24	O	8.753634	-0.753634	8.401799	-0.401799
25	H	0.475303	0.524697	0.603784	0.396216
26	O	8.739066	-0.739066	8.514573	-0.514573
27	H	0.559925	0.440075	0.637008	0.362992
28	H	0.800511	0.199489	0.837558	0.162442

2',3-dihydroxybiphenyl-4-carboxylic acid radical adduct

ROHF/6-31G(d)

C	6.0	-2.4762647060	1.2016373539	-0.3642235897
C	6.0	-1.0840521095	1.1588362538	-0.4157177919
C	6.0	-0.3861557842	0.0134322249	-0.0809469316
C	6.0	-1.1051684820	-1.1362278086	0.2893269354
C	6.0	-2.4723000718	-1.0992091386	0.3459953021
C	6.0	-3.1881888821	0.0627133106	0.0276354020
H	1.0	-0.5748072729	2.0442693628	-0.7438491119
H	1.0	-0.5918383190	-2.0435439387	0.5401948913
H	1.0	-3.0167189768	-1.9744983500	0.6430488218
C	6.0	1.7949394024	1.0797522132	0.3500842703
C	6.0	3.2221738796	1.1194359635	0.3479650588
C	6.0	3.9526755768	0.0021819462	-0.1721343539
C	6.0	3.3123943102	-1.0805619263	-0.6155169597
C	6.0	1.8138020299	-1.2220325439	-0.6057538892
C	6.0	1.1014554400	0.0159678643	-0.0921041114
H	1.0	1.2676573450	1.9319390159	0.7396291244
H	1.0	3.7363303265	1.9830185995	0.7226633912
H	1.0	3.8516346970	-1.9210743520	-1.0154871503
C	6.0	-4.6546069982	0.1020937927	0.0949436551
O	8.0	-5.3273094534	1.0610308676	-0.1789657345
O	8.0	-5.2169448049	-1.0279277807	0.4966181232
H	1.0	-6.1600025051	-0.8962594271	0.5079005061
H	1.0	5.0270912846	0.0490750743	-0.2006363662
O	8.0	-3.0526376237	2.3517830622	-0.7041170385
H	1.0	-4.0029658990	2.2739222419	-0.6398861681
O	8.0	1.3413103463	-1.6029191969	-1.8793071695
H	1.0	1.5163721157	-0.9011903559	-2.4934907089
H	1.0	1.5595189649	-2.0685630285	0.0241491835

```
Energy                                  -500821.208 KCAL/MOL
ZPE Correction                  145.717 KCAL/MOL
298.15K Temperature Correction      154.174 KCAL/MOL
```

TOTAL MULLIKEN AND LOWDIN ATOMIC POPULATIONS

ATOM		MULL.POP.	CHARGE	LOW.POP.	CHARGE
1	C	5.549903	0.450097	5.811611	0.188389
2	C	6.298185	-0.298185	6.226093	-0.226093
3	C	5.915482	0.084518	5.943766	0.056234
4	C	6.242111	-0.242111	6.210040	-0.210040
5	C	6.154231	-0.154231	6.103569	-0.103569
6	C	6.253060	-0.253060	6.154653	-0.154653
7	H	0.774925	0.225075	0.819997	0.180003
8	H	0.787398	0.212602	0.829492	0.170508
9	H	0.753704	0.246296	0.814137	0.185863
10	C	6.188829	-0.188829	6.164180	-0.164180
11	C	6.212061	-0.212061	6.149492	-0.149492

12	C	6.174205	-0.174205	6.169499	-0.169499
13	C	6.224913	-0.224913	6.180243	-0.180243
14	C	5.860121	0.139879	5.966780	0.033220
15	C	6.060562	-0.060562	6.037483	-0.037483
16	H	0.781165	0.218835	0.826077	0.173923
17	H	0.785724	0.214276	0.826514	0.173486
18	H	0.791878	0.208122	0.827298	0.172702
19	C	5.159151	0.840849	5.697336	0.302664
20	O	8.638613	-0.638613	8.374992	-0.374992
21	O	8.706706	-0.706706	8.396929	-0.396929
22	H	0.525780	0.474220	0.611804	0.388196
23	H	0.793461	0.206539	0.833652	0.166348
24	O	8.771924	-0.771924	8.423317	-0.423317
25	H	0.481868	0.518132	0.608730	0.391270
26	O	8.739063	-0.739063	8.509945	-0.509945
27	H	0.563131	0.436869	0.638317	0.361683
28	H	0.811845	0.188155	0.844052	0.155948

3,3'-dihydroxybiphenyl-4-carboxylic acid radical adduct

ROHF/6-31G(d)

C	6.0	-2.4095832461	1.1248754242	-0.4442375512
C	6.0	-1.0156830584	1.1040043427	-0.4574065922
C	6.0	-0.3154887380	-0.0097960075	-0.0383289182
C	6.0	-1.0192371881	-1.1369065694	0.4107148582
C	6.0	-2.3898459716	-1.1213617940	0.4295965638
C	6.0	-3.1125683837	0.0011797954	0.0077793599
H	1.0	-0.5094979075	1.9779292413	-0.8212565220
H	1.0	-0.4842407384	-1.9986100888	0.7613314567
H	1.0	-2.9288752863	-1.9789305068	0.7829402920
C	6.0	1.8807229690	1.1481770169	0.4484636869
C	6.0	3.3139606758	1.1768627595	0.4083694678
C	6.0	4.0181554464	0.1457524329	-0.0614750928
C	6.0	3.3730208401	-1.1105375919	-0.5775048961
C	6.0	1.8693958169	-1.0508047706	-0.5314638083
C	6.0	1.1772298002	-0.0078334024	-0.0551854009
H	1.0	1.3346586044	1.9699395840	0.8675982791
H	1.0	3.8170934200	2.0559007201	0.7715941496
H	1.0	1.3603983950	-1.9064070197	-0.9390390353
C	6.0	-4.5819284001	0.0219576449	0.0425242714
O	8.0	-5.2613530260	0.9489797287	-0.3107153335
O	8.0	-5.1351484311	-1.0870566909	0.5087071495
H	1.0	-6.0803550700	-0.9712405409	0.4934017057
H	1.0	5.0929381876	0.1759496665	-0.0953768740
O	8.0	-2.9961805400	2.2386793960	-0.8730194948

```
H           1.0  -3.9465681881   2.1505625011  -0.8237643428
O           8.0   3.8284218113  -1.4257020484  -1.8768334994
H           1.0   3.5770466520  -0.7243700091  -2.4643741911
H           1.0   3.7080172449  -1.9531980137   0.0212022921
```

```
Energy                                      -500821.208 KCAL/MOL
ZPE Correction                    145.649 KCAL/MOL
298.15K Temperature Correction      154.099 KCAL/MOL
```

TOTAL MULLIKEN AND LOWDIN ATOMIC POPULATIONS

ATOM		MULL.POP.	CHARGE	LOW.POP.	CHARGE
1	C	5.549084	0.450916	5.810479	0.189521
2	C	6.289812	-0.289812	6.224904	-0.224904
3	C	5.944039	0.055961	5.947540	0.052460
4	C	6.250052	-0.250052	6.216740	-0.216740
5	C	6.150850	-0.150850	6.102600	-0.102600
6	C	6.252012	-0.252012	6.153261	-0.153261
7	H	0.770822	0.229178	0.818377	0.181623
8	H	0.785061	0.214939	0.827185	0.172815
9	H	0.751904	0.248096	0.813119	0.186881
10	C	6.215753	-0.215753	6.149835	-0.149835
11	C	6.174347	-0.174347	6.171752	-0.171752
12	C	6.230083	-0.230083	6.180150	-0.180150
13	C	5.863042	0.136958	5.966509	0.033491
14	C	6.260728	-0.260728	6.183640	-0.183640
15	C	5.968891	0.031109	6.019944	-0.019944
16	H	0.775745	0.224255	0.822743	0.177257
17	H	0.793126	0.206874	0.830522	0.169478
18	H	0.785128	0.214872	0.825919	0.174081
19	C	5.158253	0.841747	5.697048	0.302952
20	O	8.636008	-0.636008	8.372459	-0.372459
21	O	8.706425	-0.706425	8.396216	-0.396216
22	H	0.524739	0.475261	0.611140	0.388860
23	H	0.793293	0.206707	0.831353	0.168647
24	O	8.770341	-0.770341	8.421426	-0.421426
25	H	0.481135	0.518865	0.608226	0.391774
26	O	8.743378	-0.743378	8.514266	-0.514266
27	H	0.565145	0.434855	0.639903	0.360097
28	H	0.810804	0.189196	0.842740	0.157260

3',4-dihydroxybiphenyl-4-carboxylic acid radical adduct

ROHF/6-31G(d)

```
C           6.0  -2.4225155804   1.1920693983  -0.3243644518
C           6.0  -1.0306723201   1.1593196244  -0.3690684199
```

C	6.0	-0.3274581256	-0.0005489299	-0.0872217757
C	6.0	-1.0465964045	-1.1653620284	0.2440778369
C	6.0	-2.4141371267	-1.1352480044	0.2959663838
C	6.0	-3.1328510046	0.0341747826	0.0161121122
H	1.0	-0.5288092508	2.0628798654	-0.6558597950
H	1.0	-0.5274787810	-2.0710378335	0.4914359834
H	1.0	-2.9561782211	-2.0209876436	0.5653125387
C	6.0	1.9110978473	1.1575782239	0.2431678307
C	6.0	3.2442356221	1.1621298038	0.2229138000
C	6.0	4.0701816319	-0.0229608454	-0.1923888141
C	6.0	3.2156055329	-1.2104460046	-0.5375892583
C	6.0	1.8828441688	-1.1934977316	-0.4960476253
C	6.0	1.1433785816	-0.0100262409	-0.1232689574
H	1.0	1.3844590115	2.0336115640	0.5748465035
H	1.0	3.7923483746	2.0350061936	0.5312270972
H	1.0	3.7414057700	-2.1028164020	-0.8285685794
H	1.0	1.3355735783	-2.0749579136	-0.7760948302
C	6.0	-4.5996360511	0.0661627461	0.0811342104
O	8.0	-5.2743882049	1.0333526469	-0.1549186133
O	8.0	-5.1583039076	-1.0820117388	0.4332872344
H	1.0	-6.1020330456	-0.9548039954	0.4493560136
O	8.0	-3.0026177917	2.3517065594	-0.6191469887
H	1.0	-3.9530305205	2.2686737652	-0.5612436614
O	8.0	5.0306897849	-0.3479239769	0.7904509265
H	1.0	4.5780627930	-0.5929169136	1.5874708654
H	1.0	4.6685534695	0.2456359690	-1.0583184464

```
Energy                                500823.718 KCAL/MOL
ZPE Correction                  146.122 KCAL/MOL
298.15K Temperature Correction       154.531 KCAL/MOL
```

TOTAL MULLIKEN AND LOWDIN ATOMIC POPULATIONS

ATOM		MULL.POP.	CHARGE	LOW.POP.	CHARGE
1	C	5.547135	0.452865	5.809888	0.190112
2	C	6.297186	-0.297186	6.225743	-0.225743
3	C	5.939038	0.060962	5.954654	0.045346
4	C	6.254931	-0.254931	6.220847	-0.220847
5	C	6.150384	-0.150384	6.102122	-0.102122
6	C	6.254862	-0.254862	6.154627	-0.154627
7	H	0.768716	0.231284	0.817676	0.182324
8	H	0.787168	0.212832	0.829621	0.170379
9	H	0.752318	0.247682	0.813590	0.186410
10	C	6.174235	-0.174235	6.174274	-0.174274
11	C	6.235889	-0.235889	6.177355	-0.177355
12	C	5.863911	0.136089	5.969590	0.030410
13	C	6.235355	-0.235355	6.176726	-0.176726
14	C	6.174337	-0.174337	6.175307	-0.175307

15 C	6.018599	-0.018599	5.987536	0.012464
16 H	0.782523	0.217477	0.826381	0.173619
17 H	0.790502	0.209498	0.826834	0.173166
18 H	0.791629	0.208371	0.827638	0.172362
19 H	0.786952	0.213048	0.828643	0.171357
20 C	5.158167	0.841833	5.697775	0.302225
21 O	8.636830	-0.636830	8.373197	-0.373197
22 O	8.707348	-0.707348	8.397139	-0.397139
23 H	0.524879	0.475121	0.611212	0.388788
24 O	8.769884	-0.769884	8.421010	-0.421010
25 H	0.481040	0.518960	0.608139	0.391861
26 O	8.742990	-0.742990	8.510995	-0.510995
27 H	0.565165	0.434835	0.640259	0.359741
28 H	0.808027	0.191973	0.841225	0.158775

4-hydroxybiphenyl-3-carboxylic acid (**3**)

RHF/6-31G(d)

C	6.0	-2.5490195764	1.0842591458	-0.4061042021
C	6.0	-1.1483429961	1.0841827772	-0.4552082029
C	6.0	-0.3895547893	0.0195987798	-0.0209332825
C	6.0	-1.0767613818	-1.0936869510	0.4842394914
C	6.0	-2.4462417249	-1.1347535641	0.5304578201
C	6.0	-3.2059314642	-0.0558926073	0.0725988382
H	1.0	-0.6284556732	1.9193297998	-0.8902576617
H	1.0	-0.5166437970	-1.9345983054	0.8514940123
H	1.0	-2.9671799777	-1.9909298004	0.9152842753
C	6.0	1.8202503435	1.1466690570	0.3527390671
C	6.0	3.2029796195	1.1693268323	0.2779449772
C	6.0	3.8905786614	0.0838364982	-0.2387009403
C	6.0	3.1846045641	-1.0232776638	-0.6809311704
C	6.0	1.8021210406	-1.0427639980	-0.6105472418
C	6.0	1.0986460716	0.0425498406	-0.0934476170
H	1.0	1.2994666625	1.9836961438	0.7830341237
H	1.0	3.7415922696	2.0297750655	0.6329499369
H	1.0	3.7086381030	-1.8689822738	-1.0890804404
H	1.0	1.2644063515	-1.8985257765	-0.9780953756
H	1.0	4.9641442985	0.0994082737	-0.2946755701
C	6.0	-3.3576724694	2.2415082901	-0.8704277487
O	8.0	-2.7421339799	3.3996904981	-1.0689606235
O	8.0	-4.5352957003	2.1743558779	-1.0624040085
H	1.0	-1.8523141593	3.4027625850	-0.7473971019
O	8.0	-4.5263023474	-0.1827238733	0.1352007625
H	1.0	-4.9481892790	0.5689817089	-0.2793108970

```
Energy                                  -453517.070 KCAL/MOL
ZPE Correction                  135.854 KCAL/MOL
298.15K Temperature Correction    143.306 KCAL/MOL
```

```
TOTAL MULLIKEN AND LOWDIN ATOMIC POPULATIONS
  ATOM              MULL.POP.  CHARGE        LOW.POP.   CHARGE
   1 C              6.237018  -0.237018      6.152772  -0.152772
   2 C              6.227223  -0.227223      6.140382  -0.140382
   3 C              6.022476  -0.022476      6.041282  -0.041282
   4 C              6.177954  -0.177954      6.112812  -0.112812
   5 C              6.252937  -0.252937      6.202809  -0.202809
   6 C              5.561181   0.438819      5.812722   0.187278
   7 H              0.787013   0.212987      0.833470   0.166530
   8 H              0.773053   0.226947      0.822285   0.177715
   9 H              0.766857   0.233143      0.815162   0.184838
  10 C              6.218187  -0.218187      6.174562  -0.174562
  11 C              6.196635  -0.196635      6.158656  -0.158656
  12 C              6.202294  -0.202294      6.161534  -0.161534
  13 C              6.196916  -0.196916      6.157650  -0.157650
  14 C              6.217214  -0.217214      6.170554  -0.170554
  15 C              5.981298   0.018702      6.005415  -0.005415
  16 H              0.800785   0.199215      0.836309   0.163691
  17 H              0.794000   0.206000      0.831823   0.168177
  18 H              0.792867   0.207133      0.831116   0.168884
  19 H              0.789755   0.210245      0.831478   0.168522
  20 H              0.793714   0.206286      0.834664   0.165336
  21 C              5.139451   0.860549      5.702273   0.297727
  22 O              8.702241  -0.702241      8.390797  -0.390797
  23 O              8.602671  -0.602671      8.333465  -0.333465
  24 H              0.522206   0.477794      0.619104   0.380896
  25 O              8.765864  -0.765864      8.423517  -0.423517
  26 H              0.478192   0.521808      0.603386   0.396614
```

4,5-dihydroxybiphenyl-3-carboxylic acid radical adduct

ROHF/6-31G(d)

```
 C          6.0   -2.5713349392    1.1206659252   -0.4446542387
 C          6.0   -1.1280432969    1.0728770354   -0.5500306801
 C          6.0   -0.3907369563   -0.0565934562   -0.0381052645
 C          6.0   -1.0446823375   -1.1009780774    0.4782835197
 C          6.0   -2.5368281109   -1.2135121367    0.5018979365
 C          6.0   -3.2334279367    0.0452091318    0.0459418125
 H          1.0   -0.5970104213    1.8016265132   -1.1316963901
 C          6.0    1.7989323900    1.1086945867    0.3271920760
 C          6.0    3.1821606206    1.1427486885    0.2857970101
```

```
C       6.0    3.8917885633    0.0494136214   -0.1843599186
C       6.0    3.2079104052   -1.0765094155   -0.6113762755
C       6.0    1.8237596515   -1.1097109851   -0.5688532494
C       6.0    1.1006529009   -0.0195499710   -0.0952270498
H       1.0    1.2593055169    1.9561237402    0.7112732424
H       1.0    3.7046205049    2.0190717212    0.6256469377
H       1.0    3.7495497964   -1.9272053007   -0.9846707946
H       1.0    1.3002231698   -1.9803779815   -0.9195423430
H       1.0    4.9661161154    0.0758677206   -0.2188096778
C       6.0   -3.3555405748    2.3123533236   -0.8363262426
O       8.0   -2.6959328834    3.4275333711   -1.1127725685
O       8.0   -4.5525958170    2.3163364206   -0.9009948840
H       1.0   -1.7752879659    3.3658263193   -0.9004431094
O       8.0   -4.5393953646   -0.0580549092    0.1865787054
H       1.0   -4.9667992482    0.7355277881   -0.1496395961
H       1.0   -0.5151825852   -1.9298902711    0.9103759358
H       1.0   -2.8525560430   -2.0042191602   -0.1813831033
O       8.0   -2.9377917513   -1.5440463744    1.8042581628
H       1.0   -3.8805924328   -1.6521239078    1.8186895971
```

Energy   -500816.188 KCAL/MOL
ZPE Correction   145.556 KCAL/MOL
298.15K Temperature Correction   154.073 KCAL/MOL

TOTAL MULLIKEN AND LOWDIN ATOMIC POPULATIONS

ATOM		MULL.POP.	CHARGE	LOW.POP.	CHARGE
1	C	6.250901	-0.250901	6.190452	-0.190452
2	C	6.251215	-0.251215	6.174550	-0.174550
3	C	5.956757	0.043243	6.007520	-0.007520
4	C	6.234215	-0.234215	6.181886	-0.181886
5	C	5.884177	0.115823	5.970635	0.029365
6	C	5.576847	0.423153	5.801922	0.198078
7	H	0.784315	0.215685	0.830096	0.169904
8	C	6.214033	-0.214033	6.170864	-0.170864
9	C	6.198208	-0.198208	6.160057	-0.160057
10	C	6.200249	-0.200249	6.159432	-0.159432
11	C	6.198147	-0.198147	6.159841	-0.159841
12	C	6.212137	-0.212137	6.165401	-0.165401
13	C	5.993656	0.006344	6.005980	-0.005980
14	H	0.797802	0.202198	0.835103	0.164897
15	H	0.794375	0.205625	0.832168	0.167832
16	H	0.793820	0.206180	0.831558	0.168442
17	H	0.790237	0.209763	0.830792	0.169208
18	H	0.794217	0.205783	0.834993	0.165007
19	C	5.137132	0.862868	5.698718	0.301282
20	O	8.702228	-0.702228	8.387985	-0.387985
21	O	8.622580	-0.622580	8.349906	-0.349906

22 H	0.520277	0.479723	0.618825	0.381175
23 O	8.761639	-0.761639	8.409521	-0.409521
24 H	0.467241	0.532759	0.596221	0.403779
25 H	0.775461	0.224539	0.819423	0.180577
26 H	0.813526	0.186474	0.848061	0.151939
27 O	8.735900	-0.735900	8.497867	-0.497867
28 H	0.538708	0.461292	0.630223	0.369777

4,6-dihydroxybiphenyl-3-carboxylic acid radical adduct

ROHF/6-31G(d)

C	6.0	-2.5689460547	1.0570070163	-0.3148821431
C	6.0	-1.1044303592	1.0011340275	-0.4014060345
C	6.0	-0.3587332294	-0.0536116208	-0.0740164096
C	6.0	-1.0408251774	-1.3466771818	0.3295458877
C	6.0	-2.4851568735	-1.1433900352	0.6861268667
C	6.0	-3.2248355996	0.0154484194	0.2779103452
H	1.0	-0.5909224626	1.8984850109	-0.6998940531
H	1.0	-3.0278673413	-1.9586376083	1.1236662645
C	6.0	1.7931761416	1.1527391938	0.3587157414
C	6.0	3.1753077757	1.2239820993	0.3563881308
C	6.0	3.9280165116	0.1389537918	-0.0611059657
C	6.0	3.2842071014	-1.0169682610	-0.4699170196
C	6.0	1.9011433284	-1.0888229941	-0.4727253544
C	6.0	1.1304321608	0.0021911569	-0.0697629922
H	1.0	1.2259692534	1.9898889300	0.7232252794
H	1.0	3.6620415071	2.1212587925	0.6950393167
H	1.0	3.8582069747	-1.8677327052	-0.7915085656
H	1.0	1.4182517270	-1.9895652489	-0.7981581843
H	1.0	5.0020225344	0.1906014306	-0.0587201850
C	6.0	-3.3513386884	2.2061004777	-0.7947682656
O	8.0	-2.7410852095	3.1168756750	-1.5443900646
O	8.0	-4.5174429301	2.3515401196	-0.5514965681
H	1.0	-1.8715322085	2.8528606876	-1.8085678282
O	8.0	-4.5207399130	-0.0444361118	0.5072110246
H	1.0	-4.9299397896	0.7834050394	0.2407242767
H	1.0	-0.5270465981	-1.7727364502	1.1812261968
O	8.0	-0.9383744210	-2.3463400567	-0.6690939417
H	1.0	-1.2980083701	-2.0112132143	-1.4809171853

Energy   -500812.423 KCAL/MOL
ZPE Correction   145.865 KCAL/MOL
298.15K Temperature Correction   154.342 KCAL/MOL

TOTAL MULLIKEN AND LOWDIN ATOMIC POPULATIONS

```
ATOM                 MULL.POP.  CHARGE        LOW.POP.   CHARGE
  1 C                6.286592   -0.286592     6.206453   -0.206453
  2 C                6.208825   -0.208825     6.169738   -0.169738
  3 C                6.035415   -0.035415     6.048836   -0.048836
  4 C                5.883864    0.116136     5.967537    0.032463
  5 C                6.202128   -0.202128     6.121948   -0.121948
  6 C                5.538956    0.461044     5.801137    0.198863
  7 H                0.800711    0.199289     0.836843    0.163157
  8 H                0.753874    0.246126     0.806098    0.193902
  9 C                6.223017   -0.223017     6.173215   -0.173215
 10 C                6.199990   -0.199990     6.162555   -0.162555
 11 C                6.200223   -0.200223     6.160232   -0.160232
 12 C                6.198946   -0.198946     6.161130   -0.161130
 13 C                6.234571   -0.234571     6.172914   -0.172914
 14 C                6.001989   -0.001989     6.011432   -0.011432
 15 H                0.795344    0.204656     0.834286    0.165714
 16 H                0.795773    0.204227     0.833037    0.166963
 17 H                0.794567    0.205433     0.832237    0.167763
 18 H                0.751335    0.248665     0.817043    0.182957
 19 H                0.795425    0.204575     0.835720    0.164280
 20 C                5.138441    0.861559     5.703241    0.296759
 21 O                8.706641   -0.706641     8.394301   -0.394301
 22 O                8.625959   -0.625959     8.354876   -0.354876
 23 H                0.521112    0.478888     0.618880    0.381120
 24 O                8.751147   -0.751147     8.403343   -0.403343
 25 H                0.470628    0.529372     0.598376    0.401624
 26 H                0.792487    0.207513     0.832665    0.167335
 27 O                8.733502   -0.733502     8.505420   -0.505420
 28 H                0.558541    0.441459     0.636507    0.363493
```

2',4-dihydroxybiphenyl-3-carboxylic acid radical adduct

ROHF/6-31G(d)

```
C        6.0  -2.5770663489   1.1517499647  -0.4067651589
C        6.0  -1.1771482818   1.1114456368  -0.4047628030
C        6.0  -0.4576724807  -0.0092160804  -0.0395933505
C        6.0  -1.1981862720  -1.1521681285   0.3129283141
C        6.0  -2.5691600093  -1.1501760340   0.3034645968
C        6.0  -3.2831030970  -0.0088592722  -0.0654937069
H        1.0  -0.6239901332   1.9652852529  -0.7515090136
H        1.0  -0.6786952323  -2.0460488638   0.5952936179
H        1.0  -3.1266551542  -2.0275699939   0.5717407100
C        6.0   1.7282906656   1.0958494612   0.3072252034
C        6.0   3.1456555977   1.1847715587   0.1639489415
C        6.0   3.8609552543   0.0948805523  -0.4298625155
```

```
C        6.0    3.2220112428   -1.0206781244   -0.7865250225
C        6.0    1.7575874562   -1.2460900598   -0.5245962918
C        6.0    1.0294670229    0.0053323090   -0.0594742682
H        1.0    1.2121336714    1.9481620839    0.7134618429
H        1.0    3.6637272602    2.0695653401    0.4794049096
H        1.0    3.7510809794   -1.8479975122   -1.2252524082
H        1.0    4.9209129633    0.1902490584   -0.5870577032
C        6.0   -3.3337833627    2.3704206408   -0.7923244160
O        8.0   -2.6783186321    3.5225123211   -0.8617478998
O        8.0   -4.5046404000    2.3592979278   -1.0320677772
H        1.0   -1.8042462295    3.4682098818   -0.5037948459
O        8.0   -4.6072186371   -0.0998663494   -0.0647204185
H        1.0   -4.9914843568    0.7013540187   -0.4185923626
H        1.0    1.2791286937   -1.6177770912   -1.4230581163
O        8.0    1.6085716693   -2.3110103545    0.4028007804
H        1.0    2.0742336707   -2.0828238138    1.1978757623
```

```
Energy                                -500813.050 KCAL/MOL
ZPE Correction                   145.719 KCAL/MOL
298.15K Temperature Correction       154.179 KCAL/MOL
```

TOTAL MULLIKEN AND LOWDIN ATOMIC POPULATIONS

ATOM		MULL.POP.	CHARGE	LOW.POP.	CHARGE
1	C	6.239570	-0.239570	6.156786	-0.156786
2	C	6.231007	-0.231007	6.137933	-0.137933
3	C	6.040133	-0.040133	6.048478	-0.048478
4	C	6.189800	-0.189800	6.112529	-0.112529
5	C	6.255971	-0.255971	6.206883	-0.206883
6	C	5.557099	0.442901	5.810506	0.189494
7	H	0.789889	0.210111	0.835123	0.164877
8	H	0.728390	0.271610	0.805038	0.194962
9	H	0.767646	0.232354	0.815950	0.184050
10	C	6.212309	-0.212309	6.187041	-0.187041
11	C	6.208243	-0.208243	6.149767	-0.149767
12	C	6.177456	-0.177456	6.170411	-0.170411
13	C	6.221630	-0.221630	6.182932	-0.182932
14	C	5.883986	0.116014	5.966847	0.033153
15	C	5.997702	0.002298	6.021065	-0.021065
16	H	0.804316	0.195684	0.836925	0.163075
17	H	0.787044	0.212956	0.827370	0.172630
18	H	0.791710	0.208290	0.827081	0.172919
19	H	0.792611	0.207389	0.832647	0.167353
20	C	5.139743	0.860257	5.702703	0.297297
21	O	8.703192	-0.703192	8.392289	-0.392289
22	O	8.603576	-0.603576	8.334523	-0.334523
23	H	0.523749	0.476251	0.619612	0.380388
24	O	8.765120	-0.765120	8.421714	-0.421714

25 H	0.478509	0.521491	0.604114	0.395886
26 H	0.805416	0.194584	0.841634	0.158366
27 O	8.742202	-0.742202	8.513529	-0.513529
28 H	0.561983	0.438017	0.638568	0.361432

3',4-dihydroxybiphenyl-3-carboxylic acid radical adduct

ROHF/6-31G(d)

C	6.0	-2.5387961596	1.0637528727	-0.3761735254
C	6.0	-1.1386296663	1.0659456945	-0.4260156034
C	6.0	-0.3798559297	-0.0172207771	-0.0398521724
C	6.0	-1.0655503156	-1.1465563493	0.4282982503
C	6.0	-2.4353162281	-1.1892661168	0.4749636998
C	6.0	-3.1953585380	-0.0948401440	0.0576042965
H	1.0	-0.6217844586	1.9214705091	-0.8242474342
H	1.0	-0.5037964458	-1.9993270148	0.7630608501
H	1.0	-2.9552418639	-2.0590357143	0.8293487491
C	6.0	1.8282892086	1.1571738434	0.3572633194
C	6.0	3.2558223349	1.2147748385	0.2279285324
C	6.0	3.9470274275	0.1999540156	-0.2933545055
C	6.0	3.2928900717	-1.0666400392	-0.7715409953
C	6.0	1.7921828814	-1.0209578288	-0.6599941141
C	6.0	1.1095298224	0.0033336798	-0.1311120643
H	1.0	1.2998494769	1.9544669243	0.8428414707
H	1.0	3.7649607975	2.0997550620	0.5677651992
H	1.0	1.2749286905	-1.8743927665	-1.0627123172
H	1.0	5.0168262532	0.2493828565	-0.3946619653
C	6.0	-3.3477680246	2.2393574417	-0.7914336006
O	8.0	-2.7336862516	3.4073829551	-0.9297685604
O	8.0	-4.5232213387	2.1777041843	-0.9961094259
H	1.0	-1.8500487184	3.3992424624	-0.5919044227
O	8.0	-4.5154619679	-0.2231622047	0.1171026882
H	1.0	-4.9381394137	0.5416073656	-0.2716174297
H	1.0	3.6656205203	-1.9008022277	-0.1831571589
O	8.0	3.6927205393	-1.3850347038	-2.0879193756
H	1.0	3.3979041162	-0.6962688887	-2.6700484749

Energy		-500811.795 KCAL/MOL
ZPE Correction	145.353 KCAL/MOL	
298.15K Temperature Correction	153.894 KCAL/MOL	

TOTAL MULLIKEN AND LOWDIN ATOMIC POPULATIONS

ATOM	MULL.POP.	CHARGE	LOW.POP.	CHARGE
1 C	6.237146	-0.237146	6.152311	-0.152311
2 C	6.227043	-0.227043	6.141062	-0.141062

3	C	6.019565	-0.019565	6.041462	-0.041462
4	C	6.176509	-0.176509	6.110640	-0.110640
5	C	6.253046	-0.253046	6.202526	-0.202526
6	C	5.560210	0.439790	5.812121	0.187879
7	H	0.789516	0.210484	0.835283	0.164717
8	H	0.772460	0.227540	0.821497	0.178503
9	H	0.765580	0.234420	0.814579	0.185421
10	C	6.221060	-0.221060	6.155957	-0.155957
11	C	6.175193	-0.175193	6.174122	-0.174122
12	C	6.228287	-0.228287	6.176716	-0.176716
13	C	5.860765	0.139235	5.966632	0.033368
14	C	6.269499	-0.269499	6.191887	-0.191887
15	C	5.953069	0.046931	6.017678	-0.017678
16	H	0.791833	0.208167	0.830541	0.169459
17	H	0.793435	0.206565	0.830861	0.169139
18	H	0.787824	0.212176	0.827485	0.172515
19	H	0.791222	0.208778	0.830197	0.169803
20	C	5.140323	0.859677	5.702756	0.297244
21	O	8.701799	-0.701799	8.391085	-0.391085
22	O	8.600660	-0.600660	8.331939	-0.331939
23	H	0.523240	0.476760	0.619320	0.380680
24	O	8.764923	-0.764923	8.422438	-0.422438
25	H	0.478201	0.521799	0.603394	0.396606
26	H	0.809093	0.190907	0.841861	0.158139
27	O	8.743012	-0.743012	8.513666	-0.513666
28	H	0.565486	0.434514	0.639983	0.360017

4,4'-dihydroxybiphenyl-3-carboxylic acid radical adduct

ROHF/6-31G(d)

C	6.0	-2.5254659308	1.0914706298	-0.3707723567
C	6.0	-1.1255839645	1.1034380060	-0.3965989434
C	6.0	-0.3601043918	0.0110739715	-0.0343440898
C	6.0	-1.0561579844	-1.1415515614	0.3725886624
C	6.0	-2.4244450448	-1.1915574935	0.3925643387
C	6.0	-3.1845144906	-0.0850445528	0.0051872856
H	1.0	-0.6132025884	1.9744842490	-0.7632928518
H	1.0	-0.5055649302	-2.0082050723	0.6889512479
H	1.0	-2.9456595491	-2.0773144216	0.7027104263
C	6.0	1.8479338310	1.2498376497	0.2266226179
C	6.0	3.1793639772	1.3041816861	0.1660875624
C	6.0	4.0372537031	0.1343811675	-0.2288575730
C	6.0	3.2163734416	-1.0960315911	-0.4987214596
C	6.0	1.8847190972	-1.1219984881	-0.4228916343
C	6.0	1.1110432673	0.0472773783	-0.0800184672

H	1.0	1.3012202986	2.1184944725	0.5489752413
H	1.0	3.7029243140	2.2064739864	0.4291400329
H	1.0	3.7653520440	-1.9814427808	-0.7670418741
H	1.0	1.3633600775	-2.0340377106	-0.6527845673
C	6.0	-3.3336938512	2.2781254049	-0.7571980707
O	8.0	-2.7254780765	3.4544302625	-0.8344551428
O	8.0	-4.5037643473	2.2160849166	-0.9902748347
H	1.0	-1.8506144942	3.4397705508	-0.4743607457
O	8.0	-4.5039635366	-0.2233880663	0.0340498293
H	1.0	-4.9243497528	0.5527524797	-0.3345094271
O	8.0	5.0376130426	-0.1136275118	0.7365743198
H	1.0	4.6006143388	0.3884142389	-1.1222060937
H	1.0	4.6182133504	-0.3523636000	1.5534299173

```
Energy                                  -500813.678 KCAL/MOL
ZPE Correction                   145.805 KCAL/MOL
298.15K Temperature Correction       154.306 KCAL/MOL
```

TOTAL MULLIKEN AND LOWDIN ATOMIC POPULATIONS

ATOM		MULL.POP.	CHARGE	LOW.POP.	CHARGE
1	C	6.236019	-0.236019	6.150574	-0.150574
2	C	6.232336	-0.232336	6.141262	-0.141262
3	C	6.013863	-0.013863	6.044194	-0.044194
4	C	6.181652	-0.181652	6.114565	-0.114565
5	C	6.251840	-0.251840	6.200519	-0.200519
6	C	5.560874	0.439126	5.812231	0.187769
7	H	0.784766	0.215234	0.833528	0.166472
8	H	0.773778	0.226222	0.823213	0.176787
9	H	0.764974	0.235026	0.814522	0.185478
10	C	6.176553	-0.176553	6.179414	-0.179414
11	C	6.236242	-0.236242	6.179782	-0.179782
12	C	5.862632	0.137368	5.968920	0.031080
13	C	6.239399	-0.239399	6.181366	-0.181366
14	C	6.176210	-0.176210	6.175808	-0.175808
15	C	6.005933	-0.005933	5.994929	0.005071
16	H	0.805321	0.194679	0.837244	0.162756
17	H	0.792170	0.207830	0.827884	0.172116
18	H	0.791645	0.208355	0.827526	0.172474
19	H	0.791266	0.208734	0.831412	0.168588
20	C	5.139011	0.860989	5.702481	0.297519
21	O	8.700905	-0.700905	8.390268	-0.390268
22	O	8.600289	-0.600289	8.331395	-0.331395
23	H	0.523142	0.476858	0.618709	0.381291
24	O	8.763923	-0.763923	8.420838	-0.420838
25	H	0.477660	0.522340	0.603071	0.396929
26	O	8.742845	-0.742845	8.511106	-0.511106
27	H	0.808887	0.191113	0.842296	0.157704

```
   28 H           0.565864    0.434136         0.640940    0.359060
```

benzene

ROHF/6-31G(d)

```
    1  C        6.0     0.0000000     0.0000202     0.0000000
    2  C        6.0     0.0000000    -0.0000202     0.0000000
    3  C        6.0    -0.0000020     0.0000189     0.0000000
    4  C        6.0     0.0000020     0.0000189     0.0000000
    5  C        6.0    -0.0000020    -0.0000189     0.0000000
    6  C        6.0     0.0000020    -0.0000189     0.0000000
    7  H        1.0     0.0000000    -0.0000023     0.0000000
    8  H        1.0     0.0000000     0.0000023     0.0000000
    9  H        1.0    -0.0000033    -0.0000051     0.0000000
   10  H        1.0     0.0000033    -0.0000051     0.0000000
   11  H        1.0    -0.0000033     0.0000051     0.0000000
   12  H        1.0     0.0000033     0.0000051     0.0000000
```

```
Energy                              -144768.209 KCAL/MOL
ZPE Correction                67.566 KCAL/MOL
298.15K Temperature Correction      70.136 KCAL/MOL
```

TOTAL MULLIKEN AND LOWDIN ATOMIC POPULATIONS

ATOM	MULL.POP.	CHARGE	LOW.POP.	CHARGE
1 C	6.199454	-0.199454	6.161124	-0.161124
2 C	6.199454	-0.199454	6.161124	-0.161124
3 C	6.199453	-0.199453	6.164752	-0.164752
4 C	6.199453	-0.199453	6.164752	-0.164752
5 C	6.199453	-0.199453	6.164752	-0.164752
6 C	6.199453	-0.199453	6.164752	-0.164752
7 H	0.800542	0.199458	0.838177	0.161823
8 H	0.800542	0.199458	0.838177	0.161823
9 H	0.800549	0.199451	0.835597	0.164403
10 H	0.800549	0.199451	0.835597	0.164403
11 H	0.800549	0.199451	0.835597	0.164403
12 H	0.800549	0.199451	0.835597	0.164403

hydroxybenzene radical adduct

ROHF/6-31G(d)

```
   C        6.0   -1.1295003522   -1.2380546922   -0.0577771816
   C        6.0    0.1733797150   -1.2541538519    0.2339096074
   C        6.0    0.9881236608   -0.0026585434    0.4274039960
```

```
C     6.0    0.1754843013    1.2490400942    0.2266499487
C     6.0   -1.1274589072    1.2334555035   -0.0647521189
C     6.0   -1.8441089116   -0.0021085901   -0.2056155043
H     1.0   -1.6646166868   -2.1625436735   -0.1892160675
H     1.0    0.7060821003   -2.1835813518    0.3346451577
H     1.0    0.7097165411    2.1781332762    0.3220420766
H     1.0   -1.6612347165    2.1579938041   -0.2012898466
H     1.0   -2.8915848092   -0.0019930113   -0.4367996632
O     8.0    2.1339381822   -0.0060698306   -0.4009492648
H     1.0    1.8498329770   -0.0081305995   -1.3061610718
H     1.0    1.4008952558    0.0000033763    1.4324880424
```

Energy   -192064.190 KCAL/MOL
ZPE Correction   77.122 KCAL/MOL
298.15K Temperature Correction   80.728 KCAL/MOL

TOTAL MULLIKEN AND LOWDIN ATOMIC POPULATIONS

ATOM		MULL.POP.	CHARGE	LOW.POP.	CHARGE
1	C	6.173576	-0.173576	6.173648	-0.173648
2	C	6.231660	-0.231660	6.185963	-0.185963
3	C	5.864980	0.135020	5.966950	0.033050
4	C	6.231708	-0.231708	6.185979	-0.185979
5	C	6.173546	-0.173546	6.173629	-0.173629
6	C	6.213273	-0.213273	6.149566	-0.149566
7	H	0.798692	0.201308	0.833598	0.166402
8	H	0.797840	0.202160	0.830963	0.169037
9	H	0.797840	0.202160	0.830961	0.169039
10	H	0.798686	0.201314	0.833597	0.166403
11	H	0.792240	0.207760	0.832215	0.167785
12	O	8.745133	-0.745133	8.512851	-0.512851
13	H	0.567232	0.432768	0.643507	0.356493
14	H	0.813594	0.186406	0.846573	0.153427

quinoline

ROHF/6-31G(d)

```
C     6.0    0.5425891183   -0.4874890648    0.0000000000
C     6.0    1.7059022118   -1.1882891951    0.0000000000
C     6.0    1.6842752891   -2.6056829678    0.0000000000
C     6.0    0.5046152271   -3.2792578031    0.0000000000
C     6.0   -0.7248097942   -2.5711595722    0.0000000000
C     6.0   -0.7044335023   -1.1650287974    0.0000000000
H     1.0    0.5512594503    0.5885724800    0.0000000000
H     1.0    2.6495661127   -0.6731489044    0.0000000000
H     1.0    2.6138328167   -3.1462183318    0.0000000000
```

```
  H          1.0    0.4651362506   -4.3524426142    0.0000000000
  C          6.0   -1.9526793165   -0.4931971536    0.0000000000
  C          6.0   -3.0972705861   -1.2203812195    0.0000000000
  C          6.0   -2.9981367694   -2.6344990102    0.0000000000
  N          7.0   -1.8803582031   -3.2821460345    0.0000000000
  H          1.0   -3.8985319084   -3.2257749369    0.0000000000
  H          1.0   -4.0644259063   -0.7528856901    0.0000000000
  H          1.0   -1.9771371802    0.5826160459    0.0000000000
```

Energy   -250595.719 KCAL/MOL
ZPE Correction   91.513 KCAL/MOL
298.15K Temperature Correction   95.380 KCAL/MOL

TOTAL MULLIKEN AND LOWDIN ATOMIC POPULATIONS

ATOM	MULL.POP.	CHARGE	LOW.POP.	CHARGE
1 C	6.197235	-0.197235	6.156333	-0.156333
2 C	6.209410	-0.209410	6.167590	-0.167590
3 C	6.205930	-0.205930	6.157779	-0.157779
4 C	6.186133	-0.186133	6.157089	-0.157089
5 C	5.755515	0.244485	5.943311	0.056689
6 C	6.019750	-0.019750	6.035195	-0.035195
7 H	0.792705	0.207295	0.836324	0.163676
8 H	0.794519	0.205481	0.832654	0.167346
9 H	0.793021	0.206979	0.831606	0.168394
10 H	0.776092	0.223908	0.823810	0.176190
11 C	6.129031	-0.129031	6.111587	-0.111587
12 C	6.276113	-0.276113	6.207810	-0.207810
13 C	5.924228	0.075772	6.057975	-0.057975
14 N	7.570618	-0.570618	7.185722	-0.185722
15 H	0.797688	0.202312	0.835658	0.164342
16 H	0.788490	0.211510	0.828080	0.171920
17 H	0.783522	0.216478	0.831476	0.168524

2-hydroxyquinoline radical adduct

ROHF/6-31G(d)

```
  C          6.0    0.5790332051   -0.4828512476   -0.1678369132
  C          6.0    1.7634331606   -1.2002920478   -0.2156440755
  C          6.0    1.7522726148   -2.5765843926   -0.0465912105
  C          6.0    0.5538597525   -3.2331467728    0.1714508578
  C          6.0   -0.6410616101   -2.5241006928    0.1894686733
  C          6.0   -0.6314272349   -1.1316524828    0.0273885716
  H          1.0    0.5938782819    0.5867032887   -0.2840136580
  H          1.0    2.6936594337   -0.6853066063   -0.3754634931
  H          1.0    2.6719306809   -3.1321918320   -0.0764111807
  H          1.0    0.5203429341   -4.2962643470    0.3214976976
```

```
C       6.0   -1.9118346894   -0.4174086156    0.1136115644
C       6.0   -3.0442571771   -1.0949584087    0.1701024549
C       6.0   -3.0576708413   -2.6032304151    0.0815326933
N       7.0   -1.8150076537   -3.2350694722    0.4371377827
H       1.0   -4.0032317449   -0.6122492944    0.2203799640
H       1.0   -1.8979987423    0.6582536307    0.1291939476
O       8.0   -4.1017178778   -3.1540964795    0.8216285743
H       1.0   -3.8211951902   -3.2452738143    1.7230342939
H       1.0   -3.2602169621   -2.8815898878   -0.9517827045
```

```
Energy                            -297896.720 KCAL/MOL
ZPE Correction               100.973 KCAL/MOL
298.15K Temperature Correction      106.022 KCAL/MOL
```

TOTAL MULLIKEN AND LOWDIN ATOMIC POPULATIONS

ATOM	MULL.POP.	CHARGE	LOW.POP.	CHARGE
1 C	6.227631	-0.227631	6.167048	-0.167048
2 C	6.191267	-0.191267	6.150907	-0.150907
3 C	6.211795	-0.211795	6.168422	-0.168422
4 C	6.181136	-0.181136	6.141223	-0.141223
5 C	5.809167	0.190833	5.987179	0.012821
6 C	5.990685	0.009315	6.014472	-0.014472
7 H	0.790819	0.209181	0.835379	0.164621
8 H	0.791084	0.208916	0.831043	0.168957
9 H	0.790859	0.209141	0.830470	0.169530
10 H	0.773104	0.226896	0.823042	0.176958
11 C	6.139419	-0.139419	6.161923	-0.161923
12 C	6.268974	-0.268974	6.188492	-0.188492
13 C	5.646649	0.353351	5.920664	0.079336
14 N	7.515825	-0.515825	7.152829	-0.152829
15 H	0.783328	0.216672	0.822801	0.177199
16 H	0.789266	0.210734	0.832707	0.167293
17 O	8.742871	-0.742871	8.494237	-0.494237
18 H	0.556798	0.443202	0.636146	0.363854
19 H	0.799324	0.200676	0.841014	0.158986

3-hydroxyquinoline radical adduct

ROHF/6-31G(d)

```
C       6.0    0.5973508398   -0.5145612326   -0.0352594765
C       6.0    1.7827663585   -1.2202208171    0.0372098252
C       6.0    1.7629766963   -2.6073200736    0.0985705774
C       6.0    0.5551009665   -3.2826114816    0.0826819161
C       6.0   -0.6385176831   -2.5823761199    0.0138363536
C       6.0   -0.6289315934   -1.1809714902   -0.0410965311
```

```
H           1.0    0.6114405428    0.5604033146   -0.0812404777
H           1.0    2.7199341680   -0.6933217180    0.0470552212
H           1.0    2.6846349160   -3.1578245759    0.1546051890
H           1.0    0.5161569823   -4.3553460597    0.1203385401
C           6.0   -1.8897066224   -0.4881912884   -0.1156392204
C           6.0   -3.1746157863   -1.2415199499   -0.0016691209
C           6.0   -2.9408423700   -2.7370196005   -0.0412960977
N           7.0   -1.8335790677   -3.3290301510   -0.0258677751
H           1.0   -3.8361221384   -3.3389593237   -0.0906638031
H           1.0   -1.9271167312    0.5837754814   -0.1686874258
O           8.0   -4.1227648028   -0.8679930880   -0.9736642749
H           1.0   -3.6621632233   -1.0096695927    0.9426920399
H           1.0   -3.7394785517   -0.9650853429   -1.8361002790
```

```
Energy                                -297896.720 KCAL/MOL
ZPE Correction                 100.783 KCAL/MOL
298.15K Temperature Correction     105.779 KCAL/MOL
```

TOTAL MULLIKEN AND LOWDIN ATOMIC POPULATIONS

ATOM		MULL.POP.	CHARGE	LOW.POP.	CHARGE
1	C	6.220632	-0.220632	6.159614	-0.159614
2	C	6.199055	-0.199055	6.163021	-0.163021
3	C	6.207532	-0.207532	6.163165	-0.163165
4	C	6.195716	-0.195716	6.153648	-0.153648
5	C	5.798230	0.201770	5.967045	0.032955
6	C	5.956787	0.043213	6.031060	-0.031060
7	H	0.793498	0.206502	0.836464	0.163536
8	H	0.794394	0.205606	0.832640	0.167360
9	H	0.793193	0.206807	0.831608	0.168392
10	H	0.775853	0.224147	0.824337	0.175663
11	C	6.229105	-0.229105	6.164914	-0.164914
12	C	5.893134	0.106866	5.992041	0.007959
13	C	5.942477	0.057523	6.063966	-0.063966
14	N	7.522850	-0.522850	7.176836	-0.176836
15	H	0.790997	0.209003	0.831750	0.168250
16	H	0.784414	0.215586	0.828064	0.171936
17	O	8.743127	-0.743127	8.503736	-0.503736
18	H	0.799083	0.200917	0.837264	0.162736
19	H	0.559924	0.440076	0.638827	0.361173

4-hydroxyquinoline radical adduct

ROHF/6-31G(d)

```
C           6.0    0.5379530786   -0.5250241805   -0.0911655435
C           6.0    1.7264929122   -1.2308476530   -0.0714047780
```

C	6.0	1.7035952851	-2.6169811750	0.0129220171
C	6.0	0.4969302340	-3.2837609953	0.0721957803
C	6.0	-0.7040134171	-2.5785352211	0.0489510482
C	6.0	-0.6823298065	-1.1857440643	-0.0290233357
H	1.0	0.5473605253	0.5479303276	-0.1616103233
H	1.0	2.6640340484	-0.7066563758	-0.1199032596
H	1.0	2.6244115391	-3.1719569340	0.0302595119
H	1.0	0.4536478680	-4.3551824170	0.1325237607
C	6.0	-1.9753764370	-0.3954772716	-0.0347981924
C	6.0	-3.1574491718	-1.3134425067	-0.0875013127
C	6.0	-3.0014894165	-2.7338500636	0.0177541338
N	7.0	-1.8856600650	-3.3380041258	0.0920109696
H	1.0	-3.8916368282	-3.3427042726	0.0264650218
H	1.0	-4.1352372108	-0.8805632147	-0.1816104902
O	8.0	-2.0192908994	0.5690397921	-1.0603651939
H	1.0	-1.8646544339	0.1419159479	-1.8935068740
H	1.0	-2.0347977044	0.1935360136	0.8760975799

```
Energy                              -297897.348 KCAL/MOL
ZPE Correction              101.061 KCAL/MOL
298.15K Temperature Correction       106.001 KCAL/MOL
```

TOTAL MULLIKEN AND LOWDIN ATOMIC POPULATIONS

ATOM		MULL.POP.	CHARGE	LOW.POP.	CHARGE
1	C	6.208548	-0.208548	6.153715	-0.153715
2	C	6.202451	-0.202451	6.166400	-0.166400
3	C	6.201148	-0.201148	6.159043	-0.159043
4	C	6.199945	-0.199945	6.156430	-0.156430
5	C	5.774168	0.225832	5.965773	0.034227
6	C	6.076163	-0.076163	6.062754	-0.062754
7	H	0.777608	0.222392	0.828531	0.171469
8	H	0.795094	0.204906	0.833187	0.166813
9	H	0.794101	0.205899	0.832337	0.167663
10	H	0.777376	0.222624	0.824819	0.175181
11	C	5.805910	0.194090	5.967851	0.032149
12	C	6.248517	-0.248517	6.157569	-0.157569
13	C	5.912052	0.087948	6.066760	-0.066760
14	N	7.554458	-0.554458	7.188908	-0.188908
15	H	0.793563	0.206437	0.833920	0.166080
16	H	0.777467	0.222533	0.820561	0.179439
17	O	8.741653	-0.741653	8.505426	-0.505426
18	H	0.561838	0.438162	0.638564	0.361436
19	H	0.797940	0.202060	0.837453	0.162547

5-hydroxyquinoline radical adduct

ROHF/6-31G(d)

C	6.0	0.5252075204	-0.4015834731	-0.0328775481
C	6.0	1.7495970275	-1.2747660889	-0.0792452711
C	6.0	1.7077839026	-2.6082066030	-0.0217702612
C	6.0	0.4700623393	-3.3196325022	0.0733576301
C	6.0	-0.7811319320	-2.5894947027	0.0552527259
C	6.0	-0.7691782428	-1.1947570244	-0.0107106029
H	1.0	2.6876444040	-0.7540487157	-0.1572843529
H	1.0	2.6220485688	-3.1748705674	-0.0477143111
H	1.0	0.4331729431	-4.3890841501	0.1269721276
C	6.0	-1.9926486005	-0.5410232273	-0.0555928521
C	6.0	-3.1584717861	-1.2775126355	-0.0223309652
C	6.0	-3.0533660017	-2.6611116657	0.0531502850
N	7.0	-1.9085036889	-3.3019534892	0.0880878000
H	1.0	-3.9396906371	-3.2711887919	0.0827719366
H	1.0	-4.1225118671	-0.8049696394	-0.0536978177
O	8.0	0.5361122206	0.5450212808	-1.0793663815
H	1.0	0.5047638427	0.0839595575	-1.9081835368
H	1.0	0.5727117707	0.2096533793	0.8630993446
H	1.0	-2.0197829533	0.5317905788	-0.1227572093

Energy		-297900.485 KCAL/MOL
ZPE Correction	101.175 KCAL/MOL	
298.15K Temperature Correction	106.092 KCAL/MOL	

TOTAL MULLIKEN AND LOWDIN ATOMIC POPULATIONS

ATOM		MULL.POP.	CHARGE	LOW.POP.	CHARGE
1	C	5.835945	0.164055	5.964271	0.035729
2	C	6.237050	-0.237050	6.188422	-0.188422
3	C	6.176123	-0.176123	6.169993	-0.169993
4	C	6.197756	-0.197756	6.138619	-0.138619
5	C	5.712404	0.287596	5.941339	0.058661
6	C	6.106869	-0.106869	6.074709	-0.074709
7	H	0.791993	0.208007	0.828234	0.171766
8	H	0.791306	0.208694	0.829498	0.170502
9	H	0.769024	0.230976	0.818962	0.181038
10	C	6.136526	-0.136526	6.106119	-0.106119
11	C	6.268202	-0.268202	6.208193	-0.208193
12	C	5.928109	0.071891	6.061114	-0.061114
13	N	7.583581	-0.583581	7.193540	-0.193540
14	H	0.797084	0.202916	0.834838	0.165162
15	H	0.788325	0.211675	0.827988	0.172012
16	O	8.743901	-0.743901	8.510055	-0.510055
17	H	0.563881	0.436119	0.639757	0.360243
18	H	0.804354	0.195646	0.841241	0.158759
19	H	0.767568	0.232432	0.823109	0.176891

6-hydroxyquinoline radical adduct

ROHF/6-31G(d)

C	6.0	0.4381874489	-0.4736846932	-0.1059434375
C	6.0	1.7597761700	-1.1853173095	-0.1022653466
C	6.0	1.6050790570	-2.6841074037	-0.0668269513
C	6.0	0.4351829692	-3.3002988681	0.0020099188
C	6.0	-0.8395235649	-2.5696513561	0.0461601435
C	6.0	-0.8236516164	-1.1662018898	-0.0132366096
H	1.0	2.5212343557	-3.2471515304	-0.1055476425
H	1.0	0.3643403855	-4.3722439961	0.0272543840
C	6.0	-2.0525994464	-0.5134613021	0.0107639271
C	6.0	-3.2128034503	-1.2571018631	0.0997845610
C	6.0	-3.1057573182	-2.6375587963	0.1565465633
N	7.0	-1.9519586681	-3.2782392755	0.1279242513
H	1.0	-3.9871756075	-3.2502434750	0.2261783254
H	1.0	-4.1772500592	-0.7849683974	0.1253847861
O	8.0	2.5705068939	-0.7853701684	-1.1876421896
H	1.0	2.1426214723	-1.0349400630	-1.9968238121
H	1.0	-2.0918935533	0.5608402262	-0.0360987549
H	1.0	2.3308194424	-0.8744586989	0.7682853635
H	1.0	0.4543911894	0.5984851305	-0.1717144601

Energy	-297897.348 KCAL/MOL
ZPE Correction	100.890 KCAL/MOL
298.15K Temperature Correction	105.886 KCAL/MOL

TOTAL MULLIKEN AND LOWDIN ATOMIC POPULATIONS

ATOM	MULL.POP.	CHARGE	LOW.POP.	CHARGE
1 C	6.239268	-0.239268	6.161401	-0.161401
2 C	5.854793	0.145207	5.969515	0.030485
3 C	6.238631	-0.238631	6.179838	-0.179838
4 C	6.156309	-0.156309	6.163657	-0.163657
5 C	5.759731	0.240269	5.937931	0.062069
6 C	5.985003	0.014997	6.044867	-0.044867
7 H	0.789921	0.210079	0.826888	0.173112
8 H	0.774453	0.225547	0.822218	0.177782
9 C	6.154952	-0.154952	6.119358	-0.119358
10 C	6.261041	-0.261041	6.200897	-0.200897
11 C	5.938329	0.061671	6.070084	-0.070084
12 N	7.575691	-0.575691	7.186153	-0.186153
13 H	0.795608	0.204392	0.833547	0.166453
14 H	0.787440	0.212560	0.827393	0.172607
15 O	8.743205	-0.743205	8.511742	-0.511742

16 H		0.565005	0.434995	0.640853	0.359147
17 H		0.783413	0.216587	0.831367	0.168633
18 H		0.808341	0.191659	0.841939	0.158061
19 H		0.788868	0.211132	0.830349	0.169651

7-hydroxyquinoline radical adduct

ROHF/6-31G(d)

```
C      6.0     0.4575911958   -0.4240123794   -0.0105236806
C      6.0     1.6109455797   -1.0658066038   -0.1177062162
C      6.0     1.7222741302   -2.5672036760   -0.1905428740
C      6.0     0.3812574766   -3.2415089533   -0.1860123979
C      6.0    -0.8630400008   -2.5193855628   -0.0537159079
C      6.0    -0.8351685876   -1.1187367952    0.0401883107
H      1.0     0.3427168000   -4.3095441978   -0.2763031355
C      6.0    -2.0451415348   -0.4565134955    0.1630574173
C      6.0    -3.2187519348   -1.1877404990    0.1882046517
C      6.0    -3.1307266466   -2.5670997483    0.0827163877
N      7.0    -1.9920838918   -3.2192848783   -0.0370383137
H      1.0    -4.0218912261   -3.1699641628    0.0955763535
H      1.0    -4.1750406990   -0.7084824155    0.2839795996
O      8.0     2.5026654149   -2.9654099970   -1.2978996788
H      1.0     2.0582071790   -2.7067283867   -2.0951304614
H      1.0    -2.0676396833    0.6170359565    0.2370161672
H      1.0     0.4405378553    0.6513465300    0.0414227555
H      1.0     2.2968290414   -2.9155832361    0.6632657868
H      1.0     2.5398198321   -0.5247888390   -0.1604366241
```

Energy	-297897.348 KCAL/MOL
ZPE Correction	100.969 KCAL/MOL
298.15K Temperature Correction	105.946 KCAL/MOL

TOTAL MULLIKEN AND LOWDIN ATOMIC POPULATIONS

ATOM	MULL.POP.	CHARGE	LOW.POP.	CHARGE
1 C	6.157420	-0.157420	6.160716	-0.160716
2 C	6.241861	-0.241861	6.187400	-0.187400
3 C	5.858175	0.141825	5.971143	0.028857
4 C	6.219008	-0.219008	6.146491	-0.146491
5 C	5.711170	0.288830	5.938471	0.061529
6 C	6.041015	-0.041015	6.049757	-0.049757
7 H	0.769376	0.230624	0.817530	0.182470
8 C	6.151267	-0.151267	6.118037	-0.118037
9 C	6.267233	-0.267233	6.207092	-0.207092
10 C	5.932802	0.067198	6.064549	-0.064549
11 N	7.583447	-0.583447	7.190128	-0.190128

12 H	0.795929	0.204071	0.833921	0.166079
13 H	0.788046	0.211954	0.827504	0.172496
14 O	8.742187	-0.742187	8.510766	-0.510766
15 H	0.564777	0.435223	0.640511	0.359489
16 H	0.784282	0.215718	0.832221	0.167779
17 H	0.793044	0.206956	0.835095	0.164905
18 H	0.806913	0.193087	0.840731	0.159269
19 H	0.792050	0.207950	0.827938	0.172062

8-hydroxyquinoline radical adduct

ROHF/6-31G(d)

C	6.0	0.9163524238	-1.8226339897	-0.1709834136
C	6.0	2.1452767425	-1.2755576870	-0.1150849623
C	6.0	2.3337787556	0.1247404352	-0.0437385832
C	6.0	1.1912839434	1.0818548028	-0.1822352488
C	6.0	-0.1612053020	0.4016554819	-0.0619064724
C	6.0	-0.2828575476	-0.9891596730	-0.1042747075
C	6.0	-1.5679606026	-1.5142086440	-0.0367021727
C	6.0	-2.6490814503	-0.6612553343	0.0770107272
C	6.0	-2.4059017236	0.6999623637	0.1248196831
N	7.0	-1.1916634259	1.2156496928	0.0526702137
H	1.0	-3.2168814785	1.3997760121	0.2217784637
H	1.0	-3.6534787016	-1.0375651633	0.1334398779
O	8.0	1.3345812441	2.1071100607	0.7614005894
H	1.0	0.5282976602	2.6099020037	0.7607367434
H	1.0	-1.7148759668	-2.5799512536	-0.0638550993
H	1.0	0.7900252656	-2.8891799740	-0.2212142515
H	1.0	3.0127406888	-1.9116530430	-0.1074698888
H	1.0	3.3150615792	0.5472406870	0.0540423159
H	1.0	1.2308712257	1.5189783218	-1.1839578043

```
Energy                              -297899.230 KCAL/MOL
ZPE Correction              100.651 KCAL/MOL
298.15K Temperature Correction      105.587 KCAL/MOL
```

TOTAL MULLIKEN AND LOWDIN ATOMIC POPULATIONS

ATOM	MULL.POP.	CHARGE	LOW.POP.	CHARGE
1 C	6.202814	-0.202814	6.175605	-0.175605
2 C	6.182575	-0.182575	6.163464	-0.163464
3 C	6.204653	-0.204653	6.148377	-0.148377
4 C	5.821932	0.178068	5.966961	0.033039
5 C	5.773278	0.226722	5.945689	0.054311
6 C	6.011200	-0.011200	6.041480	-0.041480
7 C	6.153688	-0.153688	6.115524	-0.115524

8 C	6.264187	-0.264187	6.199618	-0.199618
9 C	5.929954	0.070046	6.067114	-0.067114
10 N	7.606668	-0.606668	7.199722	-0.199722
11 H	0.794303	0.205697	0.832582	0.167418
12 H	0.786323	0.213677	0.827608	0.172392
13 O	8.753383	-0.753383	8.509795	-0.509795
14 H	0.536396	0.463604	0.630796	0.369204
15 H	0.782828	0.217172	0.831044	0.168956
16 H	0.794014	0.205986	0.834812	0.165188
17 H	0.792579	0.207421	0.829494	0.170506
18 H	0.783509	0.216491	0.823152	0.176848
19 H	0.825716	0.174284	0.857160	0.142840

Appendix 3: Characterization of biphenyl products

Table of Contents

Compound **1a**

^{1}H-NMR (CD$_3$OD); Identified impurities: acetone, ethyl acetate, hexanes, water

^{13}C-NMR (CD$_3$OD); Identified impurities: acetone, hexanes

Compound **1b**

^{1}H-NMR (CD$_3$OD)
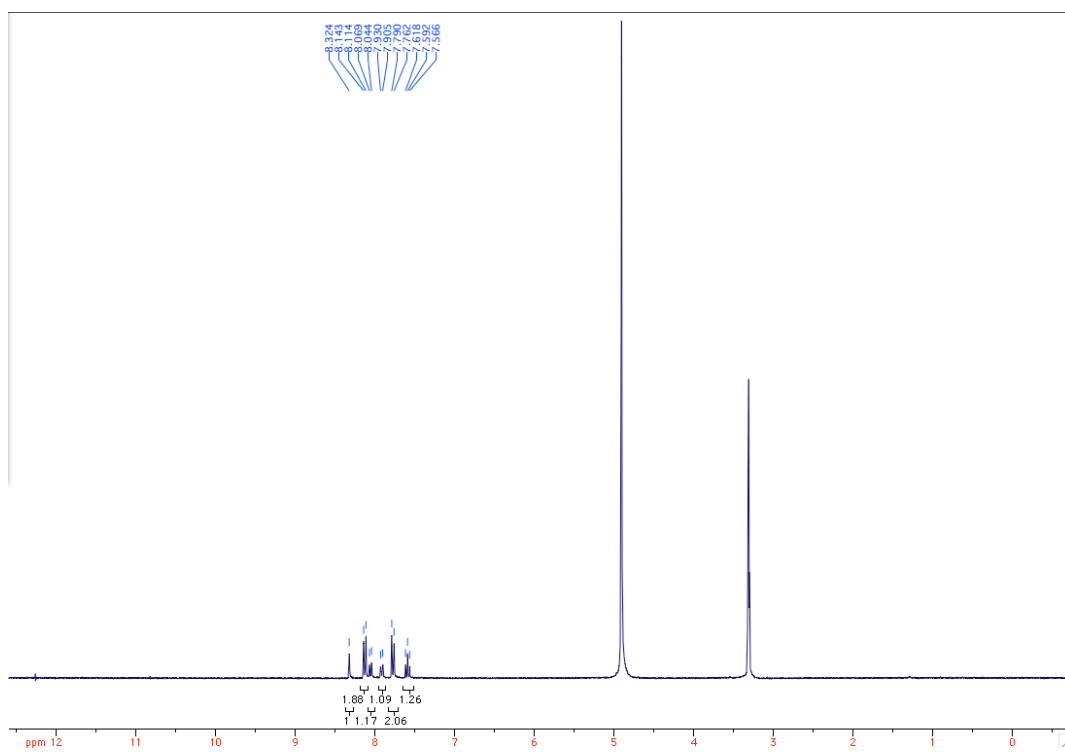
^{13}C-NMR (CD$_3$OD)
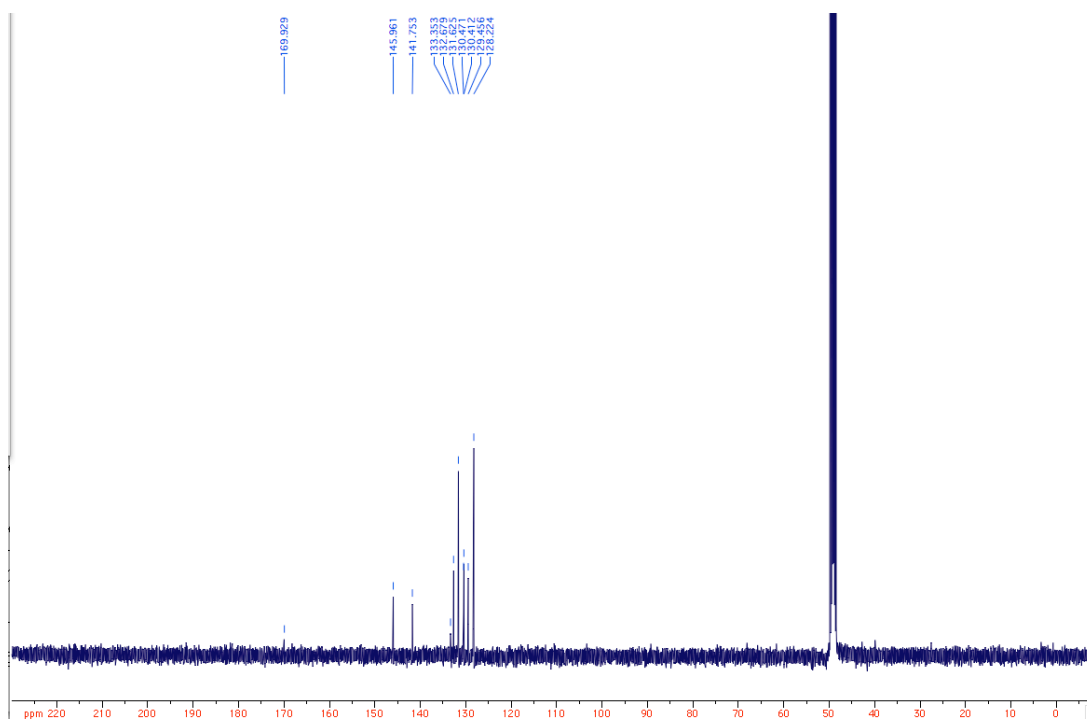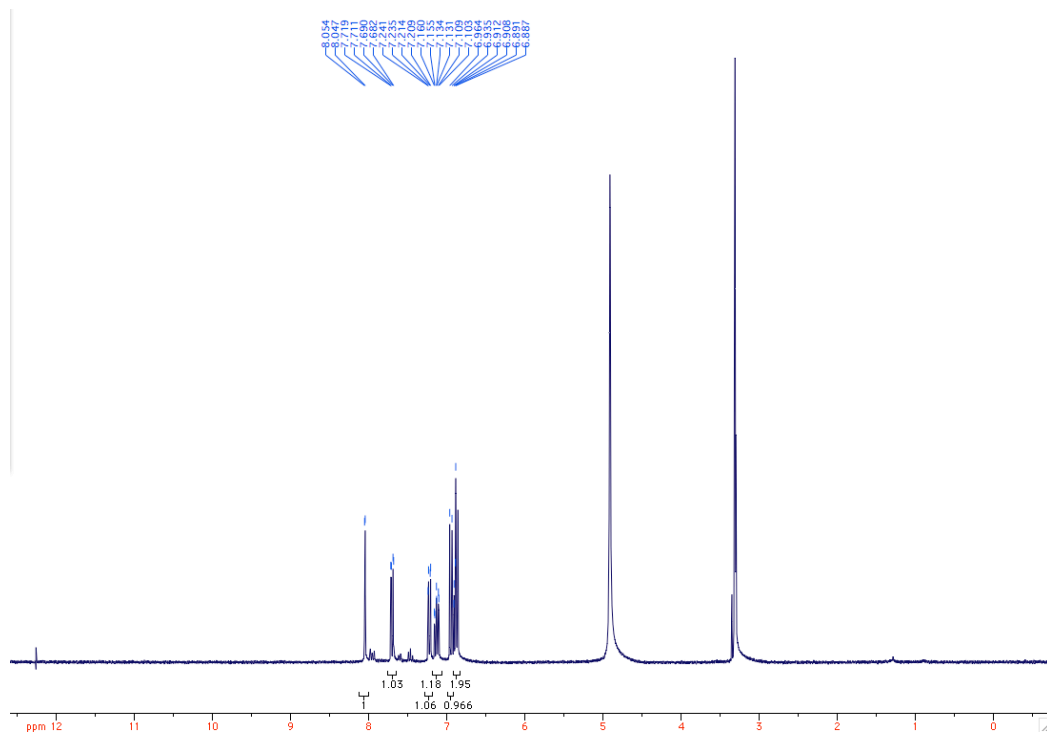
Compound **2**

^{1}H-NMR (CD$_3$OD)
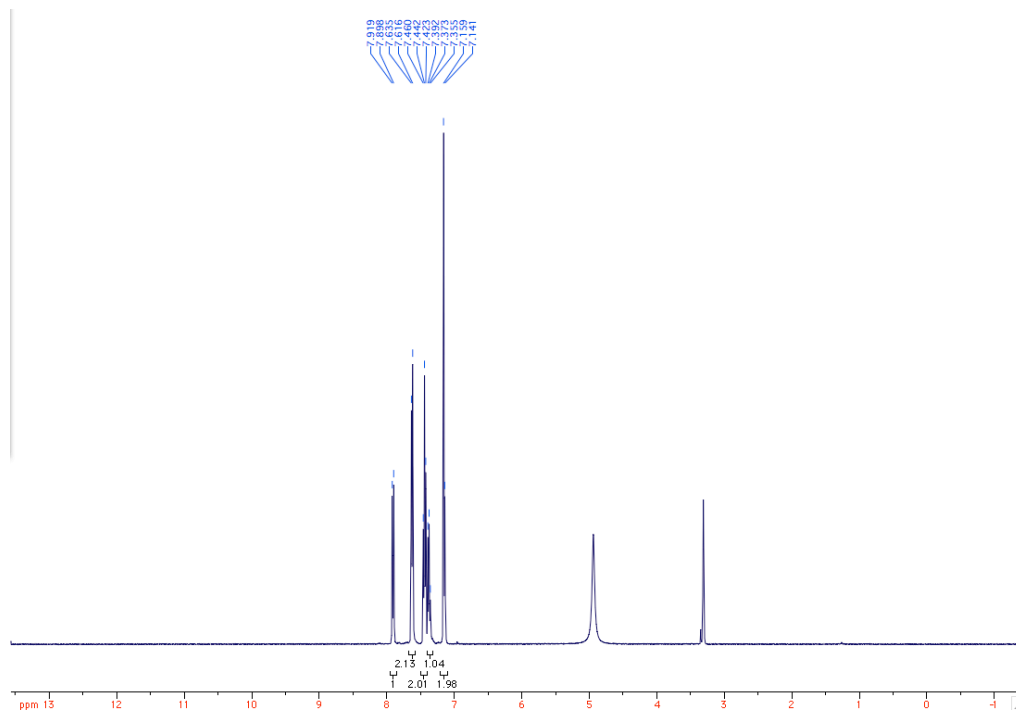
^{13}C-NMR (CD$_3$OD)
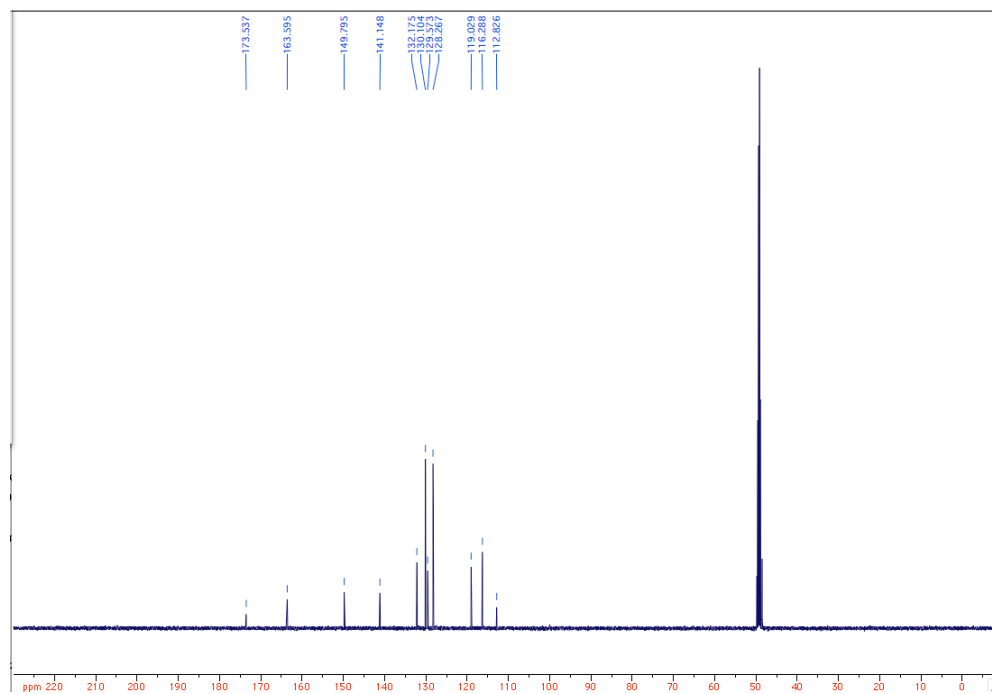
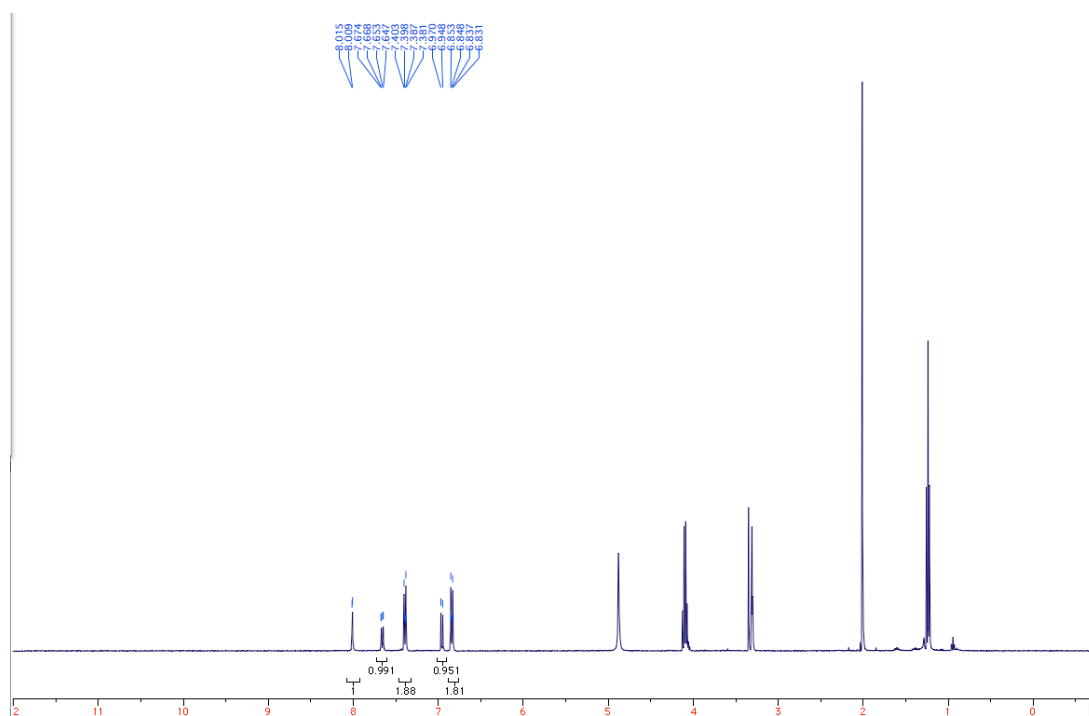Compound **2a**

^{1}H-NMR (CD$_3$OD); Identified impurities: ethanol
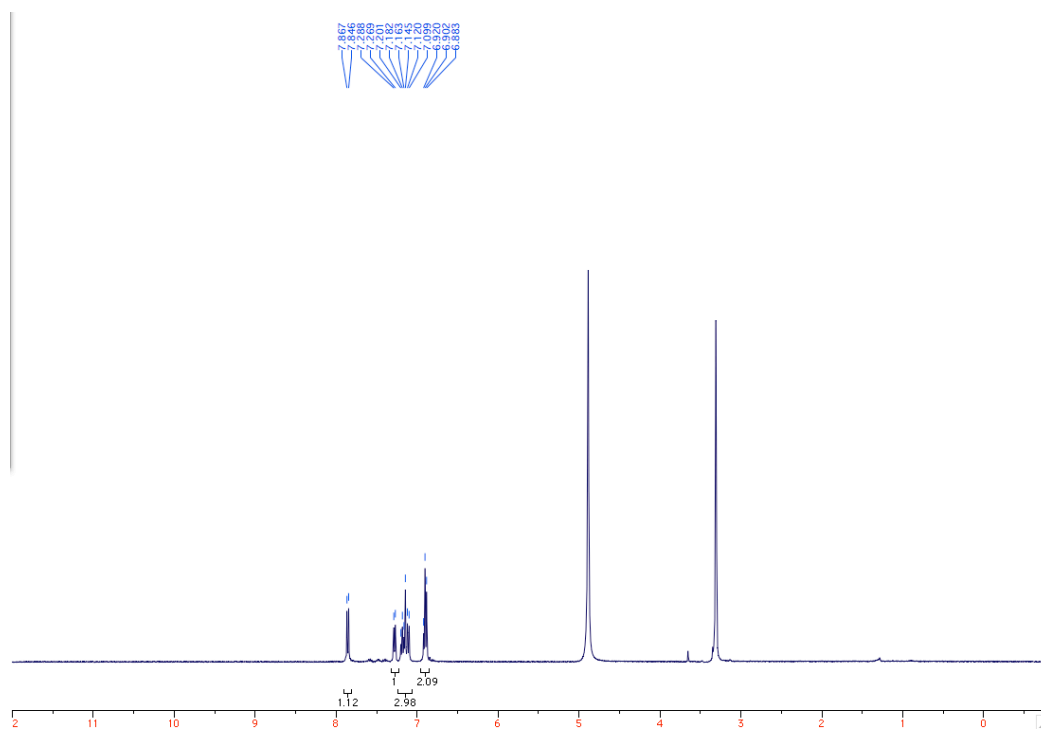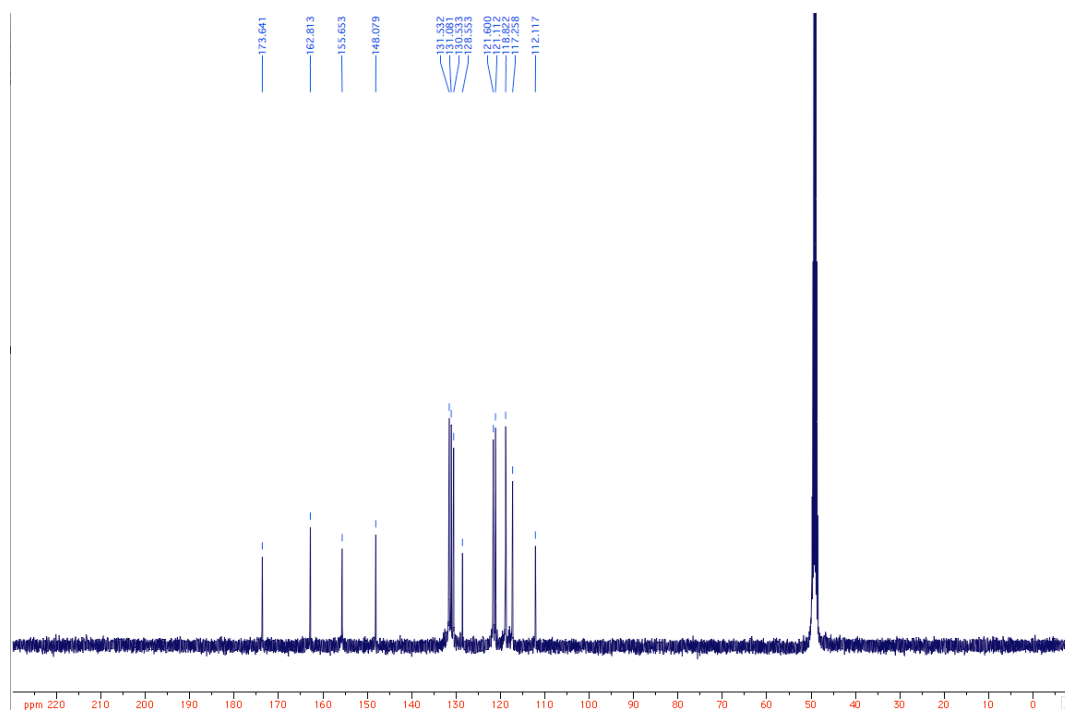
^{13}C-NMR (CD$_3$OD)

Compound **2b**

^{1}H-NMR (CD$_3$OD); Identified impurities: ethanol
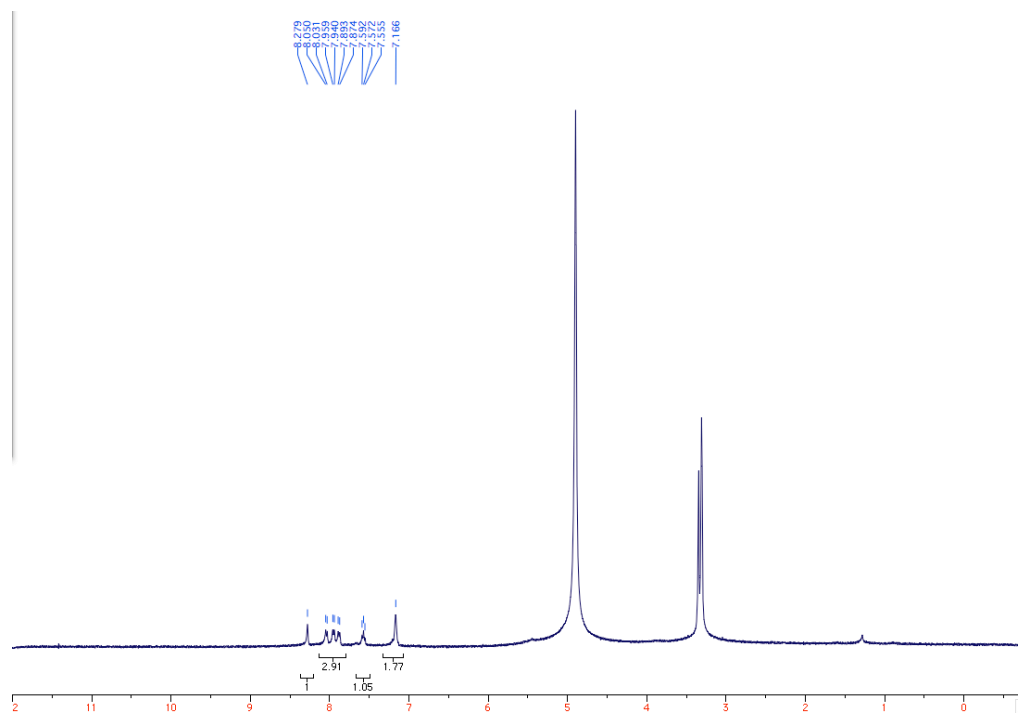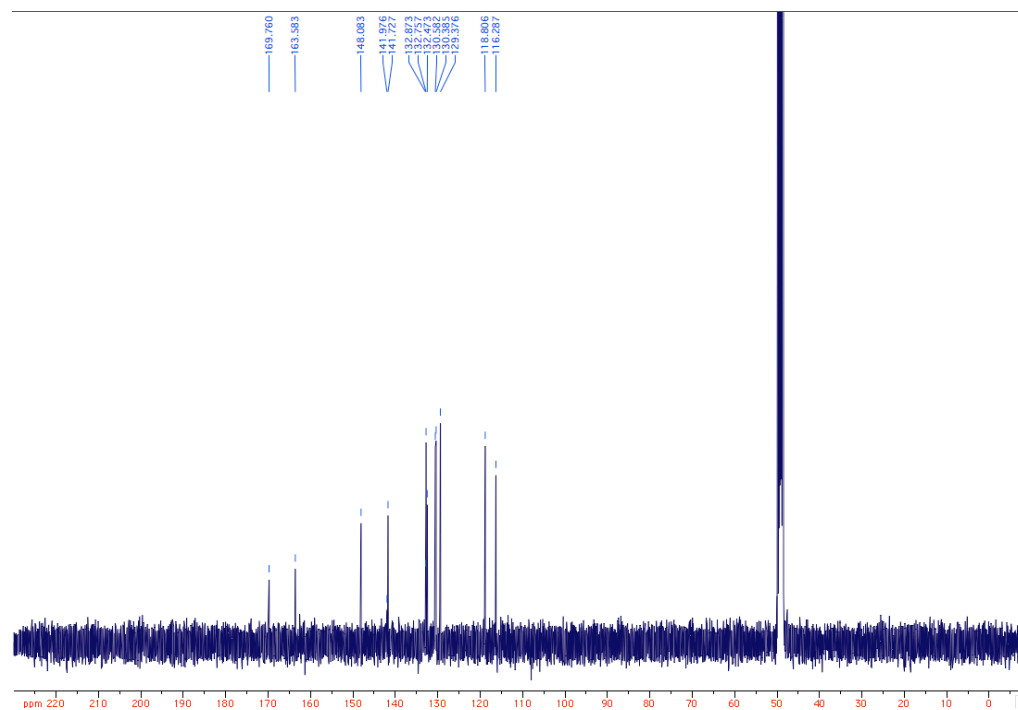
^{13}C-NMR (CD$_3$OD)

Compound **2c**

^{1}H-NMR (CD$_3$OD); Identified impurities: acetone, ethyl acetate, hexanes, water
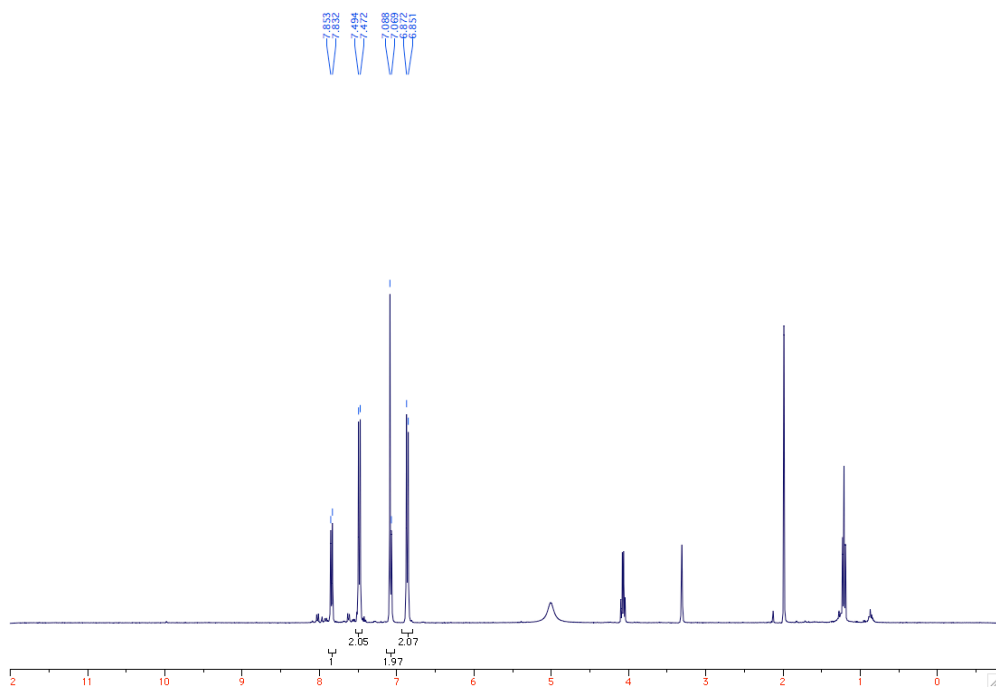
^{13}C-NMR (CD$_3$OD); Identified impurities: acetone, ethyl acetate, hexanes
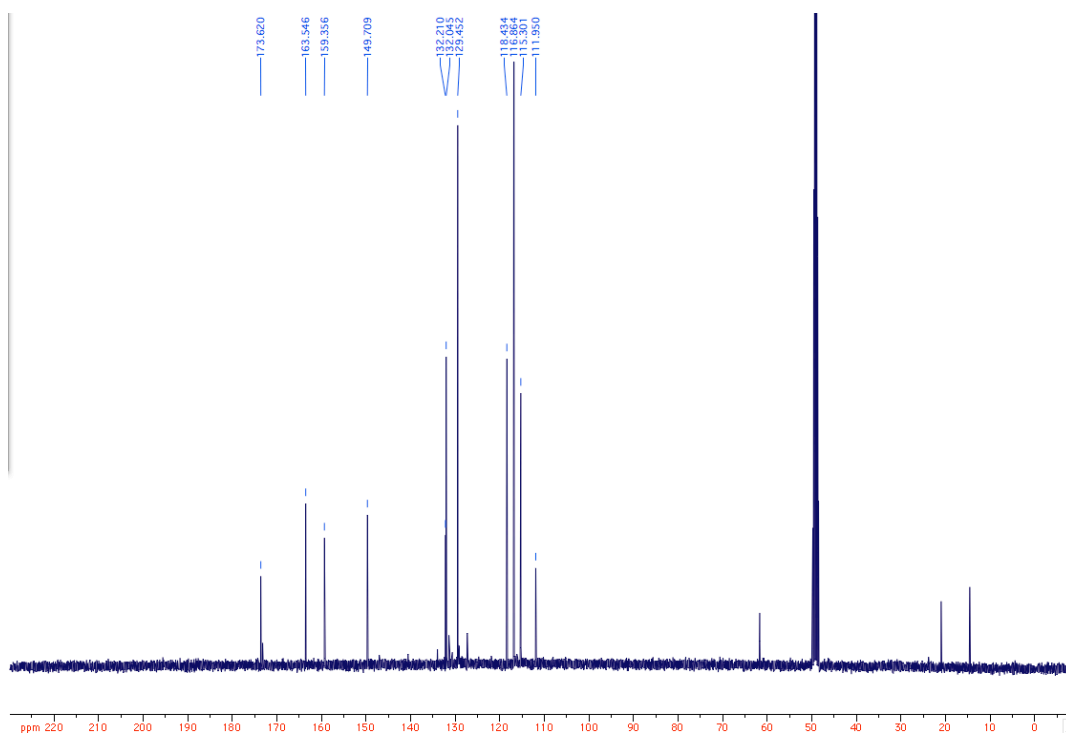
Compound **3**

^{1}H-NMR (CD$_3$OD); Identified impurities: ethanol
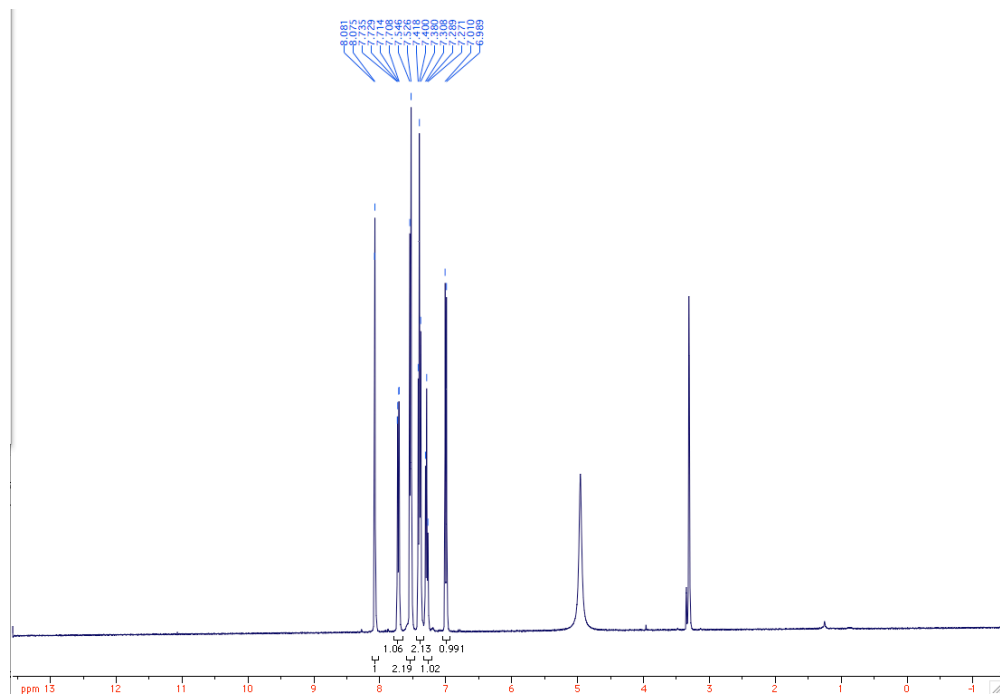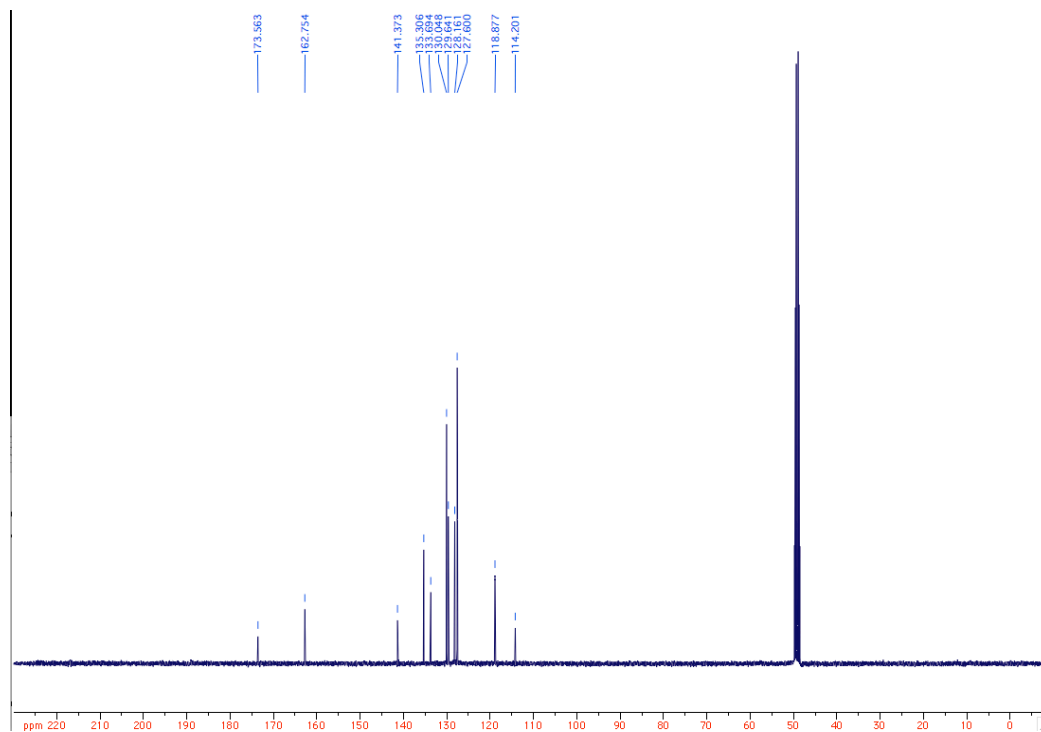
^{13}C-NMR (CD$_3$OD)

Compound **3a**

¹H-NMR (CD₃OD)

¹³C-NMR (CD₃OD)
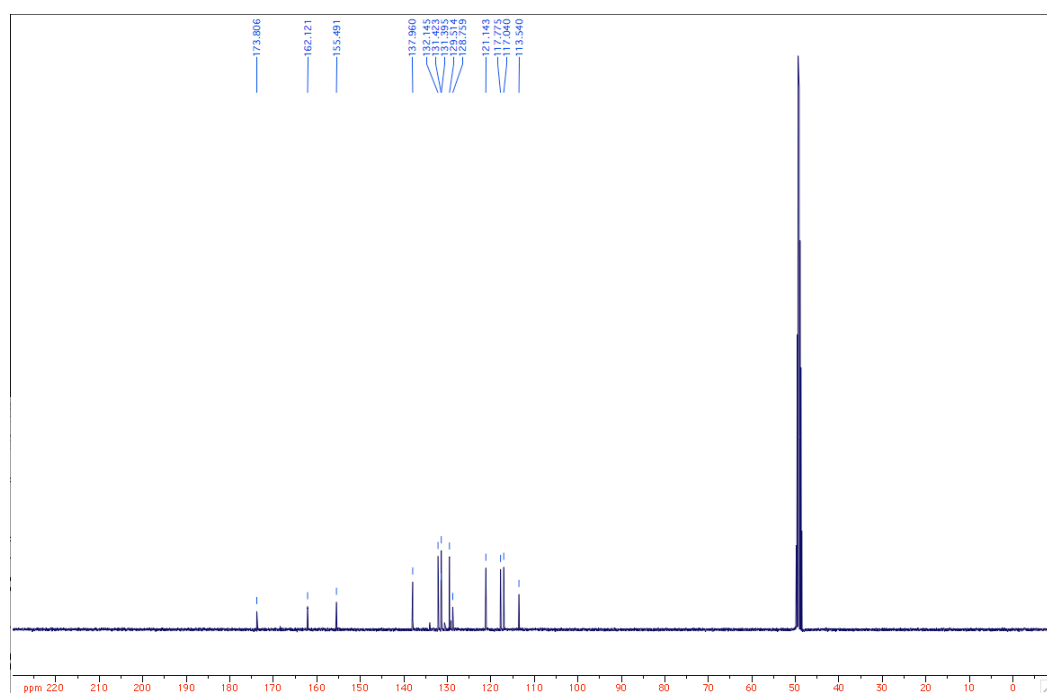
Compound **3b**

^{1}H-NMR (CD$_3$OD); Identified impurities: compound **3b'**, ethyl acetate, hexanes, methanol
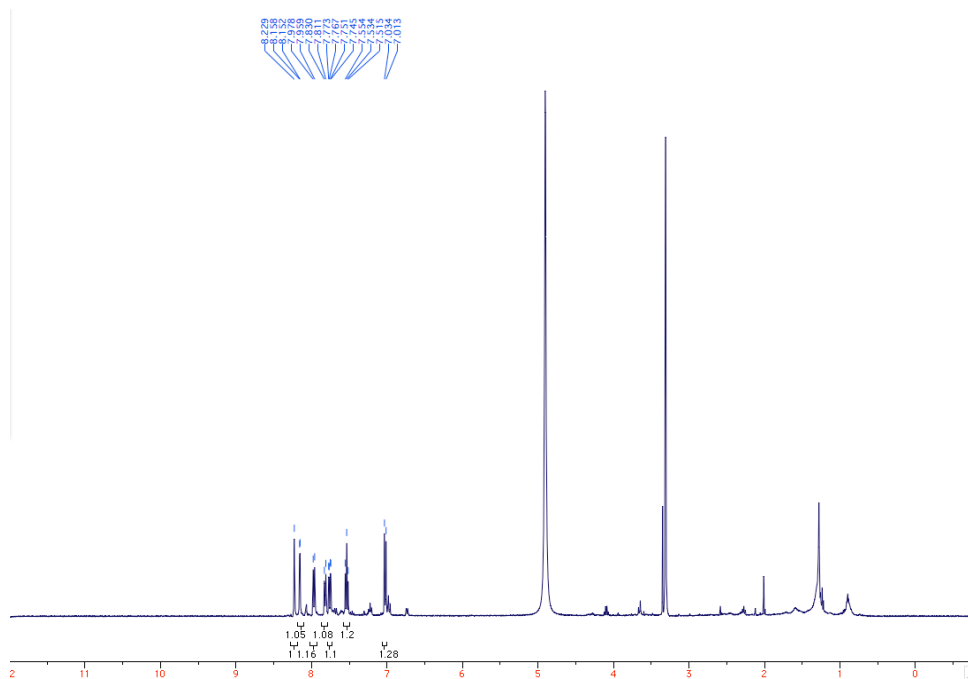
^{13}C-NMR (CD$_3$OD); Identified impurities: compound **3b'**, ethyl acetate, hexanes
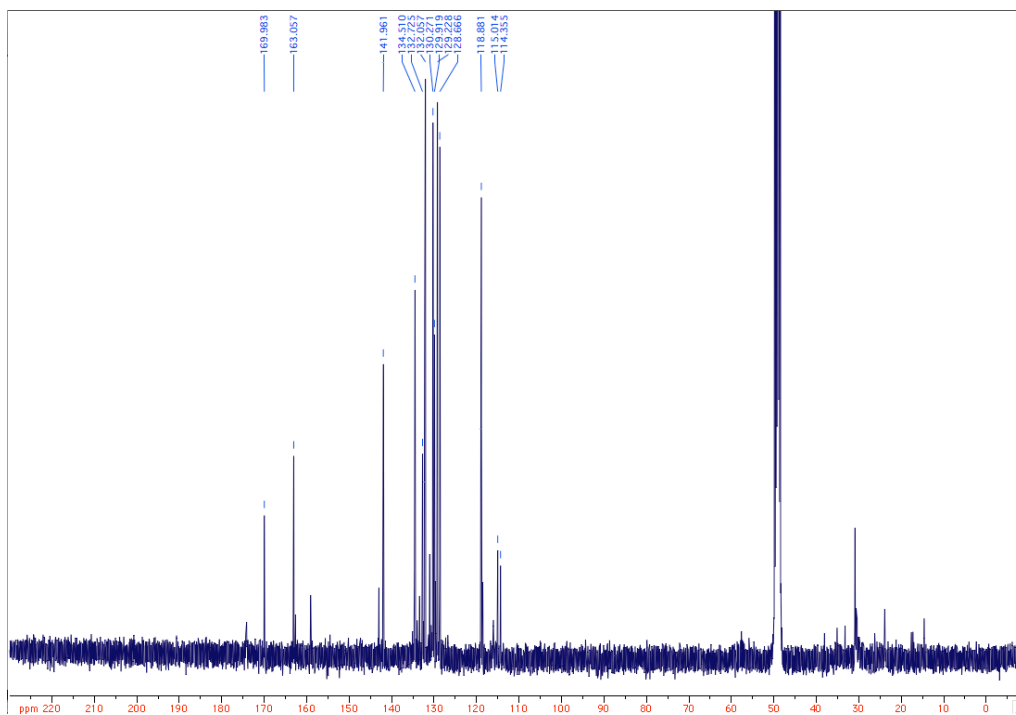
Compound **3c**

^{1}H-NMR (CD$_3$OD); Identified impurities: ethyl acetate, hexanes, methanol

^{13}C-NMR (CD$_3$OD)